The Thesis Committee for Gregory Edward McCool

Certifies that this is the approved version of the following thesis:

Evaluation of Corrosion Resistance of New and Upcoming Post-Tensioning Materials After Long-Term Exposure Testing

APPROVED BY

SUPERVISING COMMITTEE:

Supervisor: _____

John E. Breen

_____

Sharon L. Wood

_____

Harovel G. Wheat

Evaluation of Corrosion Resistance of New and Upcoming Post-Tensioning Materials After Long-Term Exposure Testing

by

Gregory Edward McCool, B.S.C.E.

Thesis

Presented to the Faculty of the Graduate School of

The University of Texas at Austin

in Partial Fulfillment

of the Requirements

for the Degree of

Master of Science in Engineering

The University of Texas at Austin

December 2010

DEDICATION

To my family and friends.

ACKNOWLEDGEMENTS

As an advisor, Dr. Breen was a great source of knowledge and guidance. I knew with certainty that, no matter what I asked, he would have a quick answer and an amusing anecdote to go along with it. I admire his attitude towards the engineering profession, and I will always carry with me the lessons I learned from him. Thank you also to Dr. Wood and Dr. Wheat for serving on my committee and answering my questions.

As my undergraduate assistant, Kevin Moyer was more tenacious than anyone I have ever worked with. His extensive knowledge of tools and equipment filled in the gaps of my own abilities, and his knack for completing tasks with military precision and speed often left me frantically trying to find more jobs for him to do. I wish him the best of luck as he continues where I left off.

Thank you to the FSEL technical and administrative staff for showing me the ropes. My involvement on the project only lasted one year, but your help made this accelerated schedule a non-issue.

Thank you to all my Longhorn, Domer, and Crimson friends for putting up with my nerdy enthusiasm for engineering over the past several years. I would say that the nerdiness will end now that I have my Masters degree, but that would be a lie.

Finally and most profoundly, thank you to my parents for believing in me and allowing me to choose my own path. Even if the content of my thesis goes over your heads, know that I couldn't have done it without your love and support.

December 3, 2010

ABSTRACT

Evaluation of Corrosion Resistance of New and Upcoming Post-Tensioning Materials After Long-Term Exposure Testing

Gregory Edward McCool, M.S.E.
The University of Texas at Austin, 2010

Supervisor: John E. Breen

This thesis focuses on the forensic analysis of ten full-scale post-tensioned beam specimens after four years of aggressive exposure testing. The research was funded by FHWA and TxDOT. Post-tensioned structures have been under scrutiny due to their vulnerability to corrosion damage. Recent corrosion failures have been traced to inadequate materials and construction procedures. The purpose of this research project is to evaluate the corrosion performance of new and upcoming post-tensioning materials and systems and to determine their suitability for preventing durability issues which were found in older structures. The following variables were tested in the full-scale beam specimens:

- Strand type
- Duct type
- Duct coupler type
- Anchorage type
- Tendon encapsulation

Non-destructive and destructive testing methods for evaluating corrosion damage were examined. Cost analysis of each material was conducted using tendon quantities from a typical post-tensioned bridge for comparison.

Galvanized steel ducts performed poorly, showing substantial pitting and area loss. Plastic ducts were intact, but elevated grout chloride levels indicate that moisture was able to enter the ducts at the locations of couplers and grout vents. Strand corrosion was minor and uniform for all the types which were examined, suggesting that chloride traveled the length of the tendons through strand interstices. Stainless steel strands were nearly corrosion-free. Pourback quality was found to protect anchorages more than galvanization of bearing plates. The electrically isolated tendon did not completely prevent strand corrosion, but the system resulted in much lower chloride concentrations along the tendon than the conventional systems.

TABLE OF CONTENTS

LIST OF TABLES

LIST OF FIGURES

CHAPTER 1
Introduction

1.1 BACKGROUND

Concrete is very weak in tension, which causes reinforced concrete members to crack in the regions which experience tensile stresses when load is applied. Prestressing introduces a large compressive stress to those regions, thus preventing cracks until the compression is overcome. When properly designed, prestressed structures allow for longer span lengths and less reinforcement than reinforced concrete structures.

Post-tensioning is a type of prestressing in which the large compressive stress is introduced to a member after casting. Concrete members are cast with ducts installed to create continuous cylindrical voids along their length. After the concrete has cured, high-strength steel strands are fed through the ducts and tensioned against anchorages located at the each end. After a desired tension has been reached, the strands are secured at the anchorages with wedges. In bonded internal post-tensioning, grout is pumped into the duct to create a protective barrier around the strands and to provide bond between the strands and surrounding concrete. Details of a typical bonded post-tensioning anchorage are shown in Figure 1.1. Post-tensioning combines the crack-control advantages of prestressing with the flexibility of being able to be cast on site.

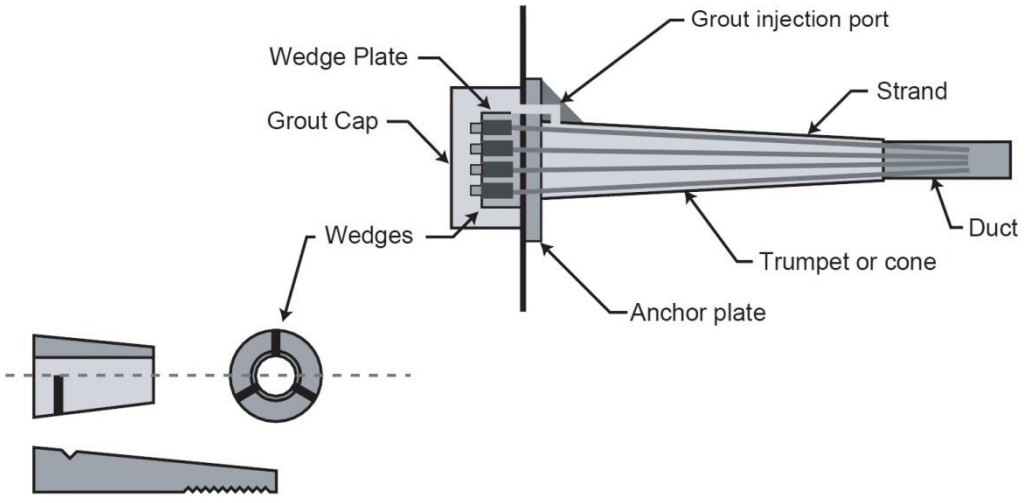

Figure 1.1: Typical Bonded Internal Post-Tensioning Anchorage[1]

1.2 CORROSION IN CONCRETE

Corrosion in concrete structures is a widespread problem with a high cost of repair. The types of structures which corrode most frequently are bridges and parking structures due to their aggressive exposure to chlorides in the form of tidal spray or deicing salts. While the high pH of concrete allows a passive layer to form around the reinforcing steel and protect it, cracks or highly porous concrete can allow chlorides to penetrate and disrupt this passive layer. Once a threshold chloride concentration has been reached at the steel level, corrosion initiates.

Corrosion is an electrochemical process in which electrons are transferred through an electrolyte from an anode to a cathode in what is known as a corrosion cell, as shown in Figure 1.2. In concrete, both the anode and cathode are on the surface of the reinforcement, and the moisture in the cement paste acts as the electrolyte. When steel corrodes, it forms several ferrous oxides. These oxides are less dense than steel itself and therefore occupy more volume than the steel they replace. In a concrete structure, this means that a corroded bar will place expansive stresses on the surrounding concrete, resulting in cracking and spalling in severe cases.

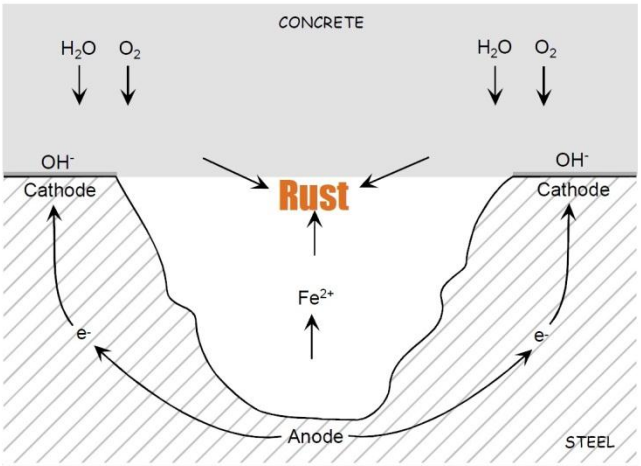

Figure 1.2: Steel Corrosion Cell[2]

Other metals are also vulnerable to corrosion. Almost all metals are thermodynamically unstable under normal conditions and will revert to their oxides over time. The corrosion tendency for each type of metal depends on its position in the galvanic series. Metals which are higher on the series are referred to as "noble," and those lower on the series are "active." Gold and platinum are the most noble metals, while zinc is among the most active. If two metals are

present and connected in the same corrosion cell, the more active one will generally corrode while the more noble will be preserved. This is the principle behind sacrificial coatings such as galvanizing zinc[3].

1.3 DURABILITY IN POST-TENSIONING

Corrosion occurs most often in bonded internal post-tensioning tendons when chloride intrusion causes the passive layer to break down on the strands. Although post-tensioned structures generally do not crack in flexure under service loads, chlorides can still enter through construction joints, inclined cracks due to diagonal tension, bursting cracks in anchorage regions, and flexural cracks due to overloads. Corrosion within post-tensioned structures is especially problematic. Seven-wire strands have much more surface area per volume than the equivalent size of reinforcing bar. This means that much more surface area is available to corrode and that area loss will occur much more quickly once corrosion initiates. Prestressed structures typically have much less steel area than an equivalent reinforced concrete structure. Also, prestressing strands are usually stressed to a very high level, often 60% to 75% of their ultimate strength. Therefore, losing just a small area of prestressing strand to corrosion could lead to a drastic loss in strength[4]. This could result in structural failure, depending on the location of the tendon and redundancy of the structure.

Originally, concrete cover and grouting were assumed to be the primary means of preventing chloride ingress for internal bonded post-tensioning tendons. Failures over the last 30 years, such as bridge collapses in the United Kingdom in the 1980s[5] as well as tendon failures in several Florida segmental bridges in the 1990s and 2000s[6], have called these assumptions into question. Many tendon corrosion problems could be traced back to[1]:

- Shrinkage cracks at construction joints and anchorage pourbacks
- Imperfect sealing at segment joints
- Grout voids caused by improper grouting procedures and poor-quality grout mixes
- Improperly installed duct splices
- Longitudinal splitting of plastic ducts.

Recent findings suggest that a more holistic approach to corrosion protection is necessary. Consideration must be given to the overall structural layout, waterproofing

membranes, concrete cover, duct, grout, and strand type to determine the durability of a post-tensioned structure[1,3] (see Figure 1.3).

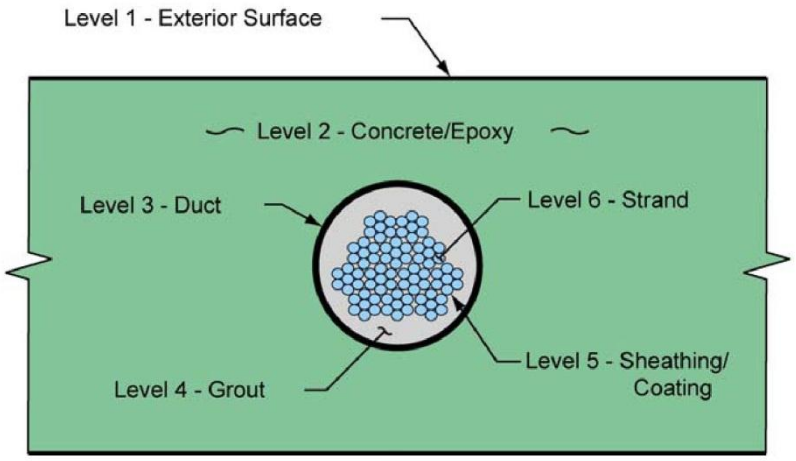

Figure 1.3: Layers of Protection in an Internal Bonded Post-Tensioned Structure[1]

Despite the corrosion problems found in some structures, post-tensioned bridges have performed much better than other types of construction. Specifications have been improving continually to reflect the state of the art. In the United States, the use of galvanized ducts has been all but discontinued in aggressive environments due to poor corrosion performance. Updated grouting specifications and training programs are expected to substantially reduce the incidence of voids and improve grout quality[7].

TxDOT Project 0-1405 was the previous project at Ferguson Structural Engineering Laboratory (FSEL) to address post-tensioning corrosion. This project focused on overall corrosion problems in post-tensioned structures. In particular, attention was paid to segmental construction joints. Level of prestress, duct type, and grout type were also studied. The beam specimens for the current project were designed to provide results which could be compared to work done by Salas[8] and Turco[9] for Project 0-1405[7].

1.4 PROJECT OBJECTIVE

The objective of TxDOT Project 0-4562 is to evaluate the corrosion performance of new and upcoming commercially available post-tensioning products with comparison to more traditional systems (steel strand, grouted in galvanized steel ducts). The project is being funded

by the Texas Department of Transportation and the Federal Highway Administration. Accelerated and passive corrosion tests as well as mechanical property tests have been conducted on each type of strand to determine their individual performance. Strand, duct, coupler, and protection system performance is being tested under aggressive chloride exposure conditions in full-scale beam specimens. Autopsies of these specimens, completed after four and six years of exposure, respectively, will determine the in-situ corrosion performance of the new materials.

1.5 THESIS OBJECTIVES AND SCOPE

The objectives of this thesis are:

- To explain the design rationale and testing procedure for the beam specimens.
- To evaluate the performance of the mild steel components, post-tensioning duct, strand, anchorages, and fully encapsulated system within 10 beam specimens after 4 years of aggressive exposure testing.
- To present the results of destructive and non-destructive monitoring of the beam specimens and evaluate the accuracy of those methods.
- To present estimates of the relative construction cost increases associated with each type of duct, strand, anchorage, and protection system for a typical segmental bridge.
- To use the results of the beam autopsies to develop corrosion design recommendations.

The scope of this thesis includes:

- Examination of non-destructive and destructive measurements taken during exposure testing of 10 beam specimens.
- Autopsy and analysis of 10 beam specimens.
- Recommendations for post-tensioned design based on research findings.

CHAPTER 2

Test Specimens

All text in this chapter was derived from Ahern[7], who developed and constructed the specimens, unless otherwise cited.

2.1 SPECIMEN CONCEPT

The test program for TxDOT Project 0-4562 was initiated in 2003 as a follow-up for Project 0-1405. The new test specimens were designed for compactness, controlled cracking, isolation of the corrosion of the post-tensioning elements, and the ability to produce results on an accelerated schedule.

Specimens from Project 0-1405 were extremely large and required equally large reaction beams. The new specimens were much smaller. Their live load was self-equilibrating, eliminating the need for reaction beams. However, the new specimens contained similar quantities of post-tensioning elements in the exposure zone as the Project 0-1405 beams. Therefore, the new specimens were expected to deliver similar results with less than 1/8 of the concrete of their predecessors. Figure 2.1 shows the size of specimens from each project for comparison.

Figure 2.1: Project 0-1405 Specimens (Background) and Project 0-4562 Specimens (Foreground)

Cracks provide a means of entry for moisture, oxygen, and chlorides into a concrete structure. While the hope in the use of prestressed concrete members is to keep them uncracked, overloading, anchorage bursting stresses, and diagonal tension can produce cracking. Thus, it

was decided that the test specimens should be intentionally overloaded to induce cracking for exposure testing.

In a prismatic concrete beam, flexural cracking can be somewhat unpredictable. In order to control crack location and limit the width to typical crack sizes, the new specimens were designed with a reduced cross-section at midspan. This decreased the moment of inertia and forced cracks to occur in that region, as shown in Figure 2.2. The presence of longitudinal steel at the top of the section helped further control crack width and quantity.

Figure 2.2: Flexural Cracks Occurring in the Reduced Midspan Region[7]

Some of the Project 0-1405 specimens had been undergoing exposure testing for eight years. While their corrosion was prominent at the time of autopsy, a much shorter project duration was desired. To that end, the new specimens were designed with a cast-in-place depression which simultaneously reduced the clear cover and served as a saltwater bath for exposure testing (see Figure 2.3). Longitudinal bars had a clear cover of 1 inch and the apex of the ducts had a clear cover of 1 3/8 inches in this region. This, combined with the specimens' controlled cracking, allowed corrosion to occur much more quickly than the previous specimens.

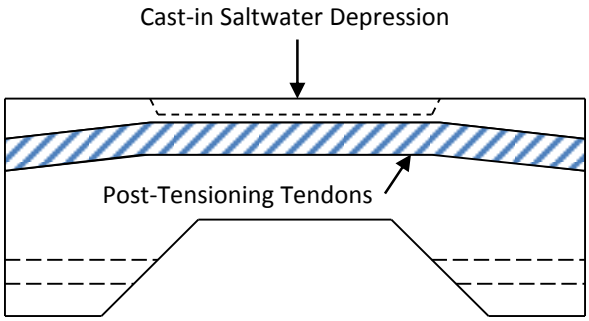

Figure 2.3: Reduced Cover at Midspan Region Due to Cast-In Depression[7]

During Project 0-1405, Salas[8] and Turco[9] observed extreme surface cracking caused by expansive stresses from the corrosion of reinforcing steel inside the specimens. This may have influenced half-cell potentials and accelerated corrosion to an uncontrolled level. To prevent this, the new specimens were constructed with epoxy-coated longitudinal bars and stirrups as well as plastic rebar chairs so that corrosion would target primarily the post-tensioning components.

2.2 SPECIMEN DESCRIPTION

The new specimens are 6 feet long by 17 inches wide. Depth varies from 15 inches at the reduced midsection to 27 inches at the end corbels. The specimens with fully encapsulated tendons are 7 feet in length due to their longer anchorage components. The corbels at each end of the specimens were fitted with PVC pipe conduits so that an axial live load could be applied down the centerline of the corbels using Dywidag bars. Springs were used to keep this force relatively constant throughout the exposure period. The application of an eccentric live load in this manner ensures that bending moment will be constant in the reduced midspan portion of the specimens.

Each specimen has two post-tensioning tendons which run along its entire length. The encapsulated specimens have one tendon due to space constraints associated with the fully encapsulated system. Each tendon has three 0.5 inch 7-wire strands. The specimens with stainless steel and stainless clad strands were constructed with 0.6 inch 7-wire strands due to availability constraints. The specimens were not designed with a particular level of prestressing in mind. Instead, the strands were stressed to a level which, after live load application, would allow the formation of flexural cracks approximately 0.010 inch in width. Complete details of the

new specimen design can be found in Reference 7, and a schematic of a typical loaded specimen is shown in Figure 2.4.

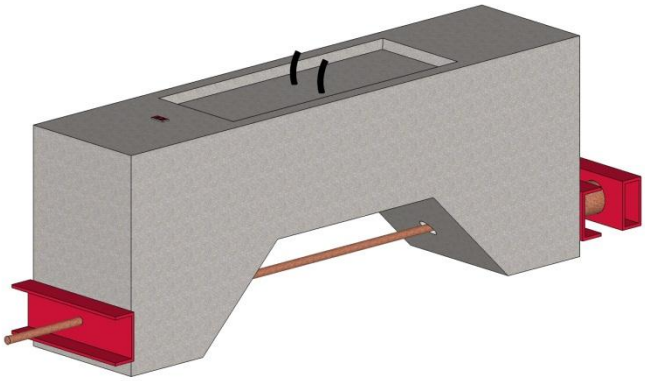

Figure 2.4: Specimen Schematic

2.3 SPECIMEN VARIABLES

Previous work by West[10], Schokker[2], Salas[8], and Turco[9] on Project 0-1405 determined that contemporary industry standards for internal bonded post-tensioned construction were inadequate. Project 0-4562 was conceived as a means of examining the corrosion performance of new and upcoming materials and systems which might result in better corrosion protection of post-tensioning tendons. A conference with members of industry and academia was held at FSEL in 2003 to identify which new post-tensioning materials to study. Although some of the materials were unable to be obtained in the United States, a specimen matrix was developed which included several types of new and upcoming post-tensioning components. The final specimen matrix is shown in Table 2.1, and the list of suppliers for each material is given in the Appendix.

Table 2.1: Final Specimen Matrix

Duct	Prestressed - Strand Type						Non-Prestressed
	Conventional	Hot Dip Galvanized	Copper Clad	Stainless Clad	Stainless	Flowfilled	Conventional Rebar
Galvanized	G - 1.4	NG - 2.2	NG - 1.2	NG - 1.3	NG - 4.1		
	NG - 1.1						
	G - T.2						
	NG - T.1						
One-Way Ribbed Plastic	NG - 2.3	NG - 3.4	NG - 2.4		NG - 4.2		
Two-Way Ribbed Plastic	G - 5.1*	NG - 3.2*	NG - 3.3*	NG - 5.2*	NG - 5.3*		
	NG - 3.1*						
Fully Encapsulated	NG - 7.1*	NG - 7.3*				NG - 7.4*	
	NG - 7.2*						
None							black - 4.4
							epoxy - 4.3

G = Galvanized Bearing Plate, NG = Non-galvanized Bearing Plate

= Autopsy performed in March 2010

* = Dead end anchorage exposure

NOTE: For each specimen with plastic ducts, one duct is coupled and the other is continuous.

2.3.1 Strand Type

Six types of strand were used to construct the test specimens:

- Conventional
- Hot-dip galvanized
- Stainless steel
- Copper-clad
- Stainless-clad
- Flow-filled epoxy-coated

All strand was 0.5-inch seven-wire except for the stainless steel and stainless clad, which were 0.6-inch diameter. Special anchor heads were obtained to accommodate the larger strand size. Special wedges were used with the epoxy-coated strand to ensure good seating during stressing. The galvanized strand was galvanized after being wound, which means that much of its interstitial space is bare steel.

2.3.2 Duct Type

Several types of duct were used in the test specimens:

- Galvanized steel
- GTI one-way plastic
- GTI two-way plastic
- VSL one-way plastic

Each type of duct had a different diameter. For each type of plastic duct, the diameter was chosen based on the smallest available coupler style for that duct.

2.3.3 Coupler Type

Because the specimens of Project 0-1405 had shown that coupling methods for galvanized ducts are quite inferior, it was decided to use continuous galvanized ducts in all specimens. For one tendon per specimen with plastic ducts, the ducts were cut in half. A coupler was placed at midspan to connect the halves. Three different types of coupler were used, each corresponding to one type of plastic duct:

- GTI slip-on (GTI two-way duct)
- GTI snap-on (GTI one-way)
- VSL snap-on (VSL one-way)

The VSL couplers did not come with a grout vent pre-installed. Instead, the project team fabricated and installed grout vents for these couplers at FSEL.

2.3.4 Anchorage Type

VSL EC5-7 bearing plates were installed in all specimens except for those with encapsulated tendons. Both galvanized and non-galvanized versions of this bearing plate were used.

2.3.5 Fully Encapsulated System

The encapsulated specimens were constructed such that the tendon is electrically isolated from the remainder of the specimen. This is achieved through the use of special anchorages, isolators between the bearing plate and anchor head, and robust, watertight connections between the duct and trumpet. Additionally, a permanent grout cap was installed over the anchor heads to

further protect the tendons. VSL supplied the fully encapsulated tendon components, including the CS-2000 bearing plate.

2.4 CONSTRUCTION PROCEDURE

All project specimens were fabricated at FSEL by Ahern. A more detailed description of the construction process can be found in his thesis[7].

2.4.1 Specimen Fabrication

The project team constructed compound wood forms which allowed the specimens to be cast in groups of four. This reduced concrete variation and saved lab space during casting. The live and dead end bearing plates were attached to the end walls of the forms in order to be imbedded in the specimens. The epoxy-coated rebar was bent off-site and assembled at FSEL using epoxy-coated wire ties (see Figure 2.5). Plastic chairs were used to support the rebar cage in the formwork. Ducts were cut to length and fitted with midspan grout vents and couplers where applicable, then installed in the rebar cage. A completed rebar cage awaiting concrete is shown in Figure 2.5.

TxDOT Class C concrete for bridge substructures was used in all specimens. Concrete was placed using a one-yard bucket and consolidated, taking care not to damage the ducts or grout vents. Just before finishing, special forms were installed on the top of the specimens to create the depressed saltwater baths. Companion cylinders were cast with each group of specimens and tested to ensure proper concrete strength before post-tensioning. After curing, strand was cut from its delivery roll and installed in the specimens.

Figure 2.5: Epoxy-Coated Rebar Cage (Left) and Completed Reinforcement Cage with Ducts in Formwork (Right)[7]

2.4.2 Post-Tensioning

Stressing was completed at FSEL using a monostrand ram with power seating capability, as shown in Figure 2.6. First, the ducts were cleaned with compressed air to remove debris. Data acquisition equipment was attached, and anchor heads and wedges were installed at each end of the specimen. The strands were stressed individually, alternating between the two tendons of each specimen to minimize elastic shortening losses. Specimens were stressed to 15% of guaranteed ultimate tensile strength in order to minimize creep and relaxation losses and to reduce the cracking live load. After all wedges were seated, the strand tails were trimmed.

Figure 2.6: Prestressing Setup[7]

2.4.3 Grouting

As required by TxDOT specifications, grouting was completed within 48 hours of stressing[11]. Temporary grouting caps were installed over the anchor heads. Prebagged Sika Grout 300 PT was batched with an electric mixer and placed in the ducts with a hand pump as shown in Figure 2.7. Grout was pumped into the dead end of the specimen, using a staged grouting sequence based on VSL guidelines to minimize the formation of voids[12].

Figure 2.7: Grouting in Progress[7]

2.4.4 Live Load Application

Live load was applied using threaded Dywidag bars which were installed through the holes in both corbels of each specimen. The bars were loaded using a hydraulic ram bearing on a stressing chair and a Dywidag nut on the specimen's live end. A spring assembly was used to maintain a constant live load. The extent of flexural cracking was carefully observed during stressing. Once crack widths of approximately 0.010 inch were reached, the Dywidag nut was tightened, and the ram was removed. On some specimens, cracks were observed extending from the re-entrant corners of the corbels during live load application. These cracks were sealed with mortar before exposure began.

2.5 SPECIMEN NOTATION

A total of 28 specimens were constructed. Of those, 24 underwent exposure testing while the remaining four remained in dry storage at FSEL due to problems obtaining a certain type of strand. The specimens were named according to their casting group and given a specimen ID derived from the materials they contained. The identification system is explained in Figure 2.8, and the complete list of all Project 0-4562 specimens is shown in the Appendix.

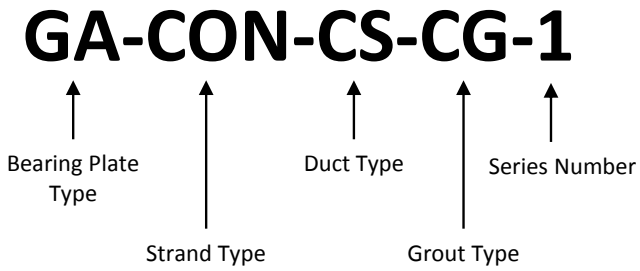

NGA = Non-Galvanized Bearing Plate
GA = Galvanized Bearing Plate

CON = Conventional Strand
HDG = Hot-Dip Galvanized Strand
SS = Stainless Steel Strand
CU = Copper-Clad Strand
SC = Stainless-Clad Strand
FF = Flowfilled Epoxy-Coated Strand

CS = Corrugated (Galvanized) Steel Duct
1P = One-Way Plastic Duct
2P = Two-Way Plastic Duct
EIT = Fully Encapsulated Tendon

CG = Cement Grout

Figure 2.8: Specimen Identification Conventions

CHAPTER 3

Experimental Procedure

3.1 LONG-TERM EXPOSURE SETUP

All specimens except for the control specimen underwent four years of exposure testing outside FSEL. The specimens were exposed to cycles of ponded saltwater at midspan, and several specimens were additionally fitted with anchorage region saltwater drippers. Non-destructive monitoring was conducted on the specimens throughout the testing period. The fourteen specimens which were not autopsied for this report will undergo the following experimental procedure for another two years. At that time, they will be autopsied to close out the project. Project 0-4562 specimens under exposure testing are shown in Figure 3.1.

Figure 3.1: Specimens under Exposure Testing

3.1.1 Ponding Cycle

The ponding cycle consisted of filling the cast-in depression on the top of each specimen with 3.5 wt% saltwater for two weeks. This concentration was chosen based on the methods outlined in ASTM G109 for aggressive corrosion testing of steel in concrete[13]. In 2007, the saltwater concentration specified in G109 changed to 3%, but 3.5% saltwater has been used in order to maintain continuity. In order to prevent leakage, the flexural cracks which extended down the sides of each specimen were patched with epoxy. After two weeks of saltwater exposure, the saltwater was rinsed out of the depressions, and any remaining water was removed

with a sponge. The specimens were then kept dry for the remainder of the month. This process was repeated every month for the entire test period, with a few gaps due to logistical factors.

Weather made maintaining the proper saltwater level in the specimens difficult. Saltwater tended to evaporate quickly out of the depressions during the hot summer months, and researchers spent much time mixing saltwater solution and refilling the depressions. In the rainier winter months, the project team had trouble keeping rainwater out of the depressions during the dry cycle. To solve these two problems, cellular polycarbonate roofs were designed and constructed in order to seal and protect the depressions on the remaining non-autopsy project specimens. The roofs were constructed using Polygal®. Each roof was assembled with construction adhesive and secured to the specimen with heavy-duty Velcro® to ensure easy access. The triangular profile and tight fit of the roofs help minimize evaporation and rainwater intrusion. Specimens with roofs attached are shown in Figure 3.1.

3.1.2 Anchorage Spray Cycle

Several specimens were chosen to receive anchorage exposure in addition to ponded saltwater exposure. All anchorage exposure specimens are referred to as "dripper specimens" in this report. Among those chosen for autopsy, Specimens 3.1, 3.2, and 7.1 were dripper specimens. For six hours every month, 3.5% saltwater was sprayed onto the dead end anchorage pockets of the dripper specimens using 45-degree stationary lawn sprinklers (see Figure 3.2). A closed-loop system was used in which saltwater was pumped from a holding tank through the pipes and out the sprinklers, then collected and channeled back into the holding tank. This minimized runoff losses and the amount of saltwater mixing required. Anchorage exposure was timed to coincide with the beginning of the ponding wet cycle so that all saltwater could be mixed at one time every month.

At the time of autopsy, the dripper system was not operational. The electric pump had seized, the holding tank had ruptured, and several pipes had broken. It was decided to use some discretionary project funds to provide permanent upgrades to the system so that all remaining dripper specimens could be reliably tested until the final round of autopsies.

Figure 3.2: Repaired Drippers in Operation (Left) and New Tank System (Right)

All broken or damaged pipe and sprinkler components were repaired. The holding tank was replaced with an outdoor-grade plastic trough and a new pump was purchased. All components in this pump which are in contact with the pumped fluid are ceramic or plastic, which should prevent the pump from seizing. Should any component fail, the pump was also sold with a 2-year unconditional warranty. A 1000-gallon elevated storage tank was assembled by FSEL technicians using lab salvage material as shown in Figure 3.2. This tank was connected to the new holding tank with a hose and a float switch. When the saltwater level in the holding tank drops due to losses, the level is automatically replenished from the elevated storage tank. The system allows several hundred gallons of saltwater to be mixed at once, so the only monthly task for the researcher is to activate the pump.

3.2 MONITORING DURING EXPOSURE TESTING

Similar methods were used to monitor the Project 0-4562 as were used to monitor Project 0-1405 specimens. Non-destructive monitoring consisted of visual inspection, half-cell potential measurements, and AC impedance measurements. As a destructive test, chloride penetration readings were only conducted at the end of the exposure period and just before autopsies.

3.2.1 Visual Examination

Specimens were monitored throughout their life for changes in appearance. Special attention was paid to extent of cracking, spalling, and the presence of corrosion stains or efflorescence on the outer surfaces of the concrete.

3.2.2 Half-Cell Potential Readings

Corrosion is an electrochemical process by which electrons are transferred from an anode to a cathode. Individually, the anodic and cathodic reactions are known as half-cells, and each has its own electrochemical potential. For the corrosion of steel in concrete, the half-cell of interest is the anodic half-cell in which iron is oxidized. This half-cell can be isolated and compared against the potential of a known reference electrode. The difference between the anodic and reference potential is known as the half-cell potential. This can be used to estimate the probability of corrosion and the time to corrosion initiation[3]. ASTM C876 provides the standard methodology for collecting and interpreting half-cell potentials of steel in concrete. The half-cell method is designed for use on uncoated rebar only[14]. However, the method had been implemented on Project 0-1405 with some success, and few other monitoring methods exist for bonded post-tensioning tendons. Therefore, the use of the half-cell method was continued for Project 0-4562 despite the presence of prestressing strand and epoxy-coated rebar[7].

Measurements were conducted just after the end of the ponding wet cycle each month. This ensured that the pore space of the concrete contained enough moisture to electrically connect the anodic and reference half-cells. The depression on top of each specimen was soaked with a wetting solution consisting of soapy water to better conduct current through the specimen (see Figure 3.3). The tip of the reference electrode was covered with a sponge to serve as a porous medium between electrode and concrete, as shown in Figure 3.3. The saturated calomel electrode (SCE) was used as the reference electrode.

The test specimens had been constructed with a lead connected to the live ends of the tendons. Half-cell potentials were measured by connecting a voltmeter to one tendon wire and the reference electrode, then touching the electrode to the surface of the concrete. Measurements were taken at every point of a regular grid within each specimen's saltwater depression, as shown in Figure 3.4. Each tendon was accounted for separately by measuring three rows of grid points with the voltmeter connected to one tendon wire, then another three while connected to the other

wire (see Figure 3.4). Half-cell potentials were recorded at every point of the grid for every specimen. Because Specimen 7.1 had only one tendon, measurements were taken at every point on the grid while connected to the same tendon wire.

Figure 3.3: Half-Cell Potential Measurements in Progress

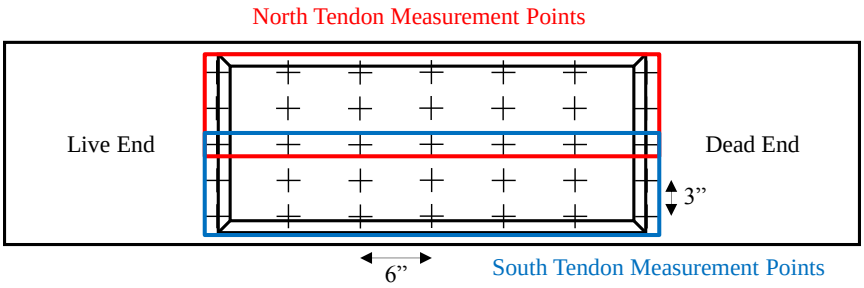

Figure 3.4: Half-Cell Potential Measurement Points (Adapted from Reference 7)

3.2.3 AC Impedance Readings

When used properly, the AC impedance method can indicate the presence of defects and chloride intrusion in fully encapsulated tendons. When alternating current is passed from the tendon to the reinforcing steel, the plastic duct acts as a capacitor in parallel with a high resistance[15]. Changes in the resistance and capacitance of this circuit throughout a structure's life can indicate defects in the tendon or chloride intrusion[4]. The tendon in each 7-series specimen was designed to be electrically isolated, making this a suitable method to monitor them.

Each 7-series specimen was constructed with one lead connected to its tendon and another to a pair of additional, uncoated steel longitudinal bars which were added to increase

conductivity (see Figure 3.5). To conduct the AC impedance measurements, a BK Model 885/886 LCR meter was connected to the two leads, as shown in Figure 3.6. Resistance, capacitance, and a loss factor were read from the meter at a frequency of 1 kHz and recorded. This procedure was conducted at the end of each month's ponding wet cycle.

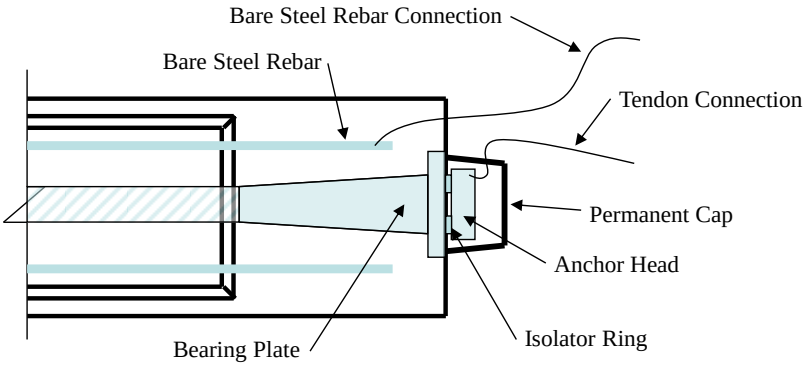

Figure 3.5: Electrically Isolated Tendon Detail[7]

Figure 3.6: LCR Meter Connected to Specimen to Measure AC Impedance

3.2.4 Chloride Content

Chloride penetration measurements were taken from the concrete and grout of all ten autopsy specimens after the end of the exposure period. Chloride content was determined for each sample using the CL-2000 Chloride Test System by James Instruments, shown in Figure 3.7. This system performs a variation of the acid-soluble chloride test procedure outlined in ASTM C1152[16]. Accuracy of the test system was validated by testing a powder sample from 1-inch depth at the top surface of Specimen T.1. Powder from the same depth was sent to Tourney Consulting Group in Kalamazoo, Michigan for acid-soluble chloride testing according to ASTM C1152.

Figure 3.7: Chloride Content Measurement Setup

3.2.4.1 Surface Chloride Penetration

Samples were extracted using a hammer drill, as shown in Figure 3.8. At all locations, powder samples were extracted at depths of 0.5 inch and 1 inch from the same hole, taking care to prevent cross-contamination. On each specimen's top surface, chloride samples were taken at a location 2 inches towards the live end from the beam's transverse centerline, as shown in Figure 3.9. Samples were also extracted at the dead end anchorage face, 5 inches from the top of the specimen (see Figure 3.10). Additional samples were extracted from the live end anchorage faces of the three dripper specimens at a distance of 6 inches from the top surface. For Specimen 7.1, samples were extracted from both ends at a depth of 6 inches. These locations correspond to the center of the dead and live end anchorage pockets, respectively.

Figure 3.8: Chloride Sample Extraction with Hammer Drill

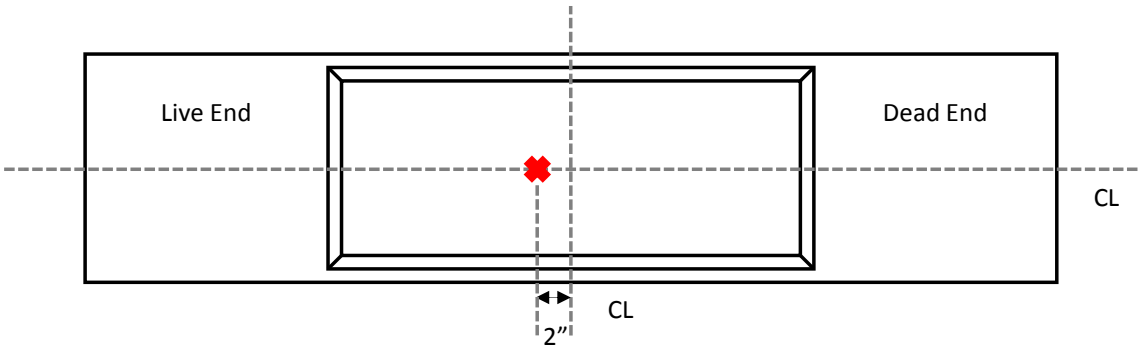

Figure 3.9: Top Surface Chloride Sample Location

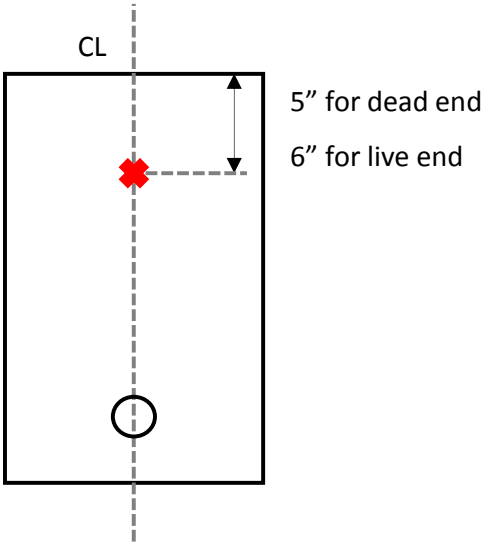

Figure 3.10: Anchorage Face Chloride Sample Location

3.2.4.2 Grout Chloride Content

In addition to surface chloride penetration, samples were extracted from the grout in the tendons of the autopsy specimens. Grout powder samples were taken after all post-tensioning elements had been removed from the main autopsy region blocks and the ducts had been cut open. For galvanized ducts, samples were taken every 2 inches along the regions of the ducts which had visible external corrosion or area loss. For plastic ducts, one sample was extracted at midspan in each tendon. The samples were extracted using a clean hammer and chisel, as shown in Figure 3.11. Care was taken to obtain a sample which included grout from the entire depth of the tendon. After pieces of grout had been chipped away from the tendon, they were ground with a mortar and pestle, as seen in Figure 3.11.

Figure 3.11: Grout Chloride Sample Extraction (Left) and Grinding (Right)

CHAPTER 4

Exposure Test Results and Analysis

Exposure testing for all specimens began on March 1, 2006 and continued until March 1, 2010. Total exposure time was 1460 days. During this time, half-cell and AC impedance readings were generally taken monthly, although some gaps in monitoring were present throughout the four year test period. Chloride samples were extracted after the end of the testing period as described in Chapter 3.

4.1 HALF-CELL POTENTIAL DATA AND ANALYSIS

The half-cell method to determine corrosion potentials was calibrated for uncoated reinforcing steel[14]. Although half-cell potentials were measured on specimens containing epoxy-coated reinforcing steel and several types of prestressing strand, the method is still useful in estimating the relative extent and severity of corrosion for the test specimens examined here.

Half-cell contour plots are presented in Figure 4.1. These plots represent the final readings taken at every point on each specimen just prior to autopsy. Note that the contour maps represent an overhead view of the autopsy region of the specimens with the live end to the left and the north tendon on the top.

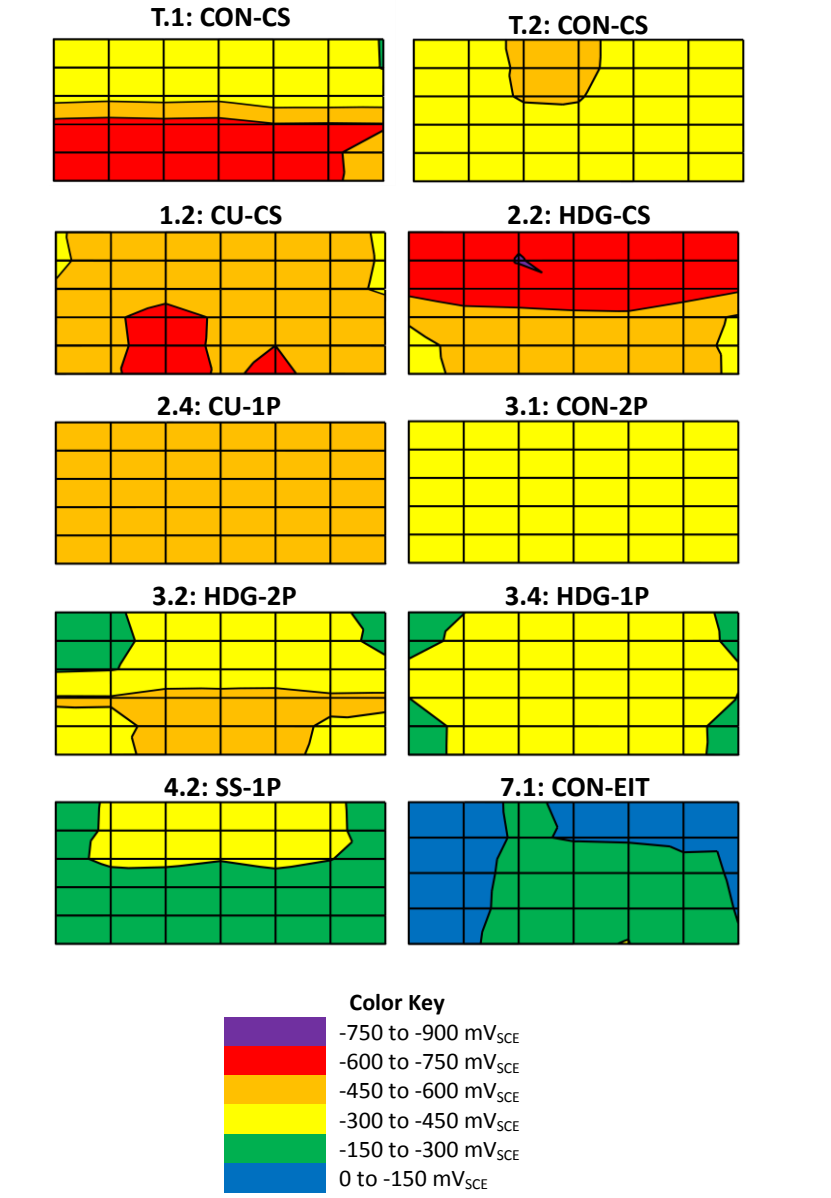

Figure 4.1: Final Half-Cell Reading Contour Maps

Spatially, there are some discernible patterns visible in the contour maps. For specimens T.1, 2.2, 3.2, and 4.2, the potentials were noticeably different between the north and south tendon

regions, implying that damage may have been more severe in one tendon. For other specimens, the difference was not as clear. Specimens 4.2 and 7.1 had the least negative readings overall, indicating that they had experienced less corrosion than the other specimens. In addition, it appears from nearly all the contour maps that potentials were least negative at the live and dead ends of the monitoring region. This may have occurred because the tendons are draped, making them slightly deeper within the specimen at the end regions. This is important because as depth to steel increases, so does the inaccuracy of the half-cell potential measurement[14]. The average final half-cell reading for each specimen is plotted in Figure 4.2.

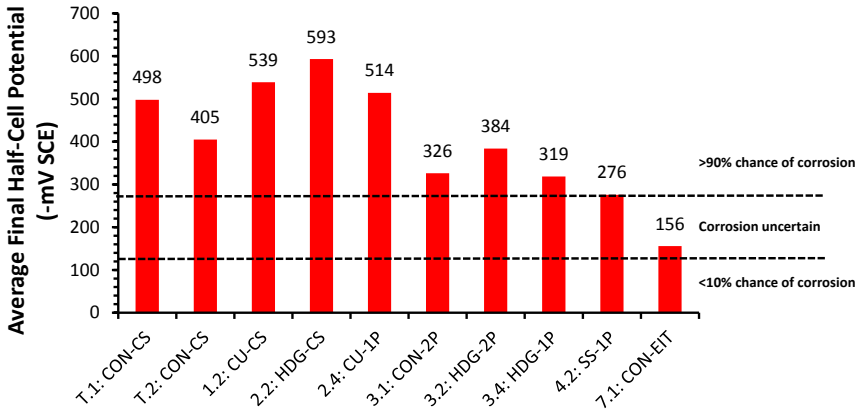

Figure 4.2: Average Final Half-Cell Readings

Specimen 2.2 had the most negative final average potential, while specimen 7.1 had the least negative potential. This probably indicates the effectiveness of the electrically isolated system used in specimen 7.1. Specimens with galvanized steel ducts had an average final half-cell potential of -509 mV_{SCE}, while those with plastic ducts had an average final potential of -329 mV_{SCE}. This suggests that specimens with plastic ducts had less corrosion at the time of autopsy. Average final potential for specimens with conventional strand was -346 mV_{SCE}, while the average for specimens with any other type of strand was -437 mV_{SCE}, indicating that the specimens with conventional strand were actually less corroded than the specimens with novel strand types at autopsy. This seems highly counterintuitive but can be explained. Averaging the final readings in this manner ignores the individual contributions of each element to corrosion. The higher potentials of the specimens with novel strand types may have occurred due to a higher

degree of corrosion in the specimens' reinforcing steel or ducts. Also, different types of strand are likely to corrode in ways which produce different potentials. Analysis of the final half-cell potentials alongside the results of the forensic analysis will shed more light on the corrosion within each specimen.

ASTM C876 defines threshold half-cell readings with respect to the copper-copper sulfate electrode which correspond to different probabilities of corrosion. These readings were converted to the saturated standard calomel electrode and are shown in Table 4.1[17]. Once again, it should be noted that these threshold potentials are truly valid only for non-prestressed concrete structures containing uncoated reinforcing steel.

Table 4.1: Probability of Corrosion by ASTM C876

Potential	Probability of Corrosion
More positive than -123 mV_{SCE}	Less than 10%
-123 to -273 mV_{SCE}	Uncertain
More negative than -273 mV_{SCE}	More than 90%

The maximum half-cell potentials from each monthly reading throughout the exposure period are plotted for every specimen in Figure 4.3. Superimposed on this plot are the probabilities of corrosion according to ASTM C876 as listed in Table 4.1.

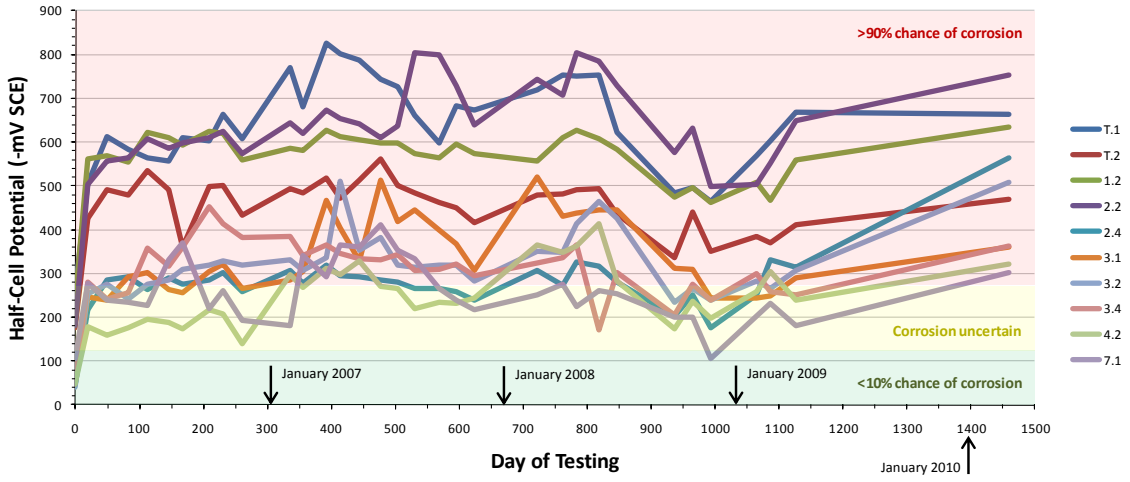

Figure 4.3: Maximum Monthly Half-Cell Potentials

From the plot of all maximum monthly readings, it appears that the most negative monthly potentials for most specimens were within the uncertain or greater than 90% probability of corrosion range for nearly the entire exposure period. Maximum readings increased quickly at the beginning of exposure, then appeared to fluctuate loosely around a mean value for each specimen. Potentials for many specimens became noticeably less negative between approximately 800 and 1000 days of exposure. Very negative but consistent potentials indicate that corrosion is electrochemically probable but limited by a lack of oxygen[14]. However, no specimen shows uniform readings over its entire life, suggesting that oxygen was never a limiting factor in corrosion for any specimen.

If the first maximum potential reading within the 90% probability of corrosion range is assumed to indicate the onset of corrosion, the approximate time of corrosion initiation can be estimated for each specimen. The estimated time to corrosion initiation for all specimens is shown in Figure 4.4.

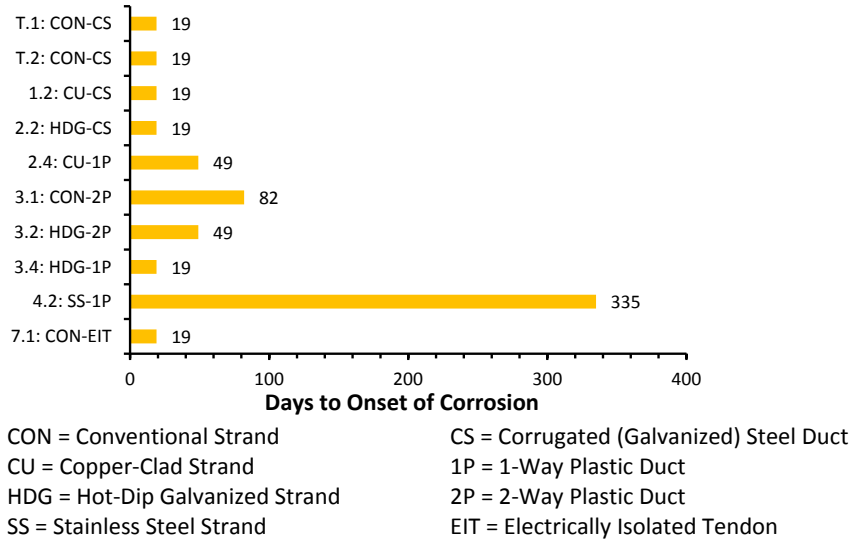

Figure 4.4: Estimated Time to Initiation of Corrosion

By this estimate, corrosion began almost immediately for most specimens; 19 days corresponds to the first half-cell reading after exposure began. The four specimens with galvanized steel ducts had a combined average time to corrosion initiation of 19 days, while the six specimens with plastic ducts averaged 92 days. This indicates that specimens with galvanized

ducts began to corrode before those with plastic ducts. Among the four specimens with conventional steel strand, the average time to corrosion was 35 days, compared to an average of 82 days for all other types of strand. The only marked difference was with Specimen 4.2, which contained stainless steel strand. Half-cell potential readings indicated that corrosion did not initiate in that specimen for nearly a year after exposure began. This indicates that stainless steel strand is much more corrosion-resistant than the other types studied in this phase of autopsies. Just as in the analysis of the average final half-cell readings, it should be noted that averaging the estimated time to corrosion in this manner ignores the individual contributions of each element to the total corrosion of the specimen. In Chapter 6, half-cell potentials are compared to the results of the forensic analysis. This will illustrate the accuracy of the half-cell method as it was implemented on this project.

In addition to using the half-cell method on prestressed specimens, error was introduced into the data in several ways. ASTM C876 contains exact specifications regarding the concentration of the wetting solution, the surface wetting procedure, the size of the porous medium, and electric potential temperature corrections[14]. There is no indication that these procedures were followed exactly throughout the duration of testing, nor can their exact effects be quantified due to the lack of detailed specimen maintenance records. In addition, several lapses in beam maintenance occurred throughout the four year exposure period due to graduate student turnover and miscommunications with FSEL staff. Half-cell readings were not taken during these periods, and the specimens were not kept on a consistent wet-dry cycle. Finally, readings were taken by several different parties throughout the exposure period. Because it is up to the researcher to wait for the half-cell voltage reading to stabilize at each measurement point, errors can occur if an inexperienced researcher does not know how long to wait for this to occur.

4.2 AC IMPEDANCE DATA AND ANALYSIS

Resistance, capacitance, and loss factor were measured each month on specimen 7.1. Outliers were omitted from the analysis at 462 and 494 days. Measured values at these times were several orders of magnitude larger or smaller than the rest of the data. Resistance and specific resistance are shown in Figure 4.5. Specific resistance is taken as the resistance multiplied by the length of the encapsulated tendon.

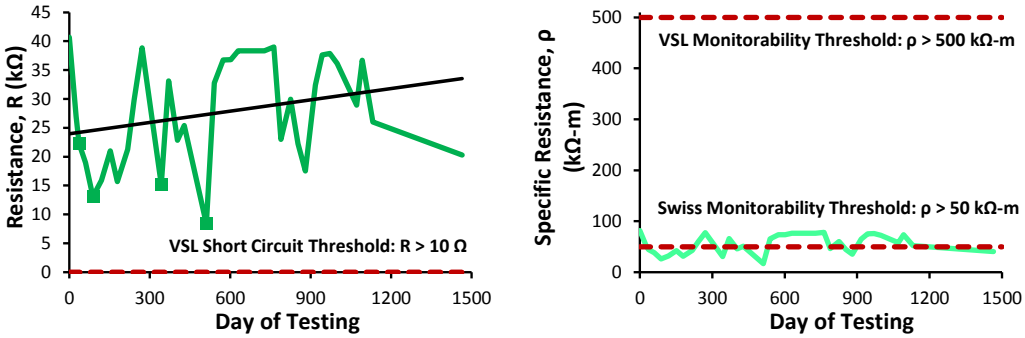

Figure 4.5: Resistance and Specific Resistance for Specimen 7.1

In general, the resistance increased throughout the test period, as shown by the trendline in Figure 4.5. This is normal behavior, as resistance tends to increase with age[4]. VSL defines the minimum resistance required to assure the absence of a short circuit to be 10 Ω. All resistance measurements easily exceed this value. Thus, it is reasonable to assume that no short circuit occurred between the tendon and reinforcing steel. VSL also defines a threshold specific resistance of 500 kΩ-m, below which a post-tensioning tendon is not considered monitorable in the long term[4]. All of the specific resistance values were well below this value, suggesting that the tendon is not suitable for accurate long-term monitoring. However, ASTRA (Swiss Federal Road Office) gives a much lower threshold for monitorability of 50 kΩ-m[18]. Approximately 60% of the specific resistance values for Specimen 7.1 were above this threshold. The Swiss standard is several years newer than that which was published in FIB Bulletin 33. The specific resistance threshold was reduced after field experience showed that 500 kΩ-m was nearly unattainable in the field[19]. Regardless of which standard is used, the monitorability of Specimen 7.1 is in question.

Low resistance values can indicate an electrolytic connection between tendon and concrete. A decrease in resistance of 30% or more indicates that moisture has entered the duct[4]. A decrease of this magnitude occurred four times throughout the life of Specimen 7.1. These points are marked with squares on the plot of resistance versus time (see Figure 4.5). While there was no direct electrical contact between tendon and reinforcement, a leak may have allowed chloride ingress at one or more points along the duct, causing the resistance to drop. However,

since resistance readings were not uniform over the life of the specimen, these four decreases could be merely scatter.

Capacitance and specific capacitance are shown in Figure 4.6. Specific capacitance is computed by dividing capacitance by the length of the encapsulated tendon.

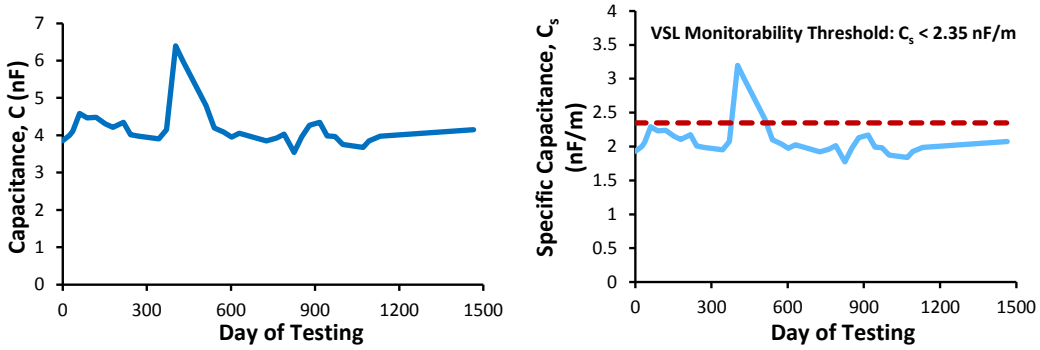

Figure 4.6: Capacitance and Specific Capacitance for Specimen 7.1

The VSL maximum specific capacitance for monitorability is 2.35 nF/m [4]. All but two measured values were below this threshold, indicating that the specimen is mostly monitorable. The Swiss document gives no guidelines for specific capacitance values.

The loss factor is plotted in Figure 4.7.

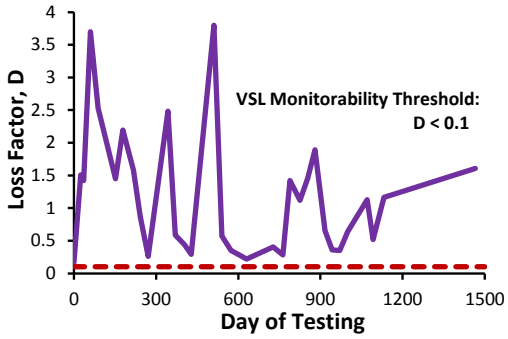

Figure 4.7: Loss Factor for Specimen 7.1

The VSL minimum threshold for the loss factor is 0.1 [4]. All measured values were greater than this, indicating that the tendon is not monitorable. The Swiss document does not mention loss factor values.

Analysis of AC impedance data for specimen 7.1 does not clearly establish its monitorability. It is certain that no short circuit occurred, and it is possible that chlorides entered the duct at some point during the life of the specimen. The extreme variation of the data is also problematic. In a truly encapsulated specimen, readings should vary little from month to month, even in a subtropical climate such as Austin. According to Dr. Hans-Rudolf Ganz, Chief Technical Officer at VSL International, the measuring device which was used does not fully comply with accepted standards for AC impedance measurement[20]. This issue will be addressed for the remaining electrically isolated specimens before the final round of autopsies begins in 2012.

4.3 CHLORIDE PENETRATION DATA AND ANALYSIS

Chloride samples were extracted from each specimen as described in Chapter 3. Grout chloride data and analyses are found in Chapter 5. The 0.033% by weight of concrete threshold for corrosion is taken from Salas' work on Project 0-1405[8]. Although the true threshold value may vary by cement content[3], 0.033% will be used for concrete and grout chloride analysis in this thesis to provide continuity from previous corrosion research at the University of Texas. The chloride contents for the top surface 2-inch offset are shown in Figure 4.8.

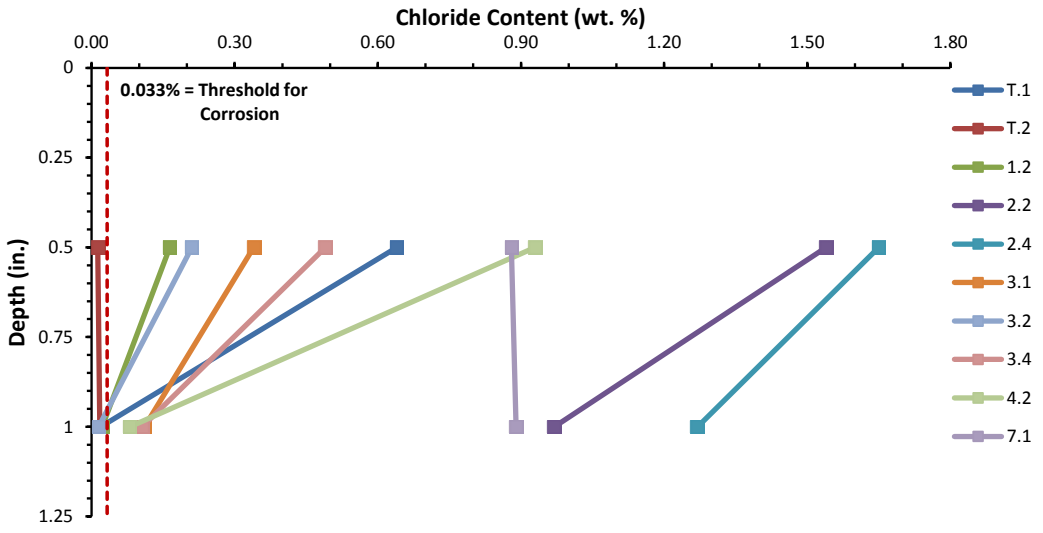

Figure 4.8: Specimen Chloride Content at Top Surface, 2-Inch Offset

Chloride content decreased with depth for all specimens except for Specimen 7.1. It is possible that the presence of additional indentations within that specimen's saltwater tray caused a chloride distribution in which concentrations were actually higher at 1 inch depth than at 0.5 inches. At a depth of 0.5 inches, chloride content was well above the corrosion threshold for every specimen except for T.2. At 1 inch depth, chloride content was above the threshold for six of the ten specimens.

The high level of chlorides within the top surface of the specimens may indicate one of two things. Either the concrete was relatively porous and allowed chlorides to permeate to a depth of at least one inch, or several samples were inadvertently extracted from a small crack. The former is certainly plausible. The surface of the specimens' saltwater trays generally appeared to be in poor condition upon autopsy, and the subsurface concrete condition could have been affected as well. The latter case is also possible, although care was taken to examine the drilling site prior to extraction to ensure that no visible cracks were present there. Had control blocks been cast alongside the post-tensioned specimens at the start of the project, there would be a better understanding of the transport of chlorides through the concrete.

Exposure procedures had not been strictly followed for at least one year prior to autopsy. This most certainly affected the chloride distribution in the concrete under the saltwater tray of each specimen. Regardless, the presence of large, deep cracks on the top of all specimens increases the probability of corrosion substantially. Because chlorides can travel so deep into the specimens through the cracks, their movement through the pore space of the concrete is expected to have a nearly negligible effect on corrosion.

Chloride contents for the anchorage regions of the dripper and non-dripper specimens are shown in separate plots in Figure 4.9. Note that on the dead end of the specimens, samples were extracted 5 inches from the top surface. On the live end, samples were extracted 6 inches from the top surface. For specimen 7.1, samples were extracted 6 inches from the top surface at both ends.

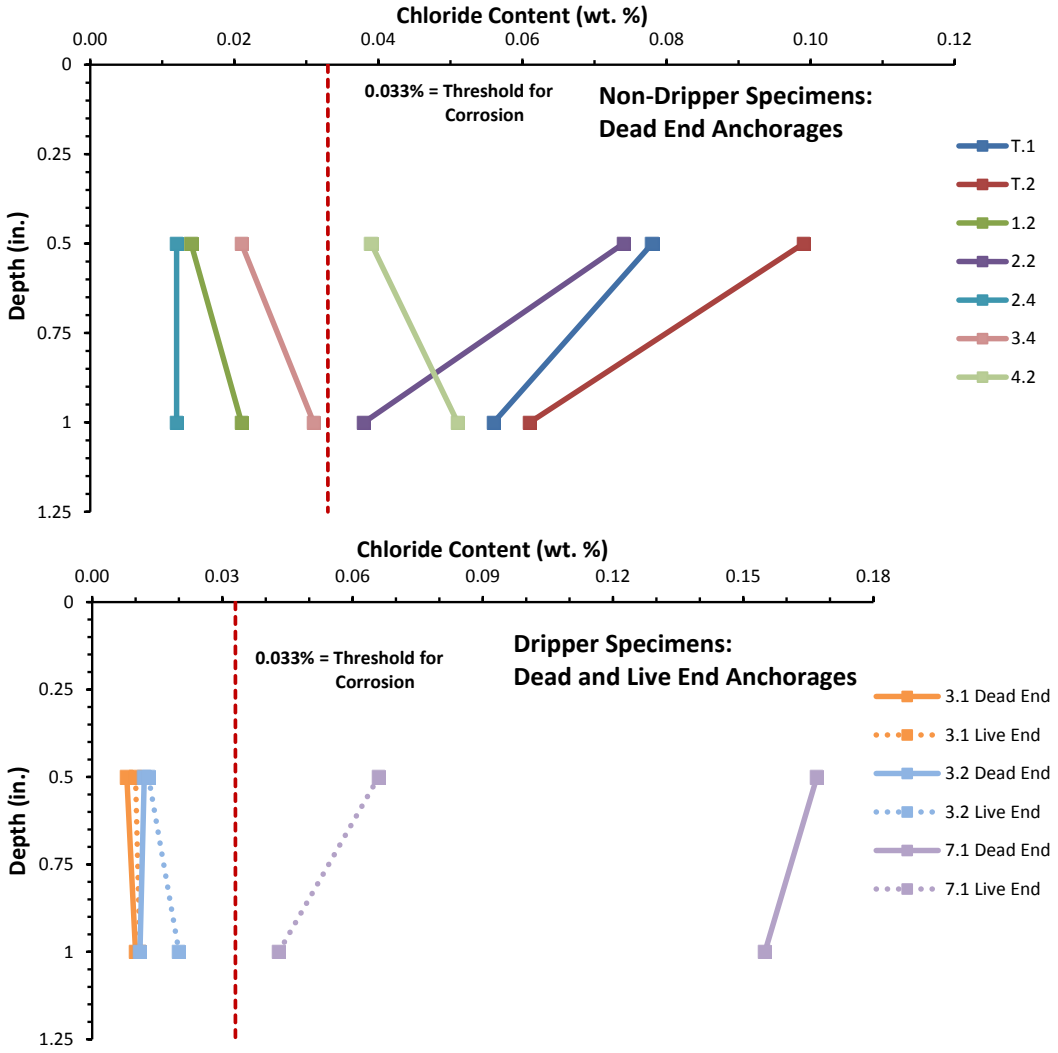

Figure 4.9: Specimen Chloride Content at Anchorages

Overall, concentrations were much lower at the dead end anchorages than at the top surfaces of the seven non-dripper specimens. Maximum chloride content for any non-dripper specimen was 1.65% (Specimen 2.4) at the top surface and 0.099% (Specimen T.2) at the dead end anchorage. Three of the seven non-dripper specimens showed chloride concentrations below the corrosion threshold at both depths. The other four specimens were above the threshold at both depths. In addition, chloride content only decreased with depth for three specimens.

Chloride content was below the corrosion threshold at the live and dead ends of dripper specimens 3.1 and 3.2. The concentrations also increased with depth at both ends for these

specimens. For Specimen 7.1, chloride content decreased with depth and was above the corrosion threshold at both ends. In addition, concentrations decreased with depth for this specimen. For the exposure specimens, anchorage region concentrations were much lower in magnitude than top surface concentrations.

For all specimens, the pourbacks were visually in much better condition upon autopsy than the saltwater trays. Therefore, concrete permeability should not have played a role in the unusual chloride distributions seen in Figure 4.9. Additionally, care was taken to avoid extracting a sample from a crack, thus negating the effects of accumulated chlorides within the pourback cracks. Anchorage chloride levels may have increased in the dead ends of all specimens and the live ends of the dripper specimens due to overflow which occurred when saltwater was flushed from the specimens' saltwater trays each month. It is important to note that there is a full order of magnitude difference between top surface chloride concentrations and the anchorage chloride concentrations. The strange distributions visible in Figure 4.9 could be partially caused by inaccuracies of the testing equipment at lower chloride contents. Regardless of the explanation, the accuracy of chloride concentrations as a predictor of internal corrosion will be examined in Chapter 6.

CHAPTER 5
Forensic Analysis

After the exposure period, ten saltwater exposure test specimens and one non-saltwater exposure control specimen were autopsied. First, the exterior of each specimen was thoroughly inspected for cracks, staining, and other signs of distress. Next, longitudinal bars, stirrups, ducts, and post-tensioning tendons were removed from the center of each specimen and inspected for signs of corrosion. Post-tensioning anchorages from the dead end of each specimen were removed and inspected, as well as from the live end of the three specimens which underwent anchorage saltwater exposure during the test period.

5.1 AUTOPSY PROCEDURE

5.1.1 Final Visual Examination

The exposed surfaces of each specimen were examined for surface defects, cracking, discoloration, efflorescence, and corrosion staining using the *Guide for Conducting a Visual Inspection of Concrete in Service*[21]. Each specimen was thoroughly photographed in its final condition. Next, surface cracks on each specimen's top surface were measured using a crack scope and crack comparator (see Figure 5.1). Cracks were highlighted with a marker for emphasis, then photographed from a vantage point approximately four feet above the midpoint of the specimen's top surface in order to facilitate the production of crack diagrams.

In order to compare the extent of cracking among specimens numerically, the crack rating was computed according to Equation 5-1, adapted from Salas[8]:

$$Crack\ Rating = \sum_{i=1}^{m} w_i^{avg} \times l_i \qquad \textbf{\textit{Equation 5-1}}$$

Where,

$w^{avg}{}_i$ = average crack width for crack i

l_i = crack length at end of testing period for crack i

m = number of longitudinal and transverse cracks within the main autopsy region

i = crack under consideration

Crack width data is presented for each autopsy specimen in Section 5.2 and analyzed in Chapter 6.

Figure 5.1: Crack Width Measurement Tools

5.1.2 Specimen Unloading

The project team attempted to remove the specimens' live load Dywidag bars using a hydraulic ram setup similar to that which was used to apply the live load. However, the extent of corrosion on the Dywidag hardware made this impossible, even after liberally applying thread lubricant to the seized components. Instead, live load was removed by cutting the Dywidag bars at midspan with an oxy-acetylene torch. In order to prevent damage from the explosive release of energy when the bars fractured, a large concrete block was placed at the live end of each Dywidag bar. The fractured Dywidag bars were discarded, and all other remaining components were placed in storage for later use.

5.1.3 Cutting of Beams

The main autopsy region consisted of a 42 inch long, 9 inch deep block, which was

removed from the top of each specimen using a 30" water-cooled concrete saw (see Figure 5.2). Additional blocks containing the anchorages were removed from the dead end of all specimens and from the live end of the three specimens which received dead end anchorage exposure. These blocks were approximately 15 inches long but varied in length by up to 4 inches due to the tendency of the concrete saw to deviate from a straight line while cutting. Additionally, the anchorage blocks for Specimen 7.1 were each 6 inches longer than the other specimens' due to their longer anchorage hardware. All cuts were centered on the specimen longitudinally and transversely, and the cut dimensions are shown in Figure 5.3. Cutting was done by the project team with assistance from FSEL lab technicians, who flipped the specimens with a forklift as needed to complete the cuts. Stacks of main autopsy region blocks are shown in Figure 5.4, and a partially chipped anchorage block is shown in Figure 5.5.

Figure 5.2: Sawcuts in Progress

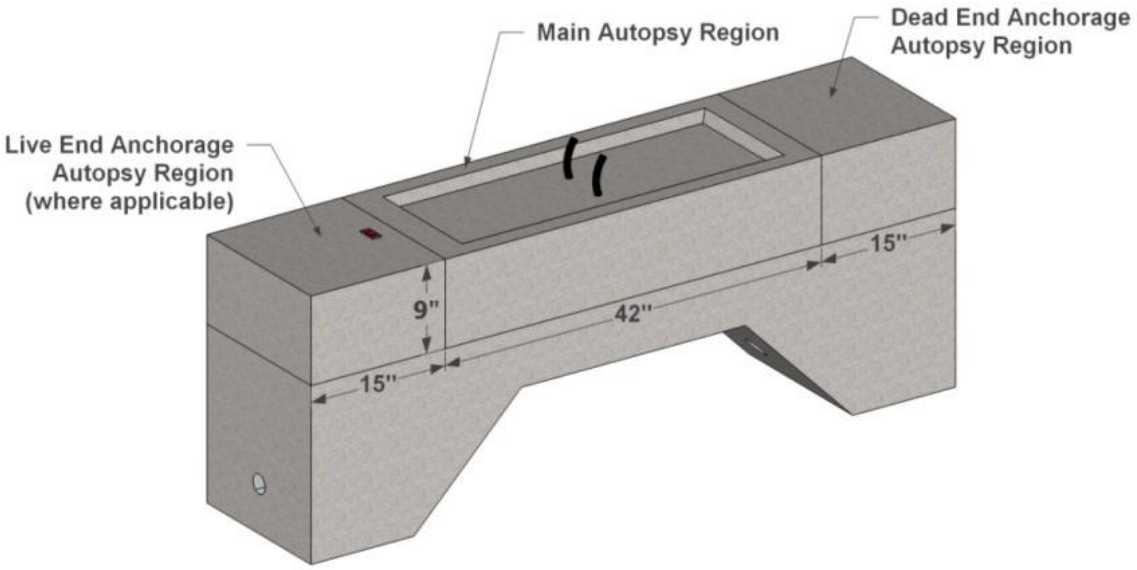

Figure 5.3: Cut Dimensions

Figure 5.4: Stacks of Main Autopsy Region Blocks

Figure 5.5: Partially Chipped Anchorage Block

The dimensions of the main autopsy region were chosen to be comparable to the ones used by Salas[8] and Turco[9] in the autopsies of TxDOT Project 0-1405 specimens. However, the length of the main autopsy region was shortened by 30 inches due to the new specimens' shorter overall length.

5.1.4 Removal of Reinforcing Elements

The mild steel elements and post-tensioning tendons were removed from the main autopsy region with a breaker and hammer drills (see Figure 5.6). Concrete was carefully chipped away in order to minimize damage to the components inside. The completely exposed reinforcement cage and tendons from Specimen 2.4 are shown in Figure 5.7. Once all concrete was chipped away, the components within each block were moved to an indoor clean room to prevent further corrosion. 42 inches of each tendon and longitudinal bar, as well as the top portion of seven stirrups were included in the main autopsy region.

Figure 5.6: Main Autopsy Block Chipping in Progress

Figure 5.7: Reinforcement Cage and Post-Tensioning Tendons from Specimen 2.4

5.1.5 Removal of Post-Tensioning Anchorages

Concrete was chipped away from the anchorage blocks using hammer drills. Care was taken to minimize damage to the anchorage components (see Figure 5.5). Bearing plates and

anchor heads were able to be removed intact for most specimens. However, a few had been damaged by the concrete saw during cutting (see Figure 5.8). The length of tendon removed with the anchorage blocks varied by specimen from 4 to 8 inches due to deviation of the concrete saw's path while cutting. Eighteen inches of tendon were removed from each anchorage block of Specimen 7.1. Immediately after chipping was complete, each set of anchorages was brought to an indoor clean room to prevent further corrosion.

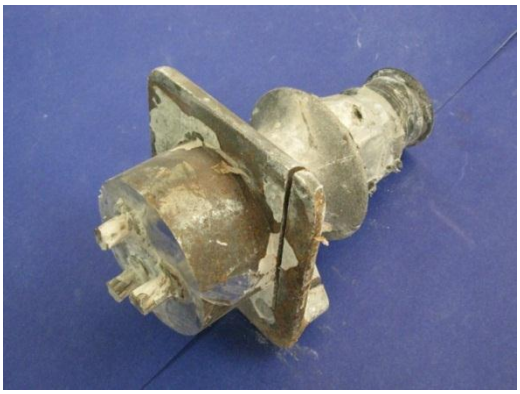

Figure 5.8: Dead End Anchorage from Specimen 4.2 Showing Saw Damage

5.1.6 Disassembly of Post-Tensioning Tendons

After both tendons had been removed from the main autopsy region block, an electric grinder was used to cut each duct in half longitudinally so that it could be separated from the grout inside (see Figure 5.9). Next, the grout was examined for the presence of cracks, staining, discoloration, and voids. Samples for chloride content analysis were extracted from the grout at 2-inch intervals over the regions in which substantial corrosion damage was observed on the surrounding duct. If no damage was observed, one sample was taken at midspan only. All grout was then cleared from the strands. Strands were examined. A screwdriver was used to pry each strand apart so that its interstices could be inspected (see Figure 5.10).

Procedures for the anchorage block tendons were identical. However, no chloride samples were taken from the anchorage zone ducts. In order to disassemble the anchorages, each anchorage was cut in half with an oxy-acetylene torch. The ducts were cut with an electric grinder and removed. Then, grout was carefully chipped away from the strands. Finally, the anchor heads were heated until the strands and wedges were able to be loosened and removed.

Figure 5.9: Removing Ducts Using Electric Grinder

Figure 5.10: Using Screwdriver to Unravel Strand

5.1.7 Element Rating System

A numerical rating system was used to evaluate and compare corrosion damage among the metal components inside each specimen. This system was developed by West[10] during his work on TxDOT Project 0-1405 and has been used by every other researcher assigned to that project since. West's system had no provisions for plastic ducts. As a result, the rating scale for galvanized steel duct was modified by the author to account for the different type of damage that plastic ducts experience.

Epoxy-Coated Steel Rating System

The top and bottom of each longitudinal bar were divided into 21 2-inch intervals. The inside and outside of the stirrups were divided into 6 2-inch intervals on the horizontal region and 2 3-inch intervals on each of their legs. The interval layout for longitudinal bars and stirrups is shown in Figure 5.11.

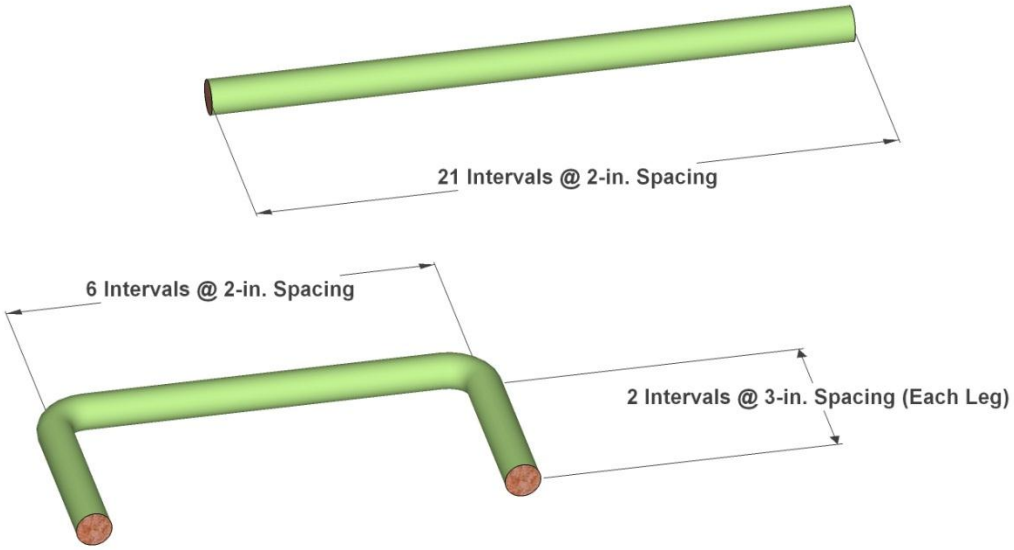

Figure 5.11: Interval Layout for Longitudinal Bars and Stirrups

The numerical rating system used to evaluate each interval of the epoxy-coated steel components is shown in Table 5.1. It should be noted that none of the specimens from earlier project 0-1405 were constructed with epoxy-coated bars. Nevertheless, West's rating system will be useful to compare corrosion damage to the epoxy-coated components among the project specimens.

Table 5.1: Numerical Rating System for Epoxy-Coated Steel Bars

Code	Meaning	Description	Rating
NC	No Corrosion	No evidence of corrosion.	0
D	Discoloration	No evidence of corrosion, but some discoloration from original color.	1
L	Light	Surface corrosion on **less** than one half of the interval, no pitting is present. Surface corrosion can be removed using a cleaning pad.	2
M	Moderate	Surface corrosion on **more** than one half of the interval, no pitting. **and/or** Any corrosion which cannot be completely removed using cleaning pad.	4
P	Pitting	Pit visible to the unaided eye.	8
AR	Area Reduction	Measurable reduction in bar cross-sectional area due to corrosion.	R^2

R = Estimated bar cross-sectional area reduction in percent.

A 3M Scotchbrite™ cleaning pad was used to determine whether the interval received a rating of L or M. When applicable, the pad was scrubbed on the component of interest with the amount of pressure used to scrub dirty pots and pans. Area loss was measured using a micrometer, then converted to percent of total cross-sectional area. The highest possible rating for an epoxy-coated steel component in one interval is 10,000, which would indicate loss of the entire section in that interval. The rating for a longitudinal bar is given by Equation 5-2:

$$R_{bar} = \sum_{i=1}^{21}\left(R_{top,i} + R_{bottom,i}\right) \qquad \textbf{\textit{Equation 5-2}}$$

The total rating for both longitudinal bars is given by Equation 5-3:

$$R_{total} = \sum_{n=1}^{2} R_{bar,n} \qquad \textbf{\textit{Equation 5-3}}$$

Where,

$R_{top,i}$ = corrosion rating on top bar surface, interval i

$R_{bottom,i}$ = corrosion rating on bottom bar surface, interval i

$R_{bar,n}$ = total bar corrosion rating, bar n

i = interval, 1 to 21

n = bar number, 1 to 2

For Specimen 7.1, n = 4 because it was constructed with two additional longitudinal bars. In order to compare longitudinal bar corrosion ratings among specimens, Equation 5-4 gives a generalized corrosion rating in units of average rating per foot of bar:

$$R_{gen,bar} = \frac{R_{total}}{2 \times 3.5} \qquad \textbf{\textit{Equation 5-4}}$$

Where 3.5 is the total length of each bar in feet.

The total rating for an individual stirrup is given by Equation 5-5:

$$R_{stirrup} = \sum_{i=1}^{10} \left(R_{top,i} + R_{bottom,i}\right) \qquad \textbf{\textit{Equation 5-5}}$$

The total rating for all seven stirrups in the specimen is given by Equation 5-6:

$$R_{total} = \sum_{n=1}^{7} R_{stirrup,n} \qquad \textbf{\textit{Equation 5-6}}$$

Where,

$R_{top,i}$ = corrosion rating on top bar surface, interval i

$R_{bottom,i}$ = corrosion rating on bottom bar surface, interval i

$R_{stirrup,n}$ = total bar corrosion rating, bar n

i = interval, 1 to 10

n = stirrup number, 1 to 7

In order to compare stirrup corrosion among specimens, Equation 5-7 gives the generalized stirrup corrosion rating:

$$R_{gen,stirrup} = \frac{R_{total}}{7 \times 2} \qquad \textbf{\textit{Equation 5-7}}$$

Where 2 is the total length of each stirrup in feet.

Galvanized Duct Rating System

Like the longitudinal bars, the galvanized ducts were divided into 21 2-inch intervals. The top and bottom halves of the duct were evaluated separately at each interval on both the inside and outside surfaces. The interval layout for the galvanized ducts is shown in Figure 5.12.

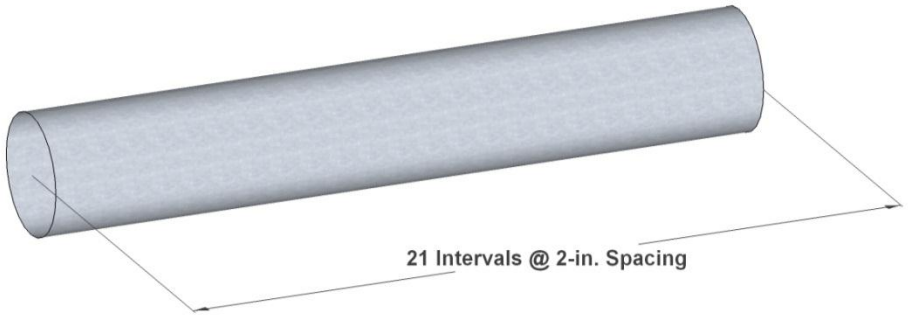

Figure 5.12: Interval Layout for Galvanized and Plastic Ducts

The length of galvanized duct removed from the anchorages was also rated using this system with the appropriate number of 2-inch intervals. The numerical rating system used to evaluate each interval of the galvanized duct is shown in Table 5.2.

Table 5.2: Numerical Rating System for Galvanized Duct

Code	Meaning	Description	Rating
NC	No Corrosion	No evidence of corrosion.	0
D	Discoloration	No evidence of corrosion, but some discoloration from original color.	1
L	Light	Surface corrosion on **less** than one half of the interval, no pitting is present.	2
M	Moderate	Surface corrosion on **more** than one half of the interval, no pitting.	4
P	Pitting	Pit visible to the unaided eye.	8
H	Hole Through Duct	Hole corroded through duct. Used in conjunction with ratings D, L, M, and S.	$32 + A_h$

A_h =Estimated area of hole(s) in mm^2.

Duct hole dimensions were measured with a micrometer. The highest possible corrosion rating for the galvanized duct in one interval would be 8,139, indicating that the entire duct is corroded away over the entire interval. The rating for the entire duct is given by Equation 5-8:

$$R_{total} = \sum_{i=1}^{21}\left(R_{top,outer,i} + R_{bottom,outer,i} + R_{top,inner,i} + R_{bottom,inner,i}\right)$$

Equation 5-8

Where,

$R_{top,outer,i}$ = top outer surface corrosion rating, interval i

$R_{bottom,outer,i}$ = bottom outer surface corrosion rating, interval i

$R_{top,inner,i}$ = top inner surface corrosion rating, interval i

$R_{bottom,inner,i}$ = bottom inner surface corrosion rating, interval i

i = interval, 1 to 21 for main autopsy region, 1 to 3 or 4 for anchorages

Each duct is given a separate generalized corrosion rating to facilitate comparison among ducts. The generalized rating is given by Equation 5-9:

$$R_{gen,duct} = \frac{R_{total}}{3.5}$$

Equation 5-9

Where 3.5 is the length of each duct in the main autopsy region in feet. Generalized anchorage zone duct corrosion ratings are calculated for each specimen according to their length.

Plastic Duct Rating System

Like the galvanized duct, plastic duct was divided into 21 2-inch intervals and evaluated on the top and bottom of both the inside and outside surfaces of each interval. The interval layout for plastic ducts is identical to that of the galvanized ducts and is shown in Figure 5.12.

The lengths of plastic duct removed from the anchorage regions was also evaluated using this system with the appropriate number of intervals. Because plastic ducts do not corrode, the numerical system developed for them has fewer damage classifications. The numerical rating system used to evaluate each interval of plastic duct is shown in Table 5.3.

Duct hole dimensions and gouge/scratch depths were measured with a micrometer. The highest possible damage rating for the plastic duct in one interval varies by duct diameter, ranging from 9,436 to 13,612. This corresponds to the entire duct being absent over the entire interval. The damage rating and generalized damage rating for an entire duct are given by Equations 5-8 and 5-9, respectively.

Table 5.3: Numerical Rating System for Plastic Duct

Code	Meaning	Description	Rating
ND	No Damage	No evidence of damage.	0
G	Gouging/Scratching	Gouges or scratches are present on the duct walls.	R^2
H	Hole Through Duct	Hole present in duct. Used in conjunction with ratings ND and G.	$32 + A_h$

R = Estimated reduction in wall thickness in percent.
A_h =Estimated area of hole(s) in mm^2.

Prestressing Strand Rating System

The strand was divided into 21 2-inch intervals. All six outer wires and the inner wire of each strand were evaluated separately for each interval. The anchorage zone strand was also evaluated by this system with the appropriate number of intervals. The numerical rating system used to evaluate the prestressing strand is shown in Table 5.4. It should be noted that this system does not take metal type into account. As such, direct comparisons among different strand types are not possible.

Table 5.4: Numerical Rating System for Prestressing Strand

Code	Meaning	Description	Rating
NC	No Corrosion	No evidence of corrosion.	0
D	Discoloration	No evidence of corrosion, but some discoloration from original color.	1
L	Light	Surface corrosion on **less** than one half of the interval, no pitting is present. Surface corrosion can be removed using a cleaning pad.	2
M	Moderate	Surface corrosion on **more** than one half of the interval, no pitting. **and/or** Any corrosion which cannot be completely removed using cleaning pad.	4
P1	Mild Pitting	Broad, shallow pits with a maximum depth not greater than 0.02 inches.	8
P2	Moderate Pitting	Pitting where the maximum depth ranges between 0.02 and 0.04 inches.	16
P3	Severe Pitting	Pitting where the maximum pit depth is greater than 0.04 inches.	32

The cleaning pad used to distinguish between light and moderate corrosion is the same as that used on the epoxy-coated steel components, applied with similar effort. Pit depth was measured with a micrometer. The three levels of pitting classification were established by Salas for Project 0-1405[8]. The highest possible rating for any one interval of strand is 224. This would indicate that severe pitting was found on every wire of the strand in that interval. The corrosion rating for an individual strand is given by Equation 5-10:

$$R_{strand} = \sum_{i=1}^{21}\left(R_{outer,i} + n_i \times R_{inner,i}\right) \qquad \textbf{\textit{Equation 5-10}}$$

The total corrosion rating for all strands in one duct is given by Equation 5-11:

$$R_{total} = \sum_{n=1}^{3} R_{strand,n} \qquad \textbf{\textit{Equation 5-11}}$$

Where,

$R_{outer,i}$ = corrosion rating on outer wires, interval i

n_i = number of corroded outer wires in interval i

$R_{inner,i}$ = corrosion rating on inner wire, interval i

n = strand number, 1 to 3

i = interval, 1 to 21 for main autopsy region

To allow strand corrosion ratings to be compared between ducts and among specimens, Equation 5-12 gives the generalized strand corrosion rating in units of rating per foot of strand:

$$R_{gen,strand} = \frac{R_{total}}{3\times3.5} \qquad \textbf{\textit{Equation 5-12}}$$

Where 3.5 is the length of each strand in feet.

5.2 RESULTS OF FORENSIC ANALYSIS

The results of the forensic analysis are presented in this section for each specimen. All longitudinal elements within the main autopsy region are pictured with a measuring tape (e.g. bars, ducts, strand). The distance on the tape corresponds to the distance from the live end of the element pictured. For elements within the live or dead end anchorage zones, the measuring tape corresponds to the distance from the end of the element closest to the outside end of the specimen. For all specimens, elements within the main autopsy region are identified as shown in Figure 5.13. Elements within the anchorage zone are identified using the same "north/south" designation according to whether they came from the live end anchorage or the dead end anchorage. All corrosion/damage rating plots in this chapter are shown with the live end to the left for the main autopsy region and with the outside end to the left for the anchorage regions. All main autopsy region crack maps are shown with the live end to the left and the north end to the top of the page.

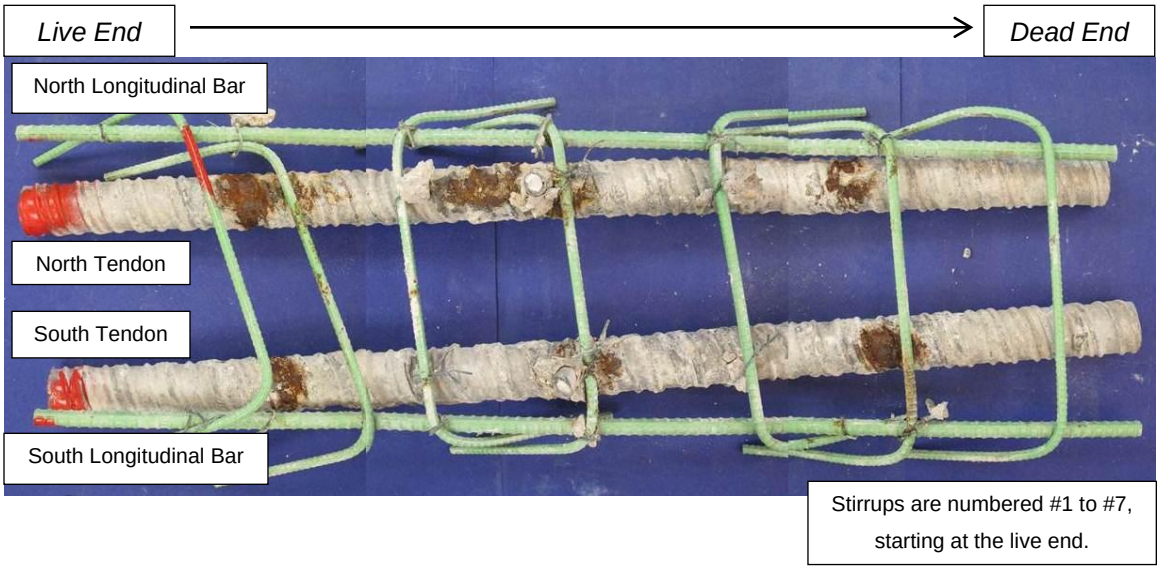

Figure 5.13: Forensic Analysis Element Naming Conventions

In order to facilitate comparison to the autopsy data from Project 0-1405, all plots in this section were formatted in a similar manner to those generated by Salas[8] and Turco[9].

5.2.1 Specimen T.1: Galvanized Duct, Conventional Strand

Figure 5.14: Specimen T.1 Overall (Right) and Grout Vents (Left)

Table 5.5: Specimen T.1 Corrosion Rating Summary

Component	Maximum	Total	Generalized
Longitudinal Bars	3	19	3
Stirrups	27	169	12
North Duct	1267	1680	480
South Duct	1580	3800	1086
North Strands	11	190	12
South Strands	18	288	27

This specimen was the first of two trial specimens which were cast prior to the others so that the project team could practice their construction methods. It did not receive anchorage exposure during the testing period.

5.2.1.1 Appearance

The exposed surfaces of the concrete showed some moderate scaling. Large aggregate was visible at many locations, especially along the specimen's edges. The surface of the saltwater tray had many shallow air voids which had developed during casting. Two approximately 6-inch-diameter hardened grout puddles were present around the vents, indicating overflow during the grouting process. A small amount of staining was visible around the base of the north grout vent, suggesting the presence of corrosion inside the specimen. This is shown in Figure 5.14.

The specimen had two large transverse cracks running across its top face, each with an average width of 0.03 inches. These cracks extended down the north and south faces of the specimen. The epoxy used to seal the cracks on these faces was intact. There was one longitudinal crack with an average width of 0.004 inches running perpendicular from the north grout vent to the transverse crack near the live end of the specimen. A large crack had formed at the re-entrant corner of the dead end corbel during live load application[7]. This crack had been sealed with non-shrink mortar which appeared intact during inspection. The dead end anchorage pocket pourback showed significant separation from the surrounding concrete at its construction joint. In addition, the entire dead end and top surfaces of this pourback displayed moderate pattern cracking, suggesting that some shrinkage occurred after the mortar was placed. Crack width data is shown in Figure 5.15, and the crack diagram is shown in Figure 5.18.

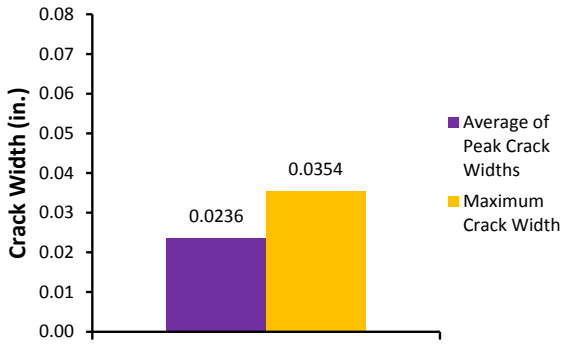

Figure 5.15: Specimen T.1 Crack Data

5.2.1.2 Longitudinal Bars and Stirrups

Both longitudinal bars were only lightly damaged, as shown in Figure 5.17. Discoloration was present at several spots along the top side of both bars, mostly coinciding with the locations where the stirrups were tied. The south bar showed more damage than the north bar. The south bar showed very light surface corrosion near midspan in addition to localized discoloration at other points. Longitudinal bar corrosion ratings are shown in Figure 5.18 and summarized in Table 5.5.

The stirrups showed more damage than the longitudinal bars. Six stirrups had corrosion which could not be completely scoured away along at least one interval, as pictured in Figure

5.17. Discoloration and light corrosion tended to occur on the underside of the stirrups near the locations where the ducts were tied, as well as on the outer side along their bends. Corrosion ratings were highest for stirrups #2 and #4, which were located underneath the two large transverse cracks. The stirrups near the dead end, where no cracking was found, were in much better condition. Stirrup #4 showed the worst damage with approximately 5% area loss at the location where the north duct was tied to it and moderate corrosion and pitting where the south duct was tied. Stirrup corrosion ratings are shown in Figure 5.18 and summarized in Table 5.5.

5.2.1.3 Ducts

The north and south ducts both had localized severe corrosion damage. Most damage on the north duct occurred at midspan and at the live end quarter point. At these locations, the outside of the duct experienced severe pitting as well as some area loss on top of the duct only. This is shown in Figure 5.17. Pitting and corrosion were more extensive on the inside of the duct, extending nearly the full length of the duct on its top inside surface. The shape and extent of the damage indicate the presence of small grout voids along the top of the entire duct. Significant corrosion and pitting also extended along the bottom inside surface. Here, the location of damage suggests that voids may have formed under the strands during grouting (see Figure 5.16). The inner surface of the duct also showed discoloration along its entire length, especially where the strands had rubbed against it.

Figure 5.16: Specimen T.1, Corrosion Along Gouges on Bottom Half of North Duct

Damage was somewhat more extensive in the south duct. Moderate to severe area loss occurred on the top of the duct at midspan, and much smaller holes were found on top of the duct near the dead end quarter point. These holes tended to form inside the helical flutes of the duct, as seen in Figure 5.17. Most of the outer dead end half of the duct had moderate corrosion and pitting, both top and bottom. Significant corrosion and pitting were found on the top of the inside of the duct along this region, as well. The bottom inside of the duct showed localized corrosion near the locations where the strands had been bearing on the duct wall as well as discoloration along its entire length. Small holes in the duct flutes were present at many of these locations. Overall, damage to both ducts was most severe near midspan. Duct corrosion ratings are shown in Figure 5.18 and summarized in Table 5.5.

5.2.1.4 Grout

The north tendon grout had very few discernible transverse cracks and no longitudinal cracks. Corrosion staining could be seen near midspan and the live end quarter point, coinciding with the corrosion observed in the duct at those locations. Orange-yellow staining was also visible at seemingly random points along the grout. Small, elliptical, uniformly-sized voids approximately 0.75 inches in width were found along nearly the entire length of grout. These voids formed in and around the uppermost flutes of the duct, as shown in Figure 5.17. Chloride content varied little within the north duct grout. Maximum chloride content was 0.085% at midspan, well above the corrosion threshold.

The south duct grout also had very few discernible transverse cracks and no longitudinal cracks. Corrosion staining was present near the grout vent at midspan and at both quarter points. Faint, yellow-colored staining was found in patches over nearly the entire length of grout. Voids, approximately 1 inch in width, and continuous bubbling were found on the top side of the grout. These occurred mostly within flutes of the duct, over most of the duct's length. The largest void occurred just towards the dead end from midspan (see Figure 5.17). This void was approximately 1.5 inches across and continuous across several duct flutes. Chloride content was 0.083% at 25 inches from the live end and 0.058% at both 10 inches and 33 inches. Chloride content for grout in both tendons is shown in Figure 5.18.

While chloride concentrations were above the corrosion threshold at every measurement point in both tendons, the measurements were relatively uniform. This suggests that chlorides

passed down through the cracks to duct level at the same rate, and that corrosion initiated at approximately the same time across the duct. There was no area loss in the north duct at 9 inches from the live end. However, chloride content was above the corrosion threshold at this location. This suggests that chlorides entered the duct through the area loss at midspan and traveled along the duct either through the top voids in the grout or through the interstices of the strands. Either scenario is possible, although the small number of cracks in the grout suggest that the chlorides traveled through the voids.

5.2.1.5 Strand

The three strands in the north tendon suffered only minor damage. Discoloration was present on some of the outer wires on many intervals, and just a few intervals experienced small flecks of light corrosion. The inner wires were more damaged, with light corrosion present on nearly all intervals. Corrosion ratings were uniform over the entire tendon, and all corrosion could be removed with a scouring pad.

The strands in the south tendon were somewhat more severely affected. On the outer wires, discoloration and light corrosion were present on many intervals. Corrosion which could not be scoured off occurred at a few points along each strand. The inner wires had light corrosion spots on almost all intervals. Corrosion ratings were mostly uniform over the entire tendon, although strand corrosion ratings were higher for the south tendon than for the north. A typical strand and inner wire are shown in Figure 5.17. Strand corrosion ratings are shown in Figure 5.18 and are summarized in Table 5.5.

Longitudinal Bar

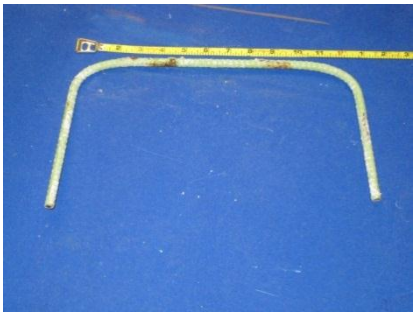

Stirrup

Top of North Duct

Top of South Duct

North Grout

South Grout

Strand

Inner Wire

Figure 5.17: Specimen T.1 Main Autopsy Region Elements

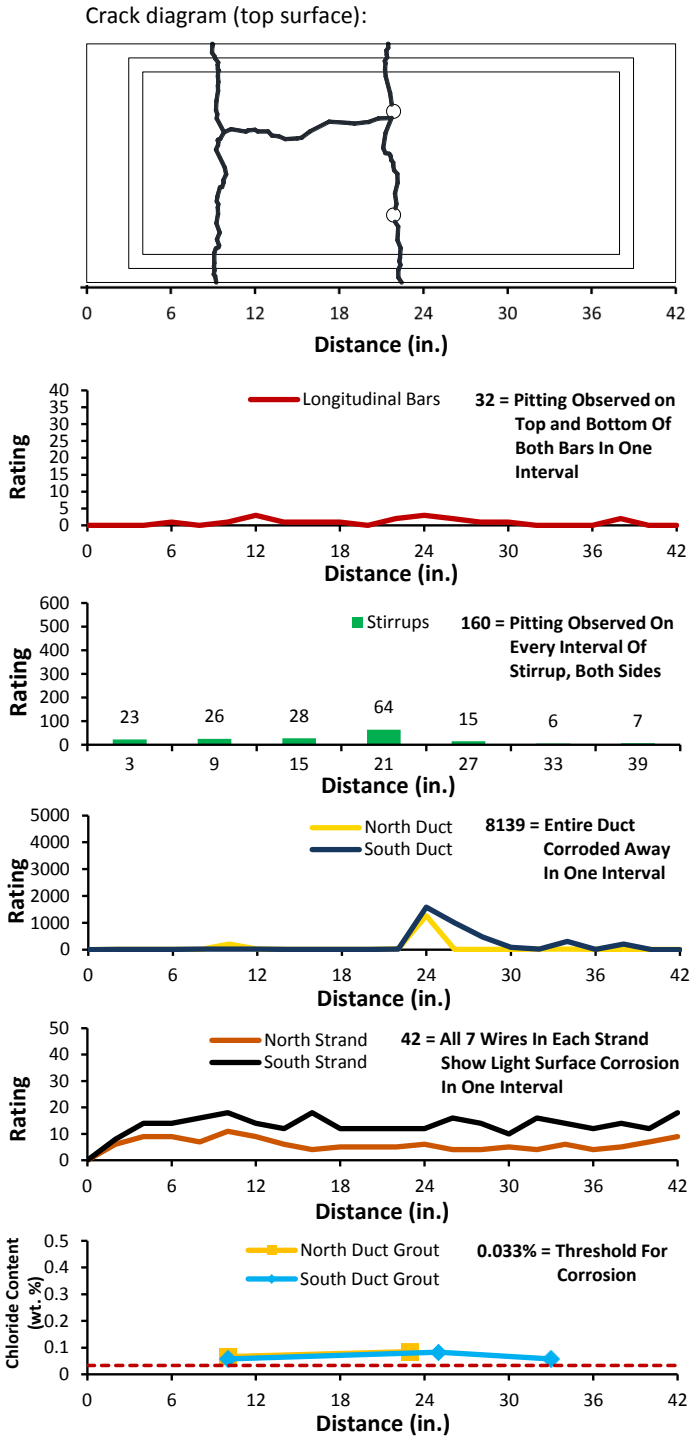

Figure 5.18: Specimen T.1 Crack Map and Corrosion Rating Plots

5.2.1.6 Dead End Anchorages

The epoxy applied to the anchorages prior to the pourback was mostly intact upon autopsy. North and south bearing plates and anchor heads had widespread light corrosion and discoloration on all epoxied surfaces. The outer surfaces of the bearing plates were mostly corrosion-free. Some light to moderate corrosion occurred on the edges and undersides of both bearing plates. The duct tape used to seal the bearing plate-duct connection was intact on both anchorages. Extensive surface corrosion was found on the surfaces covered by the duct tape. Upon removal, the anchor heads were completely intact but had widespread discoloration and some localized corrosion spots. The north and south anchorages and anchor heads are shown in Figure 5.19.

North Anchorage

South Anchorage

North Anchor Head

South Anchor Head

Figure 5.19: Specimen T.1 Anchorages and Anchor Heads

Table 5.6: Specimen T.1 Anchorage Corrosion Rating Summary

Component	Maximum	Total	Generalized
North Duct	13	35	53
South Duct	6	17	26
North Strands	38	107	36
South Strands	25	94	31

Both north and south anchorage zone ducts experienced pitting and corrosion near their splice zone, where they had been wrapped in duct tape. Some localized corrosion and discoloration were found elsewhere on the ducts' outer surfaces. Inside, the ducts were widely discolored, and some pitting and corrosion were found in the uppermost flutes of the ducts. This damage seemed to coincide with the locations of voids. North and south anchorage zone ducts are shown in Figure 5.21. Corrosion ratings for the anchorage zone ducts are shown in Figure 5.20 and are summarized in Table 5.6.

The north grout broke apart during removal. It was impossible to discern the extent of its cracking. Many small, yellowish flecks were found on the outer surface of the grout. Small, elliptical, bubble-filled voids were found on the top surface of both the north and south grout, corroborating the evidence of voids found inside the north and south ducts. The south grout showed no signs of corrosion on its outer surface. Moderate segregation occurred over the length of the anchorage zone. The grout was a light gray color near the anchorage itself and became darker moving into the specimen. North and south tendon grouts are shown in Figure 5.21.

The strands in both the north and south tendons experienced light localized corrosion and discoloration scattered across their lengths. As with the main specimen tendons, the center wire of all strands was slightly more damaged than the outer wires. Damage to both sets of strands was most severe at the ends which were outside the anchor head. One strand in each duct experienced moderate corrosion on several wires in its outermost interval. All wedges were substantially intact with only light localized corrosion. The appearance of a typical strand, with and without wedges, is shown in Figure 5.21. Corrosion ratings for the anchorage zone strands are shown in Figure 5.20 and are summarized in Table 5.6.

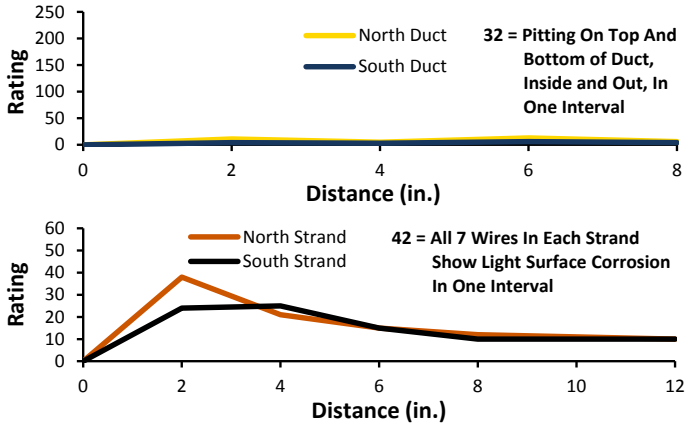

Figure 5.20: Specimen T.1 Anchorage Corrosion Rating Plots

Top of North Duct

Top of South Duct

North Grout

South Grout

Strands with Wedges

Strand

Inner Wire

Figure 5.21: Specimen T.1 Anchorage Region Elements

5.2.2 Specimen T.2: Galvanized Duct, Conventional Strand, Galvanized Bearing Plates

Figure 5.22: Specimen T.2 Overall (Left) and Grout Vents (Right)

Table 5.7: Specimen T.2 Corrosion Rating Summary

Component	Maximum	Total	Generalized
Longitudinal Bars	8	50	7
Stirrups	10	120	9
North Duct	4966	38318	10948
South Duct	1747	2256	645
North Strands	29	286	27
South Strands	29	395	38

This specimen was the second of two trial specimens which were cast prior to the others so that the project team could practice their construction methods. It did not receive anchorage exposure during the testing period.

5.2.2.1 Appearance

This specimen showed light to moderate scaling on many of its exposed surfaces, mostly on the top face and the upper north and south faces. The saltwater tray had many small surface air voids, some of which were more than ¼ inch deep. Two approximately 4 inch diameter grout puddles were present in the saltwater tray: one around each grout vent. This indicated overflow which had occurred during grouting. Extremely faint discoloration was found at the base of the north grout vent, suggesting the presence of corrosion inside the specimen there. The exterior of the specimen is shown in Figure 5.22.

The specimen had two large transverse cracks running along its top face and down its north and south faces, each with an average width of 0.03 inches. The epoxy used to seal the vertical portions of these cracks to prevent leakage was intact. The transverse crack nearest to the dead end was not continuous across the specimen. One discontinuous longitudinal crack was present approximately 6 inches from the south face of the specimen. Its maximum width was 0.01 inches. This crack was not continuous. It was not visible within about six inches of the south grout vent. Similar to specimen T.1, a large crack had formed at the re-entrant corner of the dead end corbel during live load application[7]. This crack had been sealed with non-shrink mortar, which was still intact at the time of autopsy. The dead end anchorage pourback showed significant separation as well as some delamination near its interface with the rest of the specimen. This is shown in Figure 5.23. In addition, pattern cracking was found on the top and dead end surfaces of the pourback. This suggests the action of plastic shrinkage during the life of the specimen. Crack width data is shown in Figure 5.24, and the crack diagram is shown in Figure 5.28.

Figure 5.23: Specimen T.2, Separation and Delamination Around Dead End Pourback

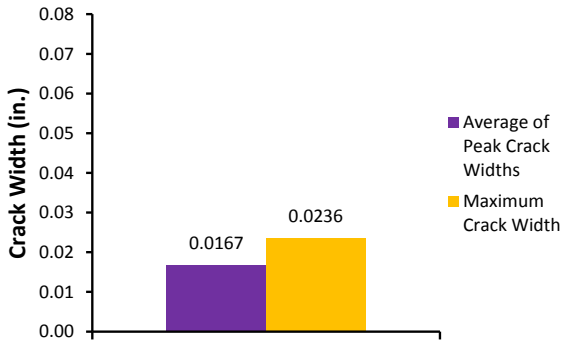

Figure 5.24: Specimen T.2 Crack Data

5.2.2.2 Longitudinal Bars and Stirrups

Both longitudinal bars were only slightly damaged, showing light localized corrosion and discoloration. All corrosion on both bars could be scrubbed away with a scouring pad. Most of the damage on both bars occurred at the locations where the stirrups were tied, and damage was the most severe near midspan. The south bar was more corroded than the north bar, but only marginally. The highest corrosion ratings coincided with the location of the transverse crack nearest to the live end. Typical longitudinal bar corrosion damage is shown in Figure 5.27. Longitudinal bar corrosion ratings are shown in Figure 5.28 and summarized in Table 5.7.

Damage to the stirrups was light to moderate. For five of the seven stirrups, all corrosion could be removed with a scouring pad. Most stirrups showed some discoloration and light corrosion at their bends and at the locations where the ducts were tied. Stirrup #4 was most damaged. It had pitting at two tie points on its outer surface. In general, corrosion ratings were highest for stirrups near midspan and lowest for those at the ends of the autopsy region. A typical stirrup is pictured in Figure 5.27. Stirrup corrosion ratings are shown in Figure 5.28 and summarized in Table 5.7.

5.2.2.3 Ducts

Both ducts were severely damaged. The north duct had substantial area loss on its top portion amounting to over half of the total cross-sectional area in several intervals. This damage occurred mostly in the intervals between transverse cracks on the beam's surface (see Figure 5.27). Where the duct was still intact, there was extensive corrosion and pitting. This damage

was more severe on the inside of the duct than the outside. The overall shape of the area loss and pitting inside the duct indicates the presence of a very large void extending over most of the duct's length. The bottom portion of the north duct was less damaged. Inside, there was widespread discoloration and light localized corrosion, mostly occurring on the same intervals as the area loss on the top half. Most of the corrosion inside the duct occurred where the strands had rubbed against it. This is shown in Figure 5.25. The outside was more damaged, with widespread pitting over the same intervals as the area loss.

Figure 5.25: Specimen T.2, Corrosion Along Gouges on Bottom Half of North Duct

Overall, the south duct was less damaged than the north duct. There was some area loss on top of the duct in the area between transverse cracks, but it amounted to far less cross-sectional area and only extended over a few intervals. Typical damage to the top of the duct is shown in Figure 5.27. The outside of the top portion also showed localized severe pitting and corrosion around midspan. Inside, the corrosion was less extensive, with pitting occurring in the intervals nearest to the area loss. The corrosion inside the south duct also indicated the presence of a large void, albeit smaller than the north duct. The bottom of the south duct had some localized pitting, corrosion, and discoloration on its outside over the same intervals as the top of the duct. Inside, the damage occurred over the same region but to a lesser extent. Duct corrosion ratings are shown in Figure 5.28 and summarized in Table 5.7.

5.2.2.4 Grout

The top of the north tendon grout had a large void extending over its entire length. This void ranged from approximately 0.5 to 1.5 inches across (see Figure 5.27). The void was deepest at midspan of the tendon and shallowest at its ends, corresponding to the curvature of the tendon.

At midspan, the top surface of the grout was heavily stained with corrosion products. Moving out toward the ends of the grout, there was less discoloration. Where the void was smaller, there grout surface was covered with dark gray air bubbles. The bottom of the north grout was poorly consolidated, with at least one strand exposed over nearly the entire autopsy region. The grout did not appear to be cracked. Chloride measurements were well above the threshold for corrosion throughout the region in which duct damage was the most severe. Maximum chloride content was 0.33% directly underneath the live end transverse crack on the specimen's surface. The chloride concentrations decreased with distance away from the peak value. This suggests that chlorides entered the duct from the transverse crack at that location and dissipated across the large grout void.

The south tendon grout had voids over most of its length. The largest void extended from near the live end of the grout to just past midspan (see Figure 5.27). This void was approximately 1.25 inches wide. The grout was moderately stained with corrosion products over this region, with the most intense discoloration occurring at midspan. The top of the grout also showed craze cracks in the middle of this large void region. On the dead end half of the specimen, voids were also present, but these were confined to the upper flutes of the duct and were approximately 0.5 inches wide. The grout vent at midspan left a deep impression in the grout. This may indicate that the grout vent was not properly seated at the top of the duct and consequently slipped downward, possibly interfering with the flow of grout through the tendon. The underside of the south tendon grout was poorly consolidated. Like the north grout, there was at least one strand exposed over the entire length of the tendon. Chloride levels were much lower in the south duct grout but still above the corrosion threshold. The maximum chloride concentration was 0.094% at midspan. Chloride content for grout in both tendons is given in Figure 5.28. Peak chloride content occurred at the location of the area loss, suggesting that chlorides entered there first and dissipated outward through the voids.

Chloride concentrations were above the corrosion threshold at all measured points in both tendons. The higher concentrations in the north tendon may have been due to the extensive buildup of corrosion products on the surface of the north tendon grout. Grout in both tendons had a large void covering at least half of its length. Because grout in neither tendon was extensively cracked, it is likely that the grout void was the primary chloride path through the grout.

5.2.2.5 Strand

One strand in the north tendon was slightly damaged. The outer wires were either undamaged or lightly discolored on all intervals, and the inner wire had light corrosion or discoloration on most intervals. At the location of the live end transverse surface crack, the inner wire of this strand showed some corrosion which could not be removed with a scouring pad. The other two strands in the north duct were substantially more damaged. Several outer wires on both strands had spots of surface corrosion which could not be scrubbed away and localized pitting at midspan, with discoloration or light corrosion over the remaining intervals (see Figure 5.26). The inner wires of these strands were also more damaged, with flecks of light to moderate corrosion over most of their length. Overall, the corrosion ratings were highest at the location of transverse surface cracks and consistent over the rest of the tendon.

Figure 5.26: Specimen T.2, North Duct Strand Showing Pitting Near Midspan

The three south duct strands all showed similar levels of damage, and were more severely corroded than the north duct strands. Spots of light to moderate corrosion occurred at the location of the live end transverse surface crack on all three strands, with light localized corrosion and discoloration occurring on other intervals. The inner wires were uniformly damaged, with light surface corrosion occurring on almost all intervals. Corrosion ratings in the south duct strands showed peaks at crack locations, and were uniform and higher than the north duct strands. A typical strand and inner wire are shown in Figure 5.27. Strand corrosion ratings are shown in Figure 5.28 and summarized in Table 5.7.

Longitudinal Bar

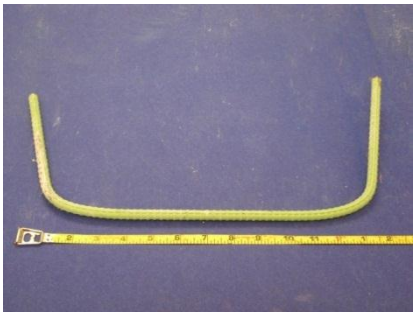

Stirrup

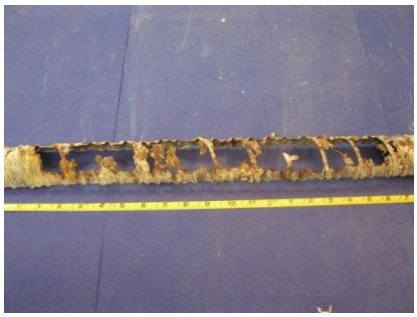

Top of North Duct

Top of South Duct

North Grout

South Grout

Strand

Inner Wire

Figure 5.27: Specimen T.2 Main Autopsy Region Elements

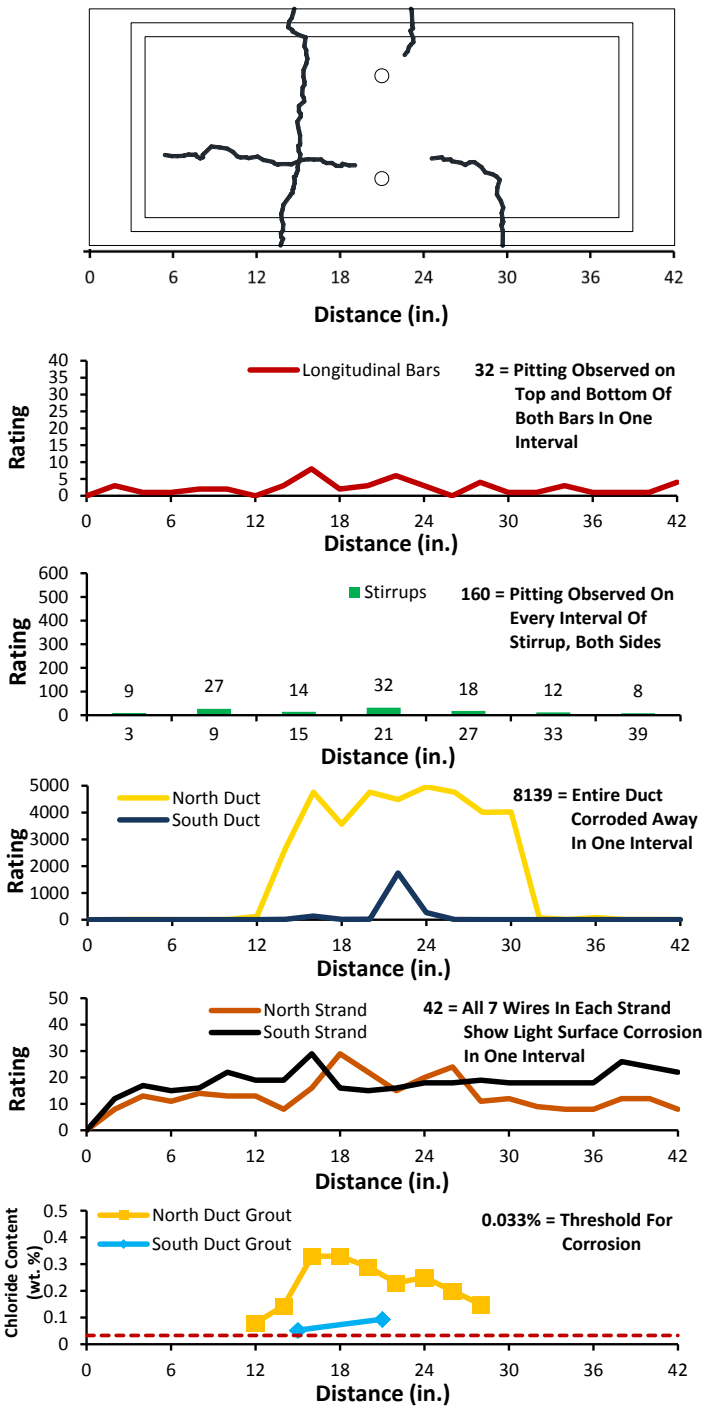

Figure 5.28: Specimen T.2 Crack Map and Corrosion Rating Plots

5.2.2.6 Dead End Anchorages

The epoxy applied to the anchorages before casting the pourback was largely intact. The epoxied surfaces were mostly either undamaged or lightly discolored. The bottom surfaces and outside edges of both bearing plates experienced some localized moderate corrosion. The duct tape used to seal the joint between the ducts and bearing plates was completely intact. Some moderate corrosion was later found on the area of the bearing plate which had been covered by the duct tape. Upon removal, the anchor heads showed uniform moderate corrosion. The area which had been covered by grout was merely discolored. North and south anchorages and anchor heads are shown in Figure 5.29.

North Anchorage

South Anchorage

North Anchor Head

South Anchor Head

Figure 5.29: Specimen T.2 Anchorages and Anchor Heads

Table 5.8: Specimen T.2 Anchorage Corrosion Rating Summary

Component	Maximum	Total	Generalized
North Duct	12	27	41
South Duct	5	19	29
North Strands	54	217	42
South Strands	42	107	36

The anchorage zone ducts were only mildly damaged. Some extremely localized pitting and surface corrosion was found on both ducts in the area which had been covered with duct tape. Light corrosion was also found on the inner top surface of the ducts, indicating the presence of small voids there. Otherwise, all surfaces of both ducts showed mild discoloration or extremely localized corrosion. North and south anchorage zone ducts are shown in Figure 5.32. Corrosion ratings for the anchorage zone ducts are shown in Figure 5.31 and summarized in Table 5.8.

The grout from both tendons fractured during removal. Thus, the extent of cracking could not be determined. The top surface of both grouts was covered with small, elliptical voids which had formed inside the flutes of the duct. The north grout also had a few very small stains near the anchorage-duct connection. The north grout showed evidence of segregation, as shown by a light gray color near the anchor head and a darker gray toward the inside of the specimen. North and south grouts are shown in Figure 5.32.

The south tendon strands shortened by approximately 0.1 inches after the anchorage had been removed from the specimen, as shown in Figure 5.30. Strands in both tendons experienced light to moderate corrosion at their exposed ends and more localized light corrosion or discoloration elsewhere. The extent of corrosion was mostly uniform between the outer wires and inner wire of each strand. Overall, corrosion ratings were higher for the north tendon strands than for the south. The wedges showed some surface corrosion but were substantially intact. The appearance of a typical strand, with and without wedges, is shown in Figure 5.32. Corrosion ratings for the anchorage zone strands are shown in Figure 5.31 and summarized in Table 5.8.

Figure 5.30: Specimen T.2, Debonded Strands in South Anchorage

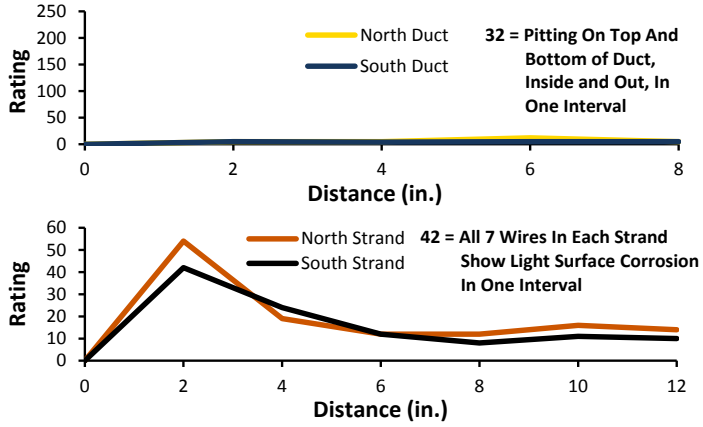

Figure 5.31: Specimen T.2 Anchorage Corrosion Rating Plots

Top of North Duct

Top of South Duct

North Grout

South Grout

Strands with Wedges

Strand

Inner Wire

Figure 5.32: Specimen T.2 Anchorage Region Elements

5.2.3 Specimen 1.2: Galvanized Duct, Copper-Clad Strand

Figure 5.33: Specimen 1.2 Top Surface (Left) and Leakage at Live End Corbel Crack (Right)

Table 5.9: Specimen 1.2 Corrosion Rating Summary

Component	Maximum	Total	Generalized
Longitudinal Bars	7	60	9
Stirrups	16	128	9
North Duct	3564	9813	2804
South Duct	3216	6190	1769
North Strands	21	441	42
South Strands	21	441	42

This specimen did not receive anchorage exposure during the testing period.

5.2.3.1 Appearance

The overall condition of the concrete was much worse around and below the ponded saltwater region than at other locations. The specimen showed widespread light scaling in these regions. The raised edges surrounding the saltwater tray were most severely scaled. Large aggregate was visible over much of this area. Some small surface air voids were visible in the saltwater tray, and many more were visible in the north and south faces. Some of these voids were up to ¼ inch deep. Two approximately 1 inch diameter popouts were present within the transverse crack near the live end of the ponded region. Corrosion staining was visible around the base of both grout vents, indicating the presence of corrosion within the specimen.

There were three large transverse cracks which crossed the top of the specimen and extended down its north and south faces. The epoxy used to seal the cracks on the side faces was

intact at the time of autopsy. These cracks were located roughly at the quarter points of the specimen. Their average width was 0.02 inches. One longitudinal crack extended from near the middle transverse crack to the live end transverse crack approximately six inches from the north edge of the specimen, and its width was 0.004 inches. The specimen also had a crack which extended from the bottom corners of the live end anchorage pourback nearly to the re-entrant corner of the corbel at the bottom of the specimen. This crack had formed long after the live load was applied. As a result, it was not sealed with mortar. After a period of wet weather, leakage was observed from this crack (see Figure 5.33). Some slight separation was observed at the joint between the live end anchorage pourback and the rest of the specimen, suggesting that some shrinkage had taken place. Crack width data is shown in Figure 5.34, and the crack diagram is shown in Figure 5.39.

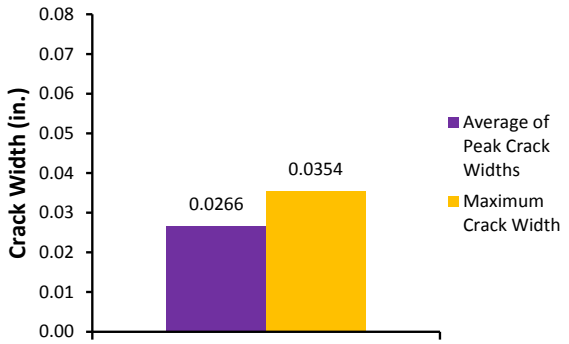

Figure 5.34: Specimen 1.2 Crack Data

5.2.3.2 Longitudinal Bars and Stirrups

Damage to both longitudinal bars was minor. Spots of discoloration and light surface corrosion occurred on the top and bottom of both bars at the locations where stirrups were tied. This damage occurred uniformly along the length of both bars. Neither bar was perceptibly more damaged than the other. The corrosion rating was highest 28 inches from the live end of the autopsy region. Typical longitudinal bar corrosion for this specimen is shown in Figure 5.38. Longitudinal bar corrosion ratings are shown in Figure 5.39 and summarized in Table 5.9.

The stirrups also showed relatively minor damage. All but two of the stirrups had corrosion which could be completely scrubbed away with a scouring pad. Light to moderate

corrosion and discoloration were most prevalent at the stirrups' bend locations and where the ducts had been tied, as shown in Figure 5.38. Stirrup #2 was most severely damaged. It had pitting on both the top and bottom of its horizontal portion over one interval. The three stirrups with the highest corrosion ratings were located underneath each of the three transverse cracks on the specimen surface. Stirrup corrosion ratings are shown in Figure 5.39 and summarized in Table 5.9.

5.2.3.3 Ducts

Both galvanized steel ducts showed severe localized corrosion damage. The outside top half of the north duct experienced area loss and extensive pitting over several intervals near midspan and its quarter points, as shown in Figure 5.38. Inside the top half, pitting and area loss were just as severe. Where the duct was still intact, corrosion and discoloration were visible in the uppermost flutes of the duct. This suggests that small voids were present in the grout. The void appeared to be continuous between 8 inches and 22 inches from the live end of the autopsy region. Corrosion may have initiated at midspan and traveled outward over this void (see Figure 5.35). The bottom half of the duct was much less damaged overall. While pitting and some slight area loss occurred on the outside at the duct's quarter points, discoloration and corrosion were less widespread in the other areas of the duct. Inside, the bottom half of the duct was widely discolored but only showed small areas of pitting near the quarter points. The pattern of the discoloration on the bottom of the duct suggests that the grout was cracked over much of its length and that at least two of the strands had rubbed against it during its life. Among large areas of discoloration, some regions of the inside even showed the characteristic sheen of new metal.

Figure 5.35: Specimen 1.2, Area Loss and Large Void on Top Inner Surface of North Duct

The south duct was similarly damaged. Its area loss was more extreme than the north duct at the live end quarter point, less extreme at midspan, and roughly comparable to the north duct at the dead end quarter point. Corrosion damage to the outside portion of the top half of the duct was extremely localized. Pitting and area loss occurred over only a few intervals near each quarter point and midspan. The remainder of the duct was only slightly discolored or lightly corroded, as shown in Figure 5.38. Inside, damage was similar. Discoloration on the top of the duct suggests the presence of small voids within its flutes. Unlike the north duct, these small voids did not appear to be continuous at any point along the duct. The outside of the bottom half had minor area loss at the quarter points along with extensive corrosion and pitting over most other intervals. Inside, there was some isolated light to moderate corrosion near the quarter points as well as at spots where the strands had rubbed on the duct. Overall, the discoloration within both ducts was much darker than expected. This may be due to the dark patina of the copper-clad strand in this specimen. Duct corrosion ratings are shown in Figure 5.39 and summarized in Table 5.9.

5.2.3.4 Grout

The north tendon grout was able to be removed from the duct fully intact. Upon examination, it showed visible transverse cracks every few inches along its entire length. The bottom portion of the grout was considerably darker than the top. This suggests density variation within the grout. Voids were clearly visible in the extracted grout. Near the ends, they were less than 1 inch across, and all were fully contained within the top flutes of the duct. The color within these voids varied from bright white on the live end of the grout to dark gray on the dead end. One continuous void was found extending from 8 inches to 22 inches from the live end of the grout. At midspan and the quarter points of the grout, heavy staining was found due to the corrosion in the surrounding duct, as shown in Figure 5.38. Isolated yellow-orange spots were seen at various points along the entire length of the grout. Two strands were partially exposed on the grout's underside over most of its length. The strands appear to have been too close to the duct for the grout to properly consolidate there. Maximum chloride content was 0.179% at 18 inches from the live end of the autopsy region. This location corresponds to the specimen's midspan transverse surface crack. Chloride concentrations decreased away from midspan of the grout. All measured chloride concentrations were well above the threshold for corrosion.

Figure 5.36: Specimen 1.2, Corrosion Staining Within South Grout

The south tendon grout was also cracked transversely every few inches along its length. Small voids were found on the top portion of the grout and appear to have formed within the top flutes of the duct, as shown in Figure 5.38. These voids were approximately 0.5 inches wide. Staining occurred at the locations corresponding to area loss and pitting of the surrounding duct. This staining permeated from the top of the grout down to the level of the strands (see Figure 5.36). Localized yellow-orange discoloration spots were also observed on all sides of the grout. Some portions of strand were exposed on the bottom of the grout, but not nearly to the extent of the north grout. The south grout was extremely well-consolidated compared to the north grout. Considerably more effort was required to crack it in order to expose the strands within. Maximum chloride concentration in the grout was 0.112% at midspan. Measurements taken at 8 and 32 inches from the live end were approximately at the threshold for corrosion. Chloride content for grout in both tendons is given in Figure 5.39.

Both tendon grouts had similar chloride distributions. However, the north tendon grout had a long continuous void on its top surface, while the south did not. This means that chlorides are transported through strand interstices and grout voids at approximately the same rate, achieving the uniform distributions shown in Figure 5.39.

5.2.3.5 Strand

Strand damage was minor and extremely uniform in both tendons. The copper-clad strands did not show any corrosion on any wire within any interval. Instead, the strands assumed a dark black patina over their entire length. The patina was darkest and glossiest on the inner wire of each strand, but could be scoured off of the outer wires more easily than the inner wires. The patina as seen on the inner and outer wires of the strands is shown in Figure 5.38. The ends of each strand took on a slightly lighter patina than the areas within the autopsy region. The

distinctive orange color of copper was even visible in spots at the ends of some strands. At the ends of several strands, a bright red color was observed, as shown in Figure 5.37. This may have been a phenomenon known as dezincification. This is a type of selective corrosion in which zinc leaches out from copper alloys and oxidizes, forming a characteristic red color[22]. The zinc content of the copper-clad strand is unknown. Transverse lines were visible on many outside wires of the strands in both ducts. These lines coincide with the locations of cracks in the north duct grout. Strand corrosion ratings are shown in Figure 5.39 and summarized in Table 5.9.

Figure 5.37: Specimen 1.2, Possible Dezincification Near Strand End

Longitudinal Bar

Stirrup

Top of North Duct

Top of South Duct

North Grout

South Grout

Strand

Inner Wire

Figure 5.38: Specimen 1.2 Main Autopsy Region Elements

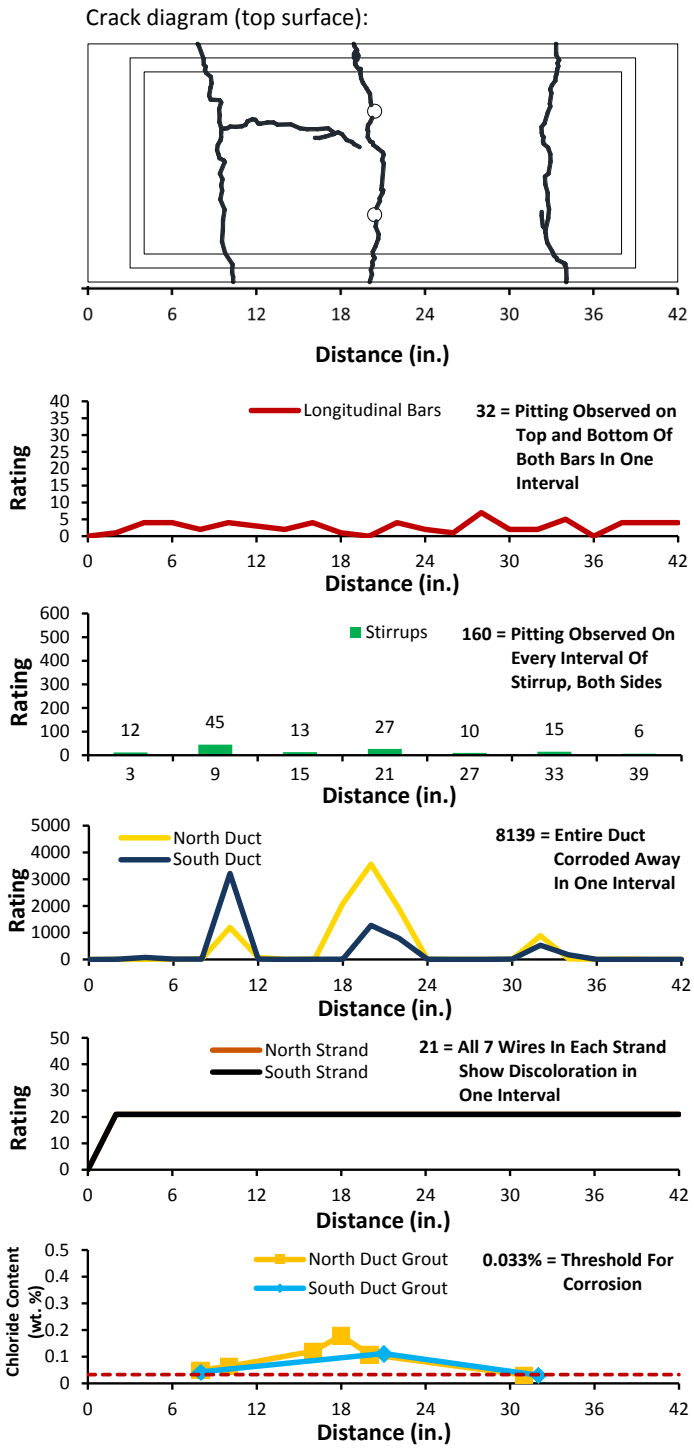

Figure 5.39: Specimen 1.2 Crack Map and Corrosion Rating Plots

5.2.3.6 Dead End Anchorages

Corrosion damage to the both anchorages was mild. Although the epoxy used to seal the anchorages prior to pourback had been scraped off during autopsy, the exposed surfaces of the bearing plates and anchor heads were mostly corrosion-free. There were some isolated spots of discoloration and light corrosion, but these represented only a small fraction of the exposed area of the bearing plates. The non-exposed surfaces of the bearing plates were dotted with isolated discoloration and light corrosion. Damage was most severe to the bottom edge of the bearing plates and grout vents, which experienced some moderate corrosion. Overall, the south anchorage was slightly more damaged than the north anchorage. Both anchor heads were completely intact. The north anchor head was only slightly discolored in spots, while the south anchor head experienced some localized moderate corrosion on its inside edge. The north and south anchorages and anchor heads are shown in Figure 5.40.

North Anchorage

South Anchorage

North Anchor Head

South Anchor Head

Figure 5.40: Specimen 1.2 Anchorages and Anchor Heads

Table 5.10: Specimen 1.2 Anchorage Corrosion Rating Summary

Component	Maximum	Total	Generalized
North Duct	5	15	30
South Duct	7	16	32
North Strands	25	135	45
South Strands	22	127	42

Unlike prior specimens, the ducts were not connected with duct tape to the anchorages[7]. The north duct experienced light localized corrosion on its top outside surface, which had been in contact with the anchorage. Elsewhere, the duct showed localized discoloration. The south duct was slightly more damaged, showing more widespread light corrosion at the end which was spliced into the anchorage. Discoloration on the bottom of both ducts was somewhat dark with undisturbed spots, just as the main autopsy region ducts had appeared. The upper portions of both ducts also showed evidence of small voids which had formed within the top flutes of the ducts. North and south anchorage zone ducts are shown in Figure 5.42. Corrosion ratings for the anchorage zone ducts are shown in Figure 5.41 and summarized in

Table 5.10.

The north tendon anchorage zone grout did not appear to be cracked. There were small voids present corresponding to the locations of the uppermost flutes of the corrugated duct. These voids had a dark gray color, matching the color of the voids near the dead end of the main autopsy region north duct grout. Some very faint flecks of discoloration were found. The north grout itself did not show any discernible color variation. The south grout appeared almost identical to the north duct grout. However, it did show some variation in color. The grout was white-gray at the anchor head and became somewhat darker gray towards the specimen interior. North and south grouts are shown in Figure 5.42.

Discoloration on the anchorage zone strands was not as uniform as in the main autopsy region. The black patina was intermittent over most of each anchorage zone strand. Multi-colored staining and some extremely localized corrosion were found in the wedge region. This suggests that the wedges may have damaged the copper coating and exposed the regular steel below. Damage to the inner wires was comparable to that of the outer wires for all strands. All wedges were found to be intact. The appearance of a typical strand, with and without wedges, is

shown in Figure 5.42. Corrosion ratings for the anchorage zone strands are shown in Figure 5.41 and summarized in

Table 5.10.

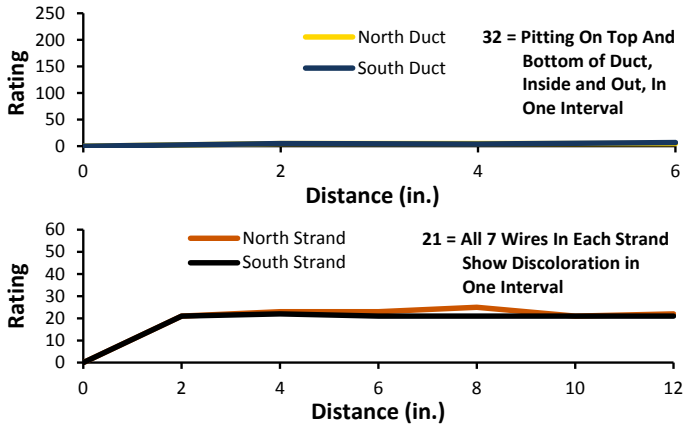

Figure 5.41: Specimen 1.2 Anchorage Corrosion Rating Plots

Top of North Duct

Top of South Duct

North Grout

South Grout

Strands with Wedges

Strand

Inner Wire

Figure 5.42: Specimen 1.2 Anchorage Region Elements

5.2.4 Specimen 2.2: Galvanized Duct, Hot-Dip Galvanized Strand

Figure 5.43: Specimen 2.2 Overall (Left) and Corrosion Stains Near Grout Vent (Right)

Table 5.11: Specimen 2.2 Corrosion Rating Summary

Component	Maximum	Total	Generalized
Longitudinal Bars	12	144	21
Stirrups	12	193	14
North Duct	2840	11350	3243
South Duct	2704	9017	2576
North Strands	23	159	15
South Strands	19	154	15

This specimen did not receive anchorage exposure during the testing period.

5.2.4.1 Appearance

The specimen showed light scaling in and around the saltwater tray and near the bottom edges of both corbels. The saltwater tray had many small surface air voids and popouts. There were a few on the north and south faces of the specimen, as well. Some light spalling was visible around the specimen's transverse cracks. This was most noticeable in the center of the saltwater tray. Corrosion staining was found around the base of both grout vents, indicating the presence of corrosion inside the specimen. This staining is shown in Figure 5.43. In addition, extensive staining was discovered just beneath the surface of the saltwater pond in this vicinity during autopsy (see Figure 5.44).

Figure 5.44: Specimen 2.2, Corrosion Staining Under North Grout Vent

Three primary transverse cracks crossed the top of the specimen and extended down its north and south faces. The epoxy used on the side faces to seal these cracks against leakage had begun to detach from the concrete at the time of autopsy. Together, the three transverse cracks had an average width of 0.035 inches. Two longitudinal cracks originated from the transverse crack nearest the live end, one of which extended fully to the transverse crack at midspan. Three more extended inward from the dead end transverse crack. These cracks tended to meander somewhat. One of the latter longitudinal cracks turned 90 degrees over its length to become transverse. The average width of the longitudinal cracks was 0.015 inches. Cracks were found extending from the reentrant corner of both the live and dead end corbels around the respective end faces of the specimen. These cracks were not sealed with mortar and were found to be leaking water at the time of autopsy. On the live end of the specimen, the corbel cracks passed through the joint between the anchorage pourback and the rest of the specimen. Some separation occurred along the construction joint as a result. Crack width data is shown in Figure 5.45, and the crack diagram is shown in Figure 5.48.

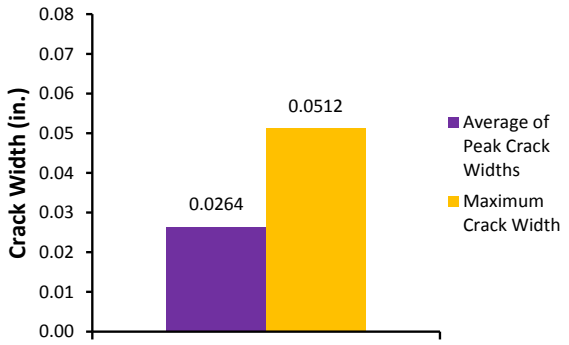

Figure 5.45: Specimen 2.2 Crack Data

5.2.4.2 Longitudinal Bars and Stirrups

The north longitudinal bar was considerably more damaged than the south bar. The north bar experienced moderate corrosion and staining on over half its length. The severity was generally greater at locations where stirrups were tied or a transverse surface crack was present. This is shown in Figure 5.47. The south bar only showed this degree of corrosion on the intervals where stirrups had been tied. This corrosion could not be removed with a scouring pad. On all other intervals, the south bar had either light localized corrosion or discoloration. Overall, corrosion ratings were highest for both bars in the vicinity of the transverse crack near the dead end of the autopsy region. Longitudinal bar corrosion ratings are shown in Figure 5.48 and summarized in Table 5.11.

The stirrups also experienced moderate but consistent damage. All but one of the stirrups had corrosion over at least one interval which could not be removed with a scouring pad. However, only two stirrups experienced pitting on any interval. Corrosion and discoloration were most prevalent at the stirrups' bend locations and the locations where the ducts were tied (see Figure 5.47). The three most severely damaged stirrups were the ones located beneath each of the specimen's transverse surface cracks. Stirrup corrosion ratings are shown in Figure 5.48 and summarized in Table 5.11.

5.2.4.3 Ducts

The north and south ducts showed severe localized corrosion damage. The north duct had significant area loss over the intervals corresponding to the locations of the specimen's

transverse surface cracks (see Figure 5.47). However, this damage was extremely concentrated. Most of the other intervals of the duct, inside and out, showed only localized light corrosion or discoloration. The inside of the duct had evidence of small voids in its uppermost flutes. The outside bottom portion of the north duct experienced substantial localized pitting at midspan and its quarter points, as well as some slight area loss at midspan. Damage was similar inside the bottom portion. However, the corrosion was at once less severe and more widespread. Overall, the highest corrosion ratings for the north duct occurred at midspan.

Damage to the south duct was comparable to that of the north duct. Significant area loss occurred within the intervals corresponding to transverse surface cracks. Most intervals which did not experience area loss were only discolored or lightly corroded, both inside and out (see Figure 5.47). The south duct also had evidence of voids in its upper flutes. The void was deep enough between 8 inches and 20 inches from the live end of the autopsy region that the duct flutes did not isolate it. It became one continuous void. In addition, there was prominent orange discoloration around the edges of this void. On the bottom portion of the south duct, much less severe area loss occurred at the same locations as on the top portion. In general, outside corrosion damage was more localized but also more severe than the inside of the duct on the bottom portion. Variations in the discoloration on the inside of the duct indicated that the grout was cracked (see Figure 5.46). Duct corrosion ratings are shown in Figure 5.48 and summarized in Table 5.11.

Figure 5.46: Specimen 2.2, Discoloration Inside South Duct Showing Signs of Cracked Grout

5.2.4.4 Grout

The north tendon grout was cracked transversely every few inches along its entire length. Small voids, approximately 0.5 inches across, were found along the length of the grout. All of them appeared to be isolated from each other by the top flutes of the duct. Significant staining was present in the areas corresponding to duct corrosion and area loss. This staining seeped down the grout through its transverse cracks, though not to the level of the strands. Localized yellow-brown discoloration was observed over nearly the entire length of the grout. Some segregation was observed in the form of color variation from white to dark gray, both over the height of the grout as well as within the duct flutes on its underside. This is shown in Figure 5.47. The grout appeared not to have consolidated well around the lowest strands in the tendon. At least one strand was partially exposed over much of the duct's length. Maximum chloride concentration in the grout was 0.084%, occurring 20 inches from the live end. Elsewhere in the north grout, the chloride levels were at or just above the corrosion threshold.

The south tendon grout was similar in appearance to the north tendon grout. A large, continuous void was present from about 8 inches to about 20 inches from the live end. This void was approximately 1 inch wide. Smaller voids, restricted to 0.5 inches in width or less by the upper flutes in the duct, were present over the rest of the grout's length (see Figure 5.47). Extensive corrosion staining was found corresponding to the regions of the duct which experienced the most severe corrosion and area loss. Like the north duct, this staining seeped downward through the grout's transverse cracks. Localized light yellow discoloration was present along the length of the grout, mostly on its bottom portion. The maximum chloride content of 0.43% occurred 18 inches from the live end of the grout. Beneath the live end transverse surface crack, the chloride concentration was 0.14%. Beneath the dead end crack, chloride levels were just above the corrosion threshold. Chloride content for grout in both ducts is given in Figure 5.48.

Grout chloride contents were higher at every measured point on the live end half of the south tendon than the same region of the north tendon. This occurred in spite of similar area loss in the north and south ducts. The higher chloride content in the south tendon may be due to the accumulation of corrosion products around the large, extensively stained void on its live end half. Concentrations were nearly equal on the dead end half of both tendons and much lower than the chloride contents on the live end half of each tendon. The lower chloride contents suggest that

the area loss experienced by both tendons at the dead end quarter point did not occur until much later than the area loss at other locations.

5.2.4.5 Strand

The north tendon strands suffered only minor damage. The outer wires of each strand had no corrosion or discoloration whatsoever in many intervals, and the inner wires had localized discoloration at worst. A few miniscule specks of corrosion were found at midspan on one strand and at midspan and the dead end quarter point of another. Although small, these specks could not be removed with a scouring pad. Corrosion ratings were highest for the north duct strands at the locations corresponding to the specimen's live end and midspan transverse surface cracks.

Damage to the south tendon strands was comparable to the north duct strands. Damage was generally mild on all wires, although small, nonremovable flecks of corrosion were present beneath the live end transverse crack on one strand and beneath the dead end transverse crack on another strand. Light surface corrosion was also more present near these critical locations than elsewhere on the strands. The inner wire of each strand was slightly more discolored or corroded than its corresponding outer wires, but only marginally so. The highest corrosion rating for the south duct strands occurred beneath the dead end transverse surface crack on top of the specimen. A typical strand and inner wire are shown in Figure 5.47. Strand corrosion ratings are shown in Figure 5.48 and summarized in Table 5.11.

The galvanized strand in this specimen had a much stronger bond with the surrounding grout than any type of strand seen thus far. Overall, grout was very difficult to remove from the strands in both tendons. In general, corrosion and discoloration appeared on the zinc coating of the outer wires in each strand. On the other hand, corrosion occurred mostly on the bare steel of the inner wire of each strand, which was exposed due to the galvanizing process occurring after the strands were wound.

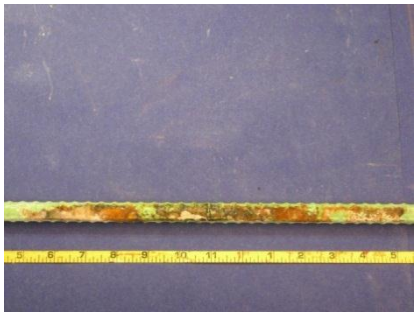

Longitudinal Bar

Stirrup

Top of North Duct

Top of South Duct

North Grout

South Grout

Strand

Inner Wire

Figure 5.47: Specimen 2.2 Main Autopsy Region Elements

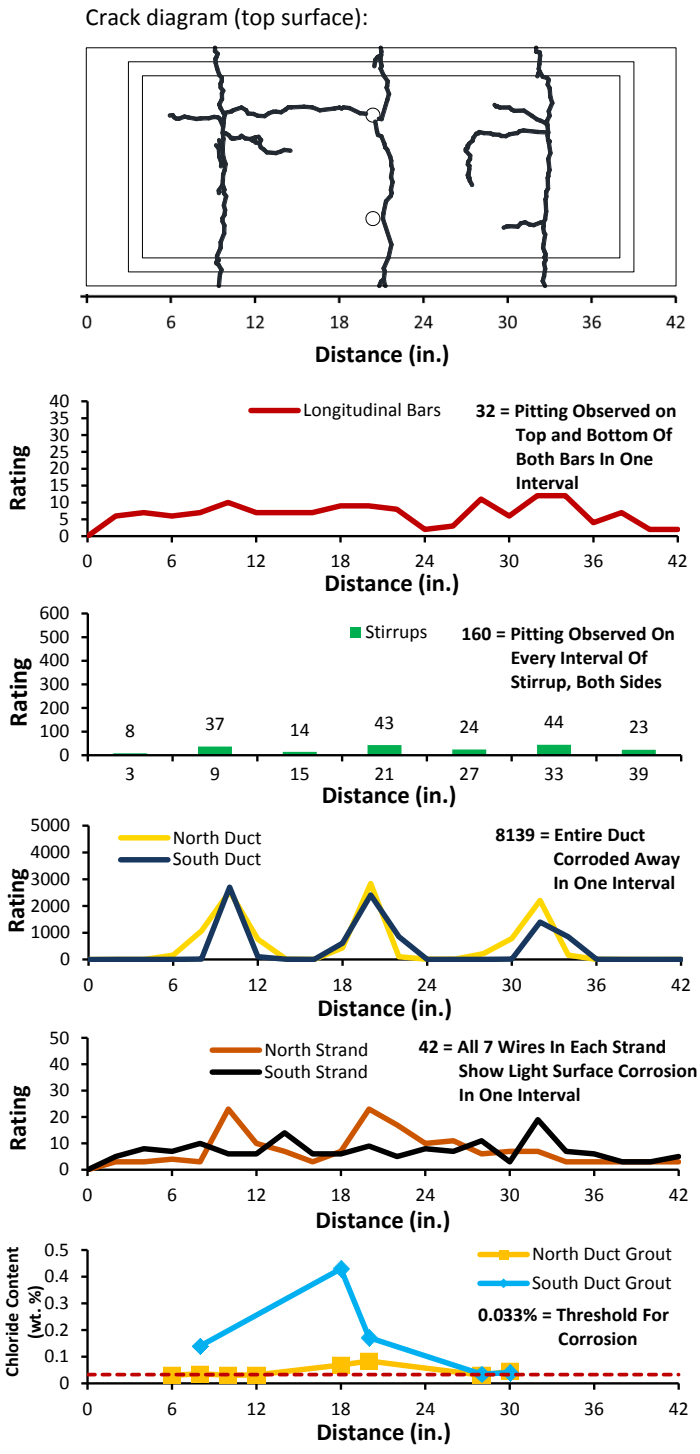

Figure 5.48: Specimen 2.2 Crack Map and Corrosion Rating Plots

5.2.4.6 Dead End Anchorages

After extraction, the epoxy used to seal the exposed surfaces of the anchorages was only partially intact on the bearing plates. The anchor heads were fully exposed. The north bearing plate showed localized spots of moderate corrosion near the bottom of its exposed area and on the surfaces against which concrete was cast. Most of this corrosion occurred on the bottom surface. The south bearing plate experienced similar damage, although the moderate corrosion was somewhat less widespread on both its exposed surface and on the bottom of the surface which had been cast against. The duct tape used to connect the ducts to the bearing plates was somewhat ripped but mostly intact. Both anchor heads experienced some localized moderate corrosion on their side and inside faces. North and south anchorages and anchor heads are shown in Figure 5.49.

North Anchorage

South Anchorage

North Anchor Head

South Anchor Head

Figure 5.49: Specimen 2.2 Anchorages and Anchor Heads

Table 5.12: Specimen 2.2 Anchorage Corrosion Rating Summary

Component	Maximum	Total	Generalized
North Duct	7	16	32
South Duct	5	13	26
North Strands	38	86	29
South Strands	20	52	17

Both the north and south anchorage zone ducts experienced very mild corrosion damage. On the outside of the ducts, some light localized corrosion was found in the areas which had been covered by duct tape. Inside, the ducts showed evidence of small voids within their top flutes. Some light corrosion spots were found in some of these voids. All duct surfaces showed widespread discoloration over all intervals. Lines visible in this discoloration suggest that the grout was cracked transversely. North and south ducts are shown in Figure 5.51. Anchorage zone duct corrosion ratings are shown in Figure 5.50 and summarized in Table 5.12.

The north and south tendon grouts appeared almost identical. Both grouts had several small voids on their top side corresponding to the upper flutes of the duct. Some extremely localized staining was found on the grout areas which had been within the anchorages. The grouts' color varied from white near the anchor heads to gray further within the specimen. This indicates that some segregation may have taken place, resulting in density variation. Two strands were visible on the surface of each grout near the anchor head. It appears that these strands were in direct contact with their respective anchorages in that region. North and south grouts are shown in Figure 5.51.

In the anchorage zone, all strands were found to have an extremely strong bond with the surrounding grout, just as was observed in the main autopsy region. Damage to all anchorage zone strands was limited to discoloration or light surface corrosion for all wires in all intervals. In general, the inner and outer wires of each strand were uniform in appearance. However, on two strands in the north tendon and one in the south tendon, damage was much less severe on the inner wires than the outer wires. For all strands, discoloration was most pronounced at the locations where the wedges had been applied. Corrosion ratings were also highest over that interval for the strands in both ducts. All wedges were found to be intact. Some localized light corrosion was found on their exteriors as well as slight discoloration in their inner regions.

Typical strands, with and without wedges, are shown in Figure 5.51. Anchorage zone strand corrosion ratings are shown in Figure 5.50 and summarized in Table 5.12.

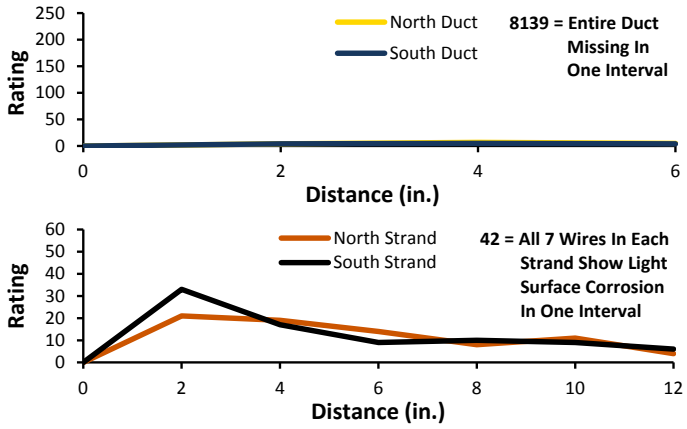

Figure 5.50: Specimen 2.2 Anchorage Corrosion Rating Plots

Top of North Duct

Top of South Duct

North Grout

South Grout

Strands with Wedges

Strand

Inner Wire

Figure 5.51: Specimen 2.2 Anchorage Region Elements

5.2.5 Specimen 2.4: One-Way Plastic Duct, Copper-Clad Strand

Figure 5.52: Specimen 2.4 Overall (Left) and Cracking at Dead End Pourback (Right)

Table 5.13: Specimen 2.4 Corrosion/Damage Rating Summary

Component	Maximum	Total	Generalized
Longitudinal Bars	14	101	14
Stirrups	530	590	49
North Duct	200	3100	886
South Duct	100	475	136
North Strands	21	441	42
South Strands	21	441	42

This specimen did not receive anchorage exposure during the testing period.

5.2.5.1 Appearance

Light to moderate scaling was found on much of the top and north and south faces of the specimen. This was most pronounced in the raised edges surrounding the saltwater tray. A few small surface air voids were visible on the surfaces of the specimen, but to a much lesser extent than seen in previous specimens. Light to moderate spalling was visible around the specimen's transverse cracks, especially toward the middle of the specimen. The top of a corroded wire tie was visible through the surface of the concrete just toward the live end from the north grout vent. This is shown in Figure 5.53.

Figure 5.53: Specimen 2.4, Corroded Wire Tie at Top Surface

The specimen had three main transverse cracks which extended across its top face and down its north and south faces. The epoxy applied to those cracks on the side faces to prevent leakage was still intact. These transverse cracks had an average width of 0.04 inches. Two secondary transverse cracks were also visible. These did not cross the entire specimen and had an average width of 0.035 inches. Two longitudinal cracks were found which connected the two transverse cracks nearest to the specimen's live end. The average width of these cracks was 0.015 inches. Most of the cracks on the specimen had more than one branch. Overall, the top of this specimen was the most cracked of any seen up to this point. Cracks were observed extending from the re-entrant corner of both corbels and around both end faces of the specimen. On the live end, this cracking occurred during live load application, and the cracks had been sealed with non-shrink mortar. On the dead end, the cracking occurred some time later. These cracks had not been sealed (see Figure 5.52). Some light efflorescence was observed around the dead end corbel cracks, indicating that leakage may have taken place at an earlier time. Crack width data is shown in Figure 5.54, and the crack diagram is shown in Figure 5.58.

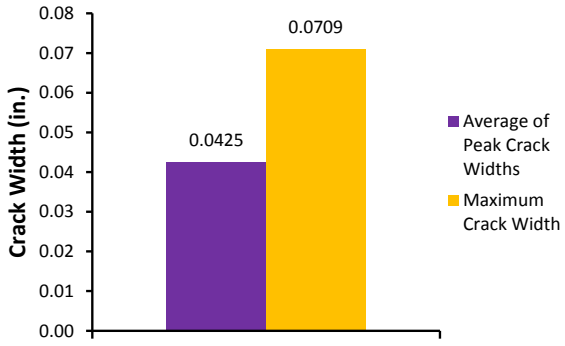

Figure 5.54: Specimen 2.4 Crack Data

5.2.5.2 Longitudinal Bars and Stirrups

Damage to the north and south longitudinal bars was moderate and localized. The north bar showed light to moderate corrosion at the locations where stirrups were tied, and some light corrosion staining at other points along its length (see Figure 5.57). Damage was more severe to the underside of the bar than to the top. The extent of corrosion was similar in the south bar, although somewhat more severe. Localized pitting was observed over one interval near the live end of the bar. Longitudinal bar corrosion ratings are shown in Figure 5.58 and summarized in Table 5.13.

Stirrups in this specimen were moderately damaged. Six of the seven stirrups had moderate corrosion or pitting over at least one interval. The worst damage tended to occur at the bend points of the stirrups and at locations where ducts were tied. However, pitting occurred over at least one interval at midspan of three stirrups' horizontal portions. This suggests that damage to the epoxy coating may have occurred at these locations. Stirrup #5 suffered the heaviest damage. This stirrup lost over 20% of its cross sectional area over a small length at midspan of its horizontal portion (see Figure 5.57). Damage did not correspond clearly to surface crack location. Although stirrup #5 was located beneath a transverse surface crack, corrosion ratings for the other six stirrups were relatively independent of location. Stirrup corrosion ratings are shown in Figure 5.58 and summarized in Table 5.13.

5.2.5.3 Ducts

The north and south plastic ducts were in near-perfect shape upon autopsy. The top of the inside of the north duct had scratches along approximately 36 inches of its length. These scratches had a depth of between 5 and 10 percent of the duct's wall thickness (see Figure 5.57). The top of the inside of the south duct was similarly damaged, although the scratches were shallower and shorter in length. The top of both ducts also showed evidence of voids which had formed inside their top flutes. The voids did not appear to be connected, and they were all approximately uniform in size and shape (see Figure 5.57). Small white crystals were found in the immediate vicinity of these voids over most of the ducts' length, but most conspicuously near midspan. A dull white residue was found on the outside of both ducts. This was more randomly distributed over the duct's length than the crystals. There were also a few localized corrosion stains on the outside of the ducts. White crystals were present over nearly the entirety of the

south duct's lower interior portion, but were completely absent from the same portion of the north duct. In fact, no discoloration whatsoever was found inside the lower north duct. Duct damage ratings are shown in Figure 5.58 and summarized in Table 5.13.

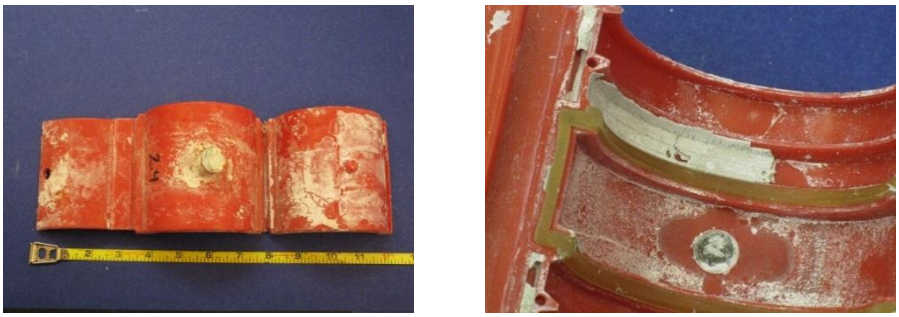

Figure 5.55: Specimen 2.4 North Duct Coupler Exterior (Left) and Gasket (Right)

The north duct coupler appeared undamaged. There were some small orange-brown flecks present on and around the coupler's grout vent outlet, and the same chalky white residue which was observed on the ducts was also present on the exterior of the coupler. The coupler's mechanical connections and gaskets were intact. The latter did not appear to be affected by the widespread scratching which occurred in the duct itself (see Figure 5.55). Cement paste was present inside the coupler but outside the gasket. Inside the gasket was grout residue and the white crystals which were present inside both ducts. There was also evidence of a small void in the vicinity of the coupler's grout vent. The south duct was continuous and did not have a coupler. The epoxy used to seal the south duct grout vent was slightly detached from the duct at midspan.

5.2.5.4 Grout

The north tendon grout was cracked transversely every few inches along its entire length. One longitudinal crack was visible on the underside of the grout. This crack appeared to terminate within approximately 6 inches of each end of the grout. Small voids, approximately 1 inch across, were found on the top surface of the grout, corresponding to the upper flutes of the duct. These voids were dark gray in color near the ends of the grout and became whiter toward midspan. A similar color change was observed in the grout itself from ends to midspan (see Figure 5.57). This may be evidence of segregation, and therefore density variation, within the

grout. One strand was visible on the underside of the grout from approximately 8 inches to 14 inches from the live end. Chloride concentration at midspan was 0.2% in the north tendon.

The south tendon grout was also cracked every few inches along its length. One longitudinal crack was observed at roughly midheight of the grout. This crack extended along the grout's entire length. Small voids were observed on the grout's upper surface. These voids were comparable in size to those found in the north grout. While these voids were mostly bounded by the upper flutes of the duct, they appeared to be slightly deeper and, as a result, more continuous than the voids in the north duct (see Figure 5.57). No color change indicating the possibility of segregation was observed. While intact, this grout was much smoother to the touch over its entire exposed surface than any grout encountered thus far. This may indicate that pressure was high and uniform during the grouting process. One strand was exposed on the underside of the grout from approximately 16 inches to 24 inches from the live end. Chloride concentration at midspan was 0.25% in the south duct. Chloride content for grout in both ducts is shown in Figure 5.58.

The chloride content at midspan of the grout in each tendon was well above the corrosion threshold despite the lack of any meaningful damage to the ducts themselves. The coupler also showed no signs of a breach. Thus, the chlorides could not have entered through either the duct or coupler. Similarly, there was no evidence to suggest that chlorides entered through the anchorage region on either end of the specimen. The only remaining means of chloride ingress would be the grout vent located at midspan of the south tendon and on top of the coupler located at midspan on the north tendon. The detached epoxy at the south duct grout vent supports the idea that chlorides entered the duct at a central location on the tendon. Chlorides entered through small imperfections in the grout vent-duct or grout vent-coupler interface and penetrated the grout through its transverse cracks. Because the copper-clad strand was uniform in appearance over the entire length of both tendons, it appears that the chlorides traveled along the tendons through the strand interstices, as well.

5.2.5.5 Strand

A uniform, glossy black patina was observed over every interval of every wire in every strand of the specimen. The patina was much glossier and somewhat darker on the inner wires than the outer wires. At the ends of each strand, the patina was less prevalent, and traces of the original copper color were visible in many spots. This can be seen in Figure 5.57. On the outer

wires, the patina could generally be removed with a scouring pad. This was not the case for the inner wires. Transverse lines were visible in the traces of grout near midspan of all strands. These lines indicated the locations of cracks in the surrounding grout (see Figure 5.56). Unlike specimen 1.2, no signs of dezincification were found. Strand corrosion ratings are shown in Figure 5.58 and summarized in Table 5.13.

Figure 5.56: Specimen 2.4, Lines in Strand Discoloration

Longitudinal Bar

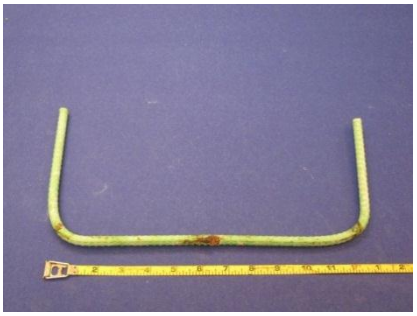

Stirrup

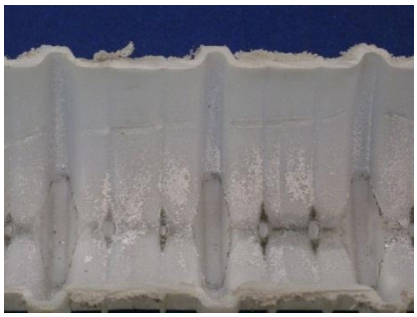

Top of North Duct

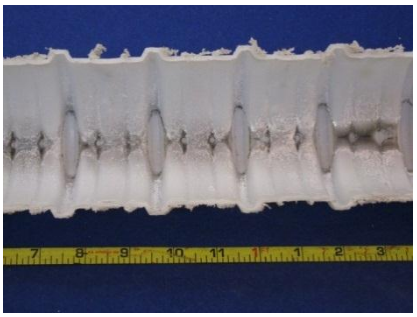

Top of South Duct

North Grout

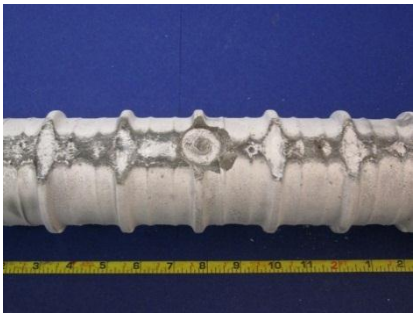

South Grout

Strand

Inner Wire

Figure 5.57: Specimen 2.4 Main Autopsy Region Elements

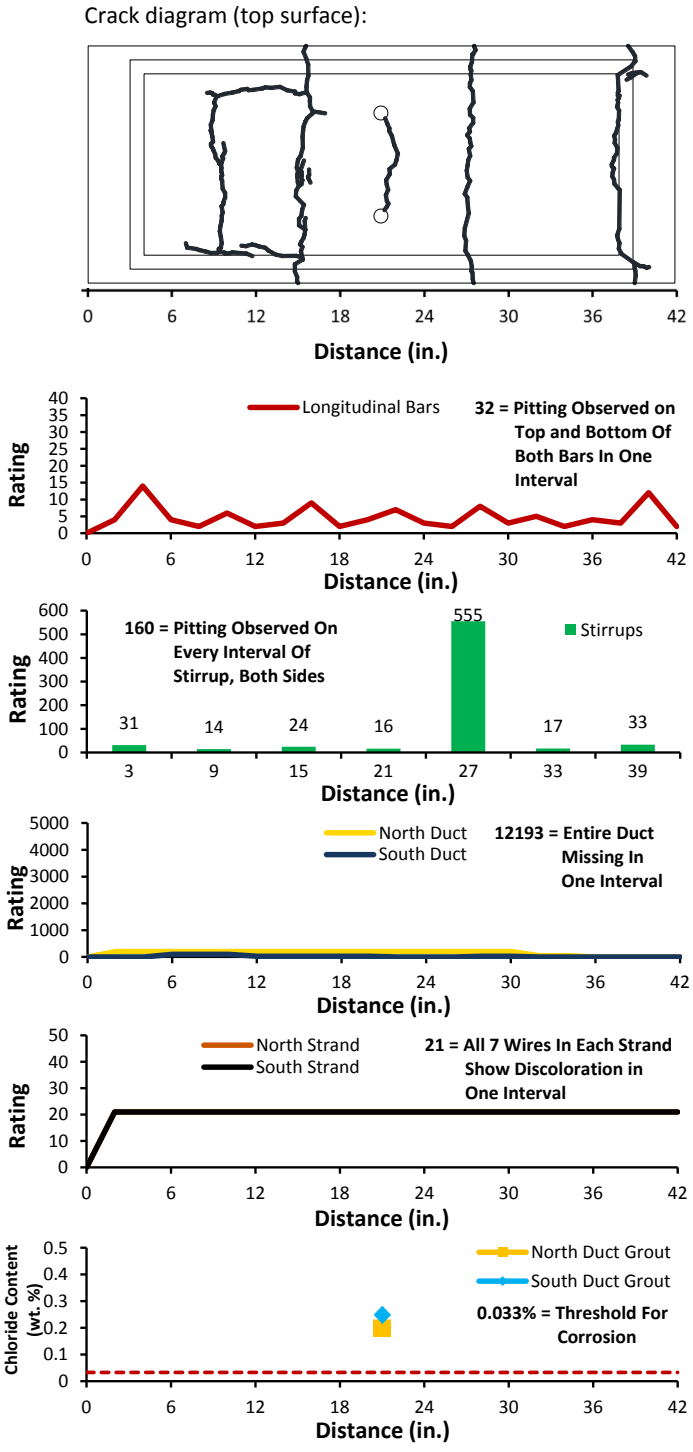

Figure 5.58: Specimen 2.4 Crack Map and Corrosion/Damage Rating Plots

5.2.5.6 Dead End Anchorages

The epoxy used to seal the exposed faces of the anchorages was almost entirely stripped away. Only small portions of the epoxy still adhered to the anchorages. The exposed face of the north bearing plate showed extensive light to moderate corrosion. The exposed face of the south bearing plate was much less affected. The undersides and outer edges of both bearing plates had moderate surface corrosion. The bottom 1 inch of each bearing plate was inadvertently sliced off by the concrete saw during autopsy. Therefore, the extent of corrosion could not be determined there. The duct tape used to seal the anchorage zone ducts was partially missing on both anchorages. Widespread moderate surface corrosion and some pitting were visible in the splice region. Both anchor heads showed patches of light to moderate corrosion, mostly concentrated around the anchor head-bearing plate interface. North and south anchorages and anchor heads are shown in Figure 5.59.

North Anchorage

South Anchorage

North Anchor Head

South Anchor Head

Figure 5.59: Specimen 2.4 Anchorages and Anchor Heads

Table 5.14: Specimen 2.4 Anchorage Corrosion/Damage Rating Summary

Component	Maximum	Total	Generalized
North Duct	0	0	0
South Duct	0	0	0
North Strands	37	156	52
South Strands	36	153	51

Both anchorage zone ducts showed evidence of voids in their upper flutes, as well as traces of the same white crystals found in the ducts of the main autopsy region. In addition, the outside of the ducts were covered with traces of the same chalky white residue which had been found on the outside of the ducts in the main autopsy region. Moderate to severe corrosion staining was found along the inside and outside rims of the end of the ducts which had been spliced to the anchorages. North and south anchorage zone ducts are shown in Figure 5.61. No scratches or gouges were found inside the ducts. Anchorage zone duct corrosion ratings are shown in Figure 5.60 and summarized in Table 5.14.

The north tendon grout shattered completely during the autopsy process. No meaningful conclusions could be drawn from it. Most of the south tendon grout shattered, as well. However, there remained one intact portion of the top of the grout adjacent to the anchor head. This grout showed many small, dark bubbles on its top side. This suggests that a small void was present inside the anchorage.

Within the first four inches from the end of the specimen of all six strands, the distinctive green color of corroding copper was visible in very localized spots. No sign of steel corrosion was found in this region on any strand. Moving in toward the specimen interior, the same patina which covered the strands in the main autopsy region was found, although the patina covered much less of the strands' overall area. Two of the specimen's dead end wedges were cracked, and some spots of moderate corrosion were found on both the inside and outside surfaces of all six wedges. Typical strands, with and without wedges, are shown in Figure 5.61. Anchorage zone strand corrosion ratings are shown in Figure 5.60 and summarized in Table 5.14.

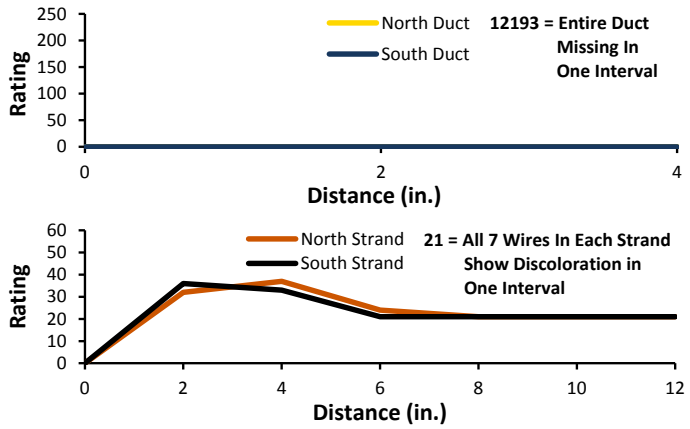

Figure 5.60: Specimen 2.4 Anchorage Corrosion/Damage Ratings

Top of North Duct

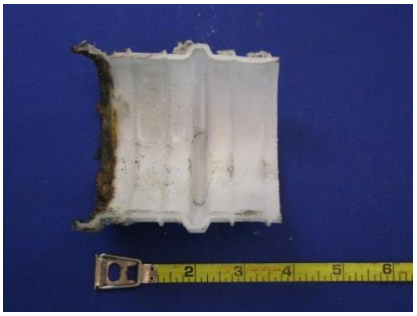

Top of South Duct

Strands with Wedges

Strand

Inner Wire

Figure 5.61: Specimen 2.4 Anchorage Region Elements

5.2.6 Specimen 3.1: Two-Way Plastic Duct, Conventional Strand

Figure 5.62: Specimen 3.1 Top Surface (Left) and Corroded Wire Tie at Top Surface (Right)

Table 5.15: Specimen 3.1 Corrosion/Damage Rating Summary

Component	Maximum	Total	Generalized
Longitudinal Bars	6	54	8
Stirrups	9	110	8
North Duct	20	120	34
South Duct	10	40	11
North Strands	16	185	18
South Strands	10	166	16

For this specimen, grouting did not occur until 5 days after post-tensioning[7]. This specimen received dead end anchorage exposure during the test period.

5.2.6.1 Appearance

The specimen showed widespread light scaling on its top surface and on the north and south faces in the vicinity of the saltwater tray. Some small surface air voids were found on the north and south faces of the specimen. Many large, shallow voids were present in the saltwater tray. Some grout appeared to have spilled out of the specimens' top vents during grouting. This grout served as a patching compound for the surface air voids in that area. The saltwater tray showed a large number of small popouts on its surface. This, combined with the voids, gave the saltwater tray a pitted, craggy appearance (see Figure 5.62). The tops of two corroded wire ties were visible on the surface of the saltwater tray along a transverse crack approximately 6 inches toward the live end from the grout vents, as shown in Figure 5.62.

The top surface of the specimen was extensively cracked. Three transverse cracks crossed the top of the specimen and extended down its north and south faces. The epoxy used to seal these cracks was intact at the time of autopsy. The transverse cracks had an average width of 0.02 inches. Two longitudinal cracks extended along almost the entire length of the autopsy region and were located approximately 4 inches from the north and south faces of the specimen, respectively. These cracks had an average width of 0.006 inches. Cracks were found on both ends of the specimen which extended nearly to the corbels there. These cracks had occurred some time after stressing and were not sealed with mortar. Efflorescence and moisture were found in the vicinity of the cracks, indicating that leakage had occurred there (see Figure 5.63). The efflorescence was slightly more extensive around the dead end cracks. Crack width data are shown in Figure 5.64, and the crack diagram is shown in Figure 5.68.

Figure 5.63: Specimen 3.1, Efflorescence at Dead End Corbel Crack

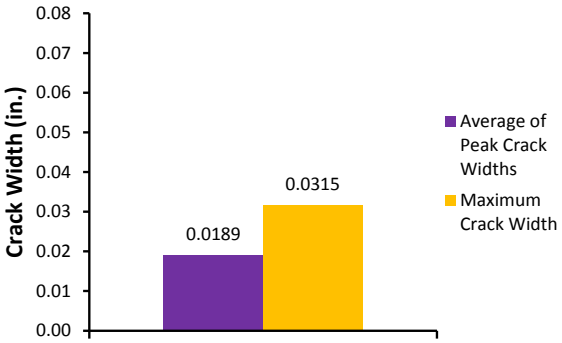

Figure 5.64: Specimen 3.1 Crack Data

5.2.6.2 Longitudinal Bars and Stirrups

Both the north and south longitudinal bars showed only minor corrosion damage. The north bar experienced corrosion which could not be scrubbed away on two intervals. Otherwise, damage was limited to light discoloration and corrosion which occurred mostly at the locations where stirrups had been tied, as shown in Figure 5.67. In general, the north bar was more corroded than the south bar, and corrosion ratings for both bars were highest underneath the location of the specimen's transverse surface cracks. Longitudinal bar corrosion ratings are shown in Figure 5.68 and summarized in Table 5.15.

The stirrups showed relatively minor damage. Only two stirrups showed pitting in any interval, and only three stirrups showed surface corrosion which could not be scrubbed away in any interval. Most corrosion and discoloration were observed at the inner and outer surfaces of the stirrups' bend radii, as well as at midspan of their horizontal regions (see Figure 5.67). The stirrups with the highest corrosion ratings were those found directly beneath the specimen's three transverse surface cracks. Stirrup corrosion ratings are shown in Figure 5.68 and summarized in Table 5.15.

5.2.6.3 Ducts

The entire north plastic duct had a chalky white residue over its entire exterior, along with several localized corrosion stains. Many of these spots were located near the heat shrink splice at midspan. The top interior portion of the north duct showed evidence of small voids which had formed in the duct's top flutes over its entire length. These voids were somewhat larger near the live end of the duct than the dead end, and all of the voids were made continuous by the duct's top longitudinal rib (see Figure 5.67). The bottom interior portion of the north duct showed some corrosion staining and extremely faint gouges near midspan. These indicate that at least one strand was either close to or bearing upon the bottom of the duct at that location. However, the scratches caused no measurable damage to the duct. Shiny white crystals were found in and around the bottom flutes of the duct, mostly near the splice region.

Damage to the south duct was similar to that of the north duct. White residue and localized corrosion stains were found on the duct's exterior. Evidence of voids was found in the upper interior portion of the duct. Voids were larger near the live end than the dead end, and maximum void size appeared somewhat larger than in the north duct. Due to the duct's top

longitudinal rib, the voids were continuous over most of the duct's length. The epoxy which sealed the grout vent at midspan appeared to have detached from the duct somewhat. It is unknown whether this occurred during autopsy or some time before (see Figure 5.67). The bottom interior portion of the duct had some light gouges between midspan and the dead end. It appeared that one strand had been bearing directly on the duct there. Shiny white crystals were observed in and around the bottom flutes of the duct on its interior. These crystals were more prevalent near midspan than elsewhere inside the duct. Duct damage ratings are shown in Figure 5.68 and summarized in Table 5.15.

The heat shrink coupler applied to the north duct was mostly intact at the time of autopsy. Both the inside and outside surfaces of the coupler showed similar discoloration and evidence of more voids than what was observed on the north duct itself. The seam between the dead end heat shrink and the coupler appeared somewhat detached around its entire circumference. This may have occurred during the autopsy process. The heat shrink tubing was somewhat brittle and easy to peel back from the duct surface. There may not have been a perfect heat shrink seal around both ducts. The coupler is pictured in Figure 5.65.

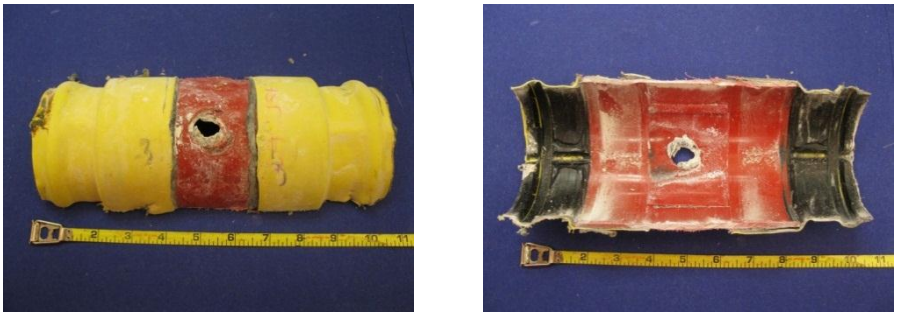

Figure 5.65: Specimen 3.1 North Duct Coupler Outer Surface (Left) and Inner Surface (Right)

5.2.6.4 Grout

The north tendon grout had transverse cracks every few inches along its entire length. No longitudinal cracks were observed. Voids, approximately 0.75 inches wide, were observed on the top surface of the grout. These were mostly contained within the transverse flutes of the duct but were connected over most of the grout's length by the top longitudinal rib of the duct (see Figure 5.67). The voids were generally white on their surface with a dark gray or black perimeter. Near

the live end of the grout, the area between voids appeared dark and porous. These factors suggest a great deal of density variation in those regions. The outside wires of one strand were visible on the grout's bottom surface approximately 28 inches from the live end. There did not appear to be any problems with consolidation in this region. Large aggregate and evidence of concrete paste intrusion were found on the underside of the splice region. This indicates that the heat shrink seal had been breached during the construction process (see Figure 5.66). The grout exterior was very smooth over its entire length, indicating high, uniform pressure during grouting. Chloride content at midspan was 0.067%.

Figure 5.66: Specimen 3.1, Cement Paste and Large Aggregate Embedded in North Grout

The south tendon grout was cracked transversely every few inches along its length. No longitudinal cracks were found. Cracking was more extensive near the dead end than the live end. One continuous void, approximately 1.25 inches wide, was found on the top of the grout extending from the live end to near midspan. The remainder of the grout showed smaller voids, about 0.5 inches across, on its top surface, connected by the top longitudinal rib of the duct. The surface of the large void was white in color with a gray perimeter and many small gray craze cracks. The smaller voids were uniformly gray in color, as shown in Figure 5.67. On the underside, the dead end region was much darker in color than the rest of the grout. This indicates that segregation took place during grouting. One wire of a strand was observed intermittently on the bottom surface of the grout from approximately 18 to 28 inches from the live end. Chloride content at midspan was 0.145%. Chloride content for north and south grouts is shown in Figure 5.68.

The presence of chloride concentrations above the corrosion threshold in both tendons indicates that chlorides entered by way of leaks. Breaches appeared to have occurred around the south duct grout vent interface and at the north duct coupler. The presence of cement paste and aggregate inside the coupler confirm that it was not watertight. It is possible that chlorides may have also entered through the north duct grout vent, but this was broken off during autopsy. No evidence was found to suggest that chlorides entered the tendon through either anchorage. The presence of strand corrosion along the entire north and south tendons suggests that chlorides were able to travel the entire length of duct from their midspan entry point through the strand interstices.

5.2.6.5 Strand

Corrosion damage to the north tendon strands was minor. The outer wires of all strands showed isolated flecks of light surface corrosion or somewhat more widespread discoloration. Over many intervals, no damage was observed at all. Clear lines were observed within the discoloration in some regions, indicating the presence of transverse grout cracks there. The inner wires were more affected, with corrosion spots over much of their length. The inner wires of two strands showed corrosion which could not be removed with a scouring pad over several intervals. Overall, damage was most severe to the north duct strands near midspan of the tendon.

The south tendon strands showed similar damage. The outer wires of all strands showed light localized discoloration. No corrosion spots were found in any intervals. Lines were observed among the discoloration, indicating cracks in the surrounding grout. The inner wires were more damaged than the outer wires in all strands. Many small corrosion flecks were observed along the length of all inner wires. In a few intervals, this corrosion could not be scrubbed away. This occurred near midspan and the dead end of all three strands' inner wires. Corrosion ratings were nearly uniform along the strands' length. No clear correlation with crack location was observed. A typical strand and inner wire are shown in Figure 5.67. Strand corrosion ratings are shown in Figure 5.68 and summarized in Table 5.15.

Longitudinal Bar

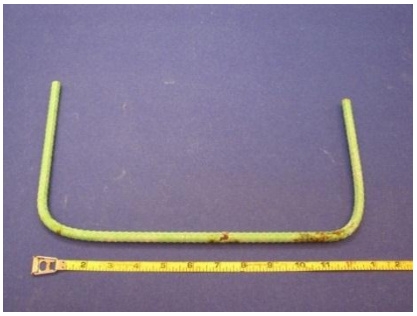

Stirrup

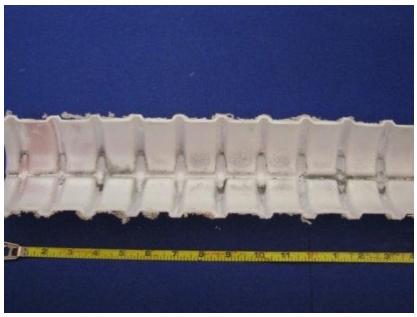

Top of North Duct

Top of South Duct

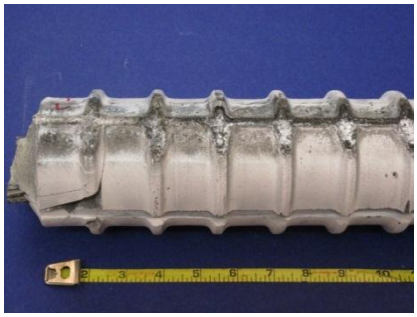

North Grout

South Grout

Strand

Inner Wire

Figure 5.67: Specimen 3.1 Main Autopsy Region Elements

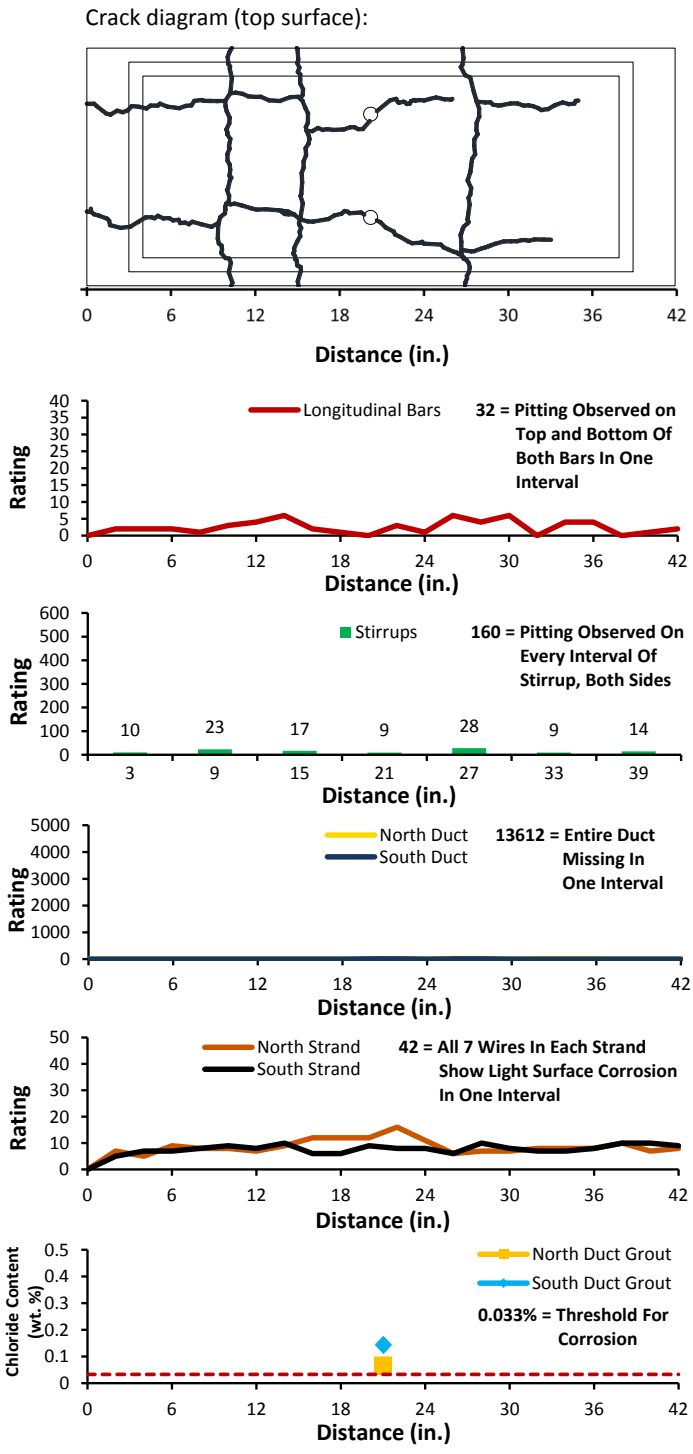

Figure 5.68: Specimen 3.1 Crack Map and Corrosion/Damage Rating Plots

5.2.6.6 Dead End Anchorages

The epoxy used to seal the exposed areas of the anchorages was mostly intact on the bearing plates, but largely missing on the anchor heads. The exposed surface of the north bearing plate showed widespread moderate surface corrosion, mostly concentrated on the bottom half of the plate. The south bearing plate was much more affected, with moderate corrosion covering most of its outer surface. Extensive surface corrosion was found on the bottom surface of both bearing plates. Although the duct tape used to connect both ducts to the bearing plates was mostly intact, widespread corrosion and pitting were found underneath. This damage was more severe to the south bearing plate than to the north. The outer surfaces of both anchor heads had localized spots of light to moderate surface corrosion. The surfaces which had been bearing on the anchorages showed much more widespread moderate corrosion, corresponding to the respective level of corrosion in both bearing plates. The north and south anchorages and anchor heads are shown in Figure 5.69.

North Anchorage

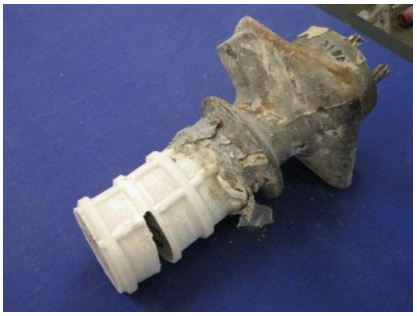

South Anchorage

North Anchor Head

South Anchor Head

Figure 5.69: Specimen 3.1 Dead End Anchorages and Anchor Heads

The outside of both the north and south ducts showed the same chalky white residue which was found on the ducts in the main autopsy region. In addition, prominent corrosion stains were found on the outer surface of the ducts where they had been spliced with the anchorages. Some very light gouges were observed in the interior of the south duct. However, the ducts were moderately damaged during the autopsy process, so the damage may have occurred at that time. The bottom interior surfaces of both ducts showed traces of the white crystals which were found in the main autopsy regions, but to a much lesser extent. North and south ducts are shown in Figure 5.70. Dead end anchorage zone duct corrosion ratings are shown in Figure 5.73 and summarized in Table 5.16.

Both the north and south tendon grout had small voids corresponding to the top of the transverse duct flutes. Heavy corrosion staining was visible on the edge of the grout nearest to the corroded anchorage-duct splices. Both grouts were damaged during the duct removal process, so the extent of cracking could not be determined. North and south grouts are shown in Figure 5.70.

Damage to the strands in both ducts was most severe in the regions outside the anchor head and inside the wedges. Light to moderate surface corrosion spots were found on several outer wires per strand in these regions. Further into the specimen, the outer wires were far less damaged, showing light discoloration and the occasional light corrosion spot. The inner wires of all strands were much more uniformly damaged, with light surface corrosion spots on most intervals. All 6 sets of wedges showed light to moderate corrosion on their outer surfaces and some discoloration spots inside. Damage to the wedges tended to be more extreme near their narrow end. Typical strands, with and without wedges, are shown in Figure 5.70. Dead end anchorage zone strand corrosion ratings are shown in Figure 5.73 and summarized in Table 5.16.

Top of North Duct

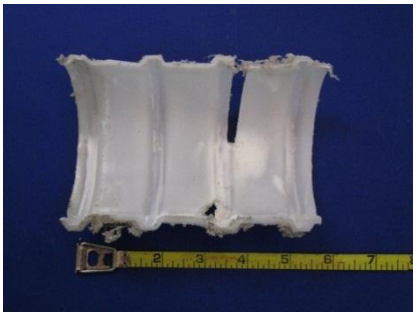

Top of South Duct

North Grout

South Grout

Strands with Wedges

Strand

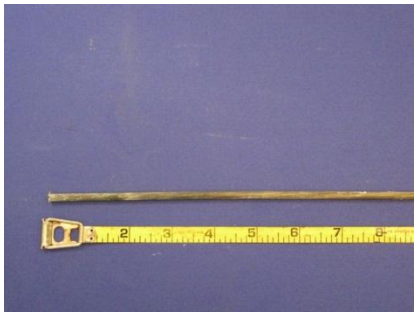

Inner Wire

Figure 5.70: Specimen 3.1 Dead End Anchorage Region Elements

5.2.6.7 Live End Anchorages

The epoxy used to seal the exposed surfaces of both live end anchorages was almost entirely missing. The exposed front of the bearing plates were mostly covered with widespread moderate surface corrosion and some localized pitting. This damage tended to be more severe toward the bottom of the bearing plates. All outer surfaces showed some isolated surface corrosion, but widespread surface corrosion was found on the bottom surfaces of both bearing plates. This was most pronounced on the north bearing plate, whose bottom surface was nearly covered with corrosion. Some isolated damage occurred on the interior edges of both bearing plates, as well. The duct tape used to seal the bearing plate-duct connections was mostly intact on the north anchorage but mostly missing on the south anchorage. Heavy corrosion and some pitting were found underneath the duct tape. The inside surfaces of both anchor heads showed widespread moderate to heavy corrosion, while the outside surfaces were only slightly discolored. Corrosion on the sides of the anchor heads was more severe in the vicinity of the bearing plates. North and south anchorages and anchor heads are shown in Figure 5.71.

North Anchorage

South Anchorage

North Anchor Head

South Anchor Head

Figure 5.71: Specimen 3.1 Live End Anchorages and Anchor Heads

The outside surface of both ducts showed the same chalky white residue as the duct in the rest of the specimen. The south duct had deep corrosion staining on both its inner and outer surfaces near the splice region. This staining was absent on the north duct. Both ducts showed signs of a continuous void spanning their entire length within their upper flutes. Very light gouges were found on both the top and bottom inner surfaces of the north duct. The south duct was not damaged in this manner. Some traces of white crystals were found in the inside of the bottom ribs of both ducts. North and south ducts are shown in Figure 5.72. Anchorage zone duct corrosion ratings are shown in Figure 5.73 and summarized in Table 5.16.

Both north and south tendon grouts were heavily damaged during the autopsy process. As a result, the extent of cracking and voids could not be ascertained. The grout appeared well-consolidated and uniform in color. Significant staining was present at the grout-anchorage interface for both the north and south duct grouts.

Damage to the anchorage zone strands was minor. Only two strands showed any corrosion spots which could not be scrubbed away. In general, the most severe corrosion occurred underneath the wedges and outside the anchor head. Corrosion spots were found on several wires per strand in these intervals. The outer wires on the remainder of the strands showed only minor surface corrosion spots or discoloration. The damage was only slightly more severe on the inner wires away from the anchor head region. All 6 wedges showed light to moderate surface corrosion on their outer surfaces and spots of discoloration on their inner surfaces. Typical strands, both with and without wedges, are shown in Figure 5.72. Anchorage zone strand corrosion ratings are shown in Figure 5.73 and summarized in Table 5.16.

Top of North Duct

Top of South Duct

Strands with Wedges

Strand

Inner Wire

Figure 5.72: Specimen 3.1 Live End Anchorage Region Elements

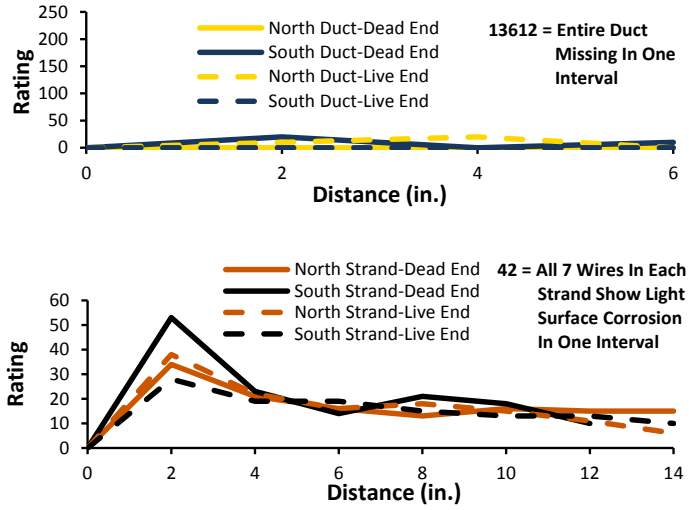

Figure 5.73: Specimen 3.1 Live and Dead End Anchorage Corrosion/Damage Ratings

Table 5.16: Specimen 3.1 Dead and Live End Anchorage Corrosion/Damage Rating Summary

	Dead End Anchorage			Live End Anchorage		
Component	**Maximum**	**Total**	**Generalized**	**Maximum**	**Total**	**Generalized**
North Duct	0	0	0	20	30	60
South Duct	20	30	60	0	0	0
North Strands	34	130	37	38	126	36
South Strands	53	139	46	28	117	33

5.2.6.8 Comparison of Anchorage Corrosion

Overall, the live end bearing plates and anchor heads showed more severe and more widespread corrosion than the dead end components. The ducts in this specimen were made of plastic and no holes were discovered in the anchorage regions. Chloride ingress would have had no effect on their damage. Generalized corrosion ratings are roughly equal for the north tendon strands, while the south tendon strands have a much higher rating at the dead end than the live end. This suggests that more chlorides may have been present at the dead end than at the live. However, the extent of corrosion in the strands is small enough that human error may have played a role in discerning the corrosion rating. Additionally, south tendon strand corrosion ratings were

only significantly higher at the dead end in the region which lay within and outside of the anchor head. Otherwise, ratings were relatively consistent.

The inconsistent corrosion between the dead end anchorage components and their live end counterparts suggests that the observed corrosion was independent of exposure. It appears that either the pourback was of high enough quality to prevent chloride ingress at the dead end, or the chlorides entered the specimen but never moved past the anchorage hardware. It is also possible that saltwater entered the specimen through the large corbel crack on the dead end and exited the sides of the specimen where efflorescence was observed. It is worth noting that at the time of autopsy, the dripper system had not been functional for at least a year. Any chlorides present within the anchorages at both ends may have entered the beam as rainwater, resulting in similar damage.

5.2.7 Specimen 3.2: Two-Way Plastic Duct, Hot-Dip Galvanized Strand

Figure 5.74: Specimen 3.2 Overall (Left) and Efflorescence at Live End Corbel Crack

Table 5.17: Specimen 3.2 Corrosion/Damage Rating Summary

Component	Maximum	Total	Generalized
Longitudinal Bars	6	42	6
Stirrups	12	126	9
North Duct	10	80	23
South Duct	20	180	51
North Strands	13	140	13
South Strands	15	182	17

During the grouting process, small air bubbles were seen at the base of the south duct grout vent on top of the specimen[7]. This specimen received dead end anchorage exposure during the testing period.

5.2.7.1 Appearance

The specimen was lightly to moderately scaled on its top, north, and south faces. Damage was most severe in and around the saltwater tray. Large, shallow surface air voids were visible on the surface of the saltwater tray. Many of those near the grout vents appear to have been "patched" by spilled grout. Numerous small popouts were present in the saltwater tray. Many contained a powdery black residue which could have been a microbial or fungal growth, as shown in Figure 5.75. No signs of corrosion were visible on the surface of the specimen.

Figure 5.75: Specimen 3.2, Black Residue in Saltwater Tray

Three primary transverse cracks crossed the top face of the specimen and extended down its sides. The side face portions of the cracks had been sealed with epoxy, which was intact at the time of autopsy. The average width of these cracks was 0.015 inches. Several longitudinal cracks extended along various portions of the top surface. These were mostly located above the specimen's ducts. Average width of the longitudinal cracks was 0.004 inches. Cracks were found extending from the live end anchorage pourback to near the re-entrant corner of the live end corbel on both faces of the specimen. A short distance of these cracks had been patched with mortar, but most of their length was not patched. This suggests that the cracks expanded some time after live load application. Efflorescence was observed at points along these cracks, suggesting the presence of moisture inside the specimen (see Figure 5.74). Crack width data is shown in Figure 5.76, and the crack diagram is shown in Figure 5.80.

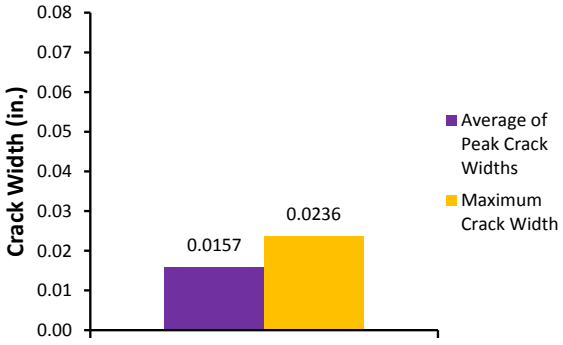

Figure 5.76: Specimen 3.2 Crack Data

5.2.7.2 Longitudinal Bars and Stirrups

Both longitudinal bars experienced very minor corrosion damage. The bars showed localized discoloration and light surface corrosion, occurring mostly at locations where stirrups had been tied (see Figure 5.79). Neither bar experienced any non-removable corrosion in any interval. The highest corrosion ratings occurred beneath the transverse surface crack nearest the live end of the autopsy region. Longitudinal bar corrosion ratings are shown in Figure 5.80 and summarized in Table 5.17.

All stirrups showed localized corrosion damage. Discoloration and corrosion were observed on all stirrups, generally occurring at the stirrups' bend points and at midspan of their horizontal regions, as shown in Figure 5.79. Pitting was observed on 2 stirrups, and corrosion which could not be scrubbed away was observed on 4 stirrups. Stirrup #1 showed the worst corrosion damage. This stirrup experienced localized pitting at the midpoint of its horizontal span. In general, corrosion ratings decreased across the autopsy region from live end to dead end. Stirrup corrosion ratings are shown in Figure 5.80 and summarized in Table 5.17.

5.2.7.3 Ducts

The exterior of the north duct was covered in chalky white residue. Some localized, dull corrosion staining was visible, as well. The top interior portion of the duct showed evidence of small voids which had formed within the top ribs of the duct. These voids appeared slightly larger on the live end half of the duct than on the dead end half. Traces of shiny white crystals were found around the upper ribs in the duct's interior, as well as intermittently on the lower region (see Figure 5.79). Light scratches were observed near midspan and near both ends of the duct on its bottom portion. This indicates that the duct was slightly damaged by the strand as it was passed through prior to stressing.

Chalky white residue and dull corrosion staining was observed on the outside of the south duct. The epoxy used to seal the joint between the duct and grout vent had separated somewhat from the duct surface. It is uncertain whether this occurred during autopsy or during construction. The inner top portion of the duct showed signs of voids within its upper transverse ribs. These voids were uniform in size along the duct's length and were made continuous by the duct's longitudinal rib, as shown in Figure 5.79. White crystals were observed near the upper ribs and on the bottom of the duct's interior. The bottom half of the duct had widespread light

gouging over more than a foot of its length, centered at midspan. It appeared that one strand had been bearing directly on the duct in that region. Duct damage ratings are shown in Figure 5.80 and summarized in Table 5.17.

The outer surfaces of the heat shrink splice showed the same chalky white residue as the rest of the north duct. The interfaces between the heat shrinks and the plastic coupler were somewhat detached. This damage may have occurred during the autopsy process (see Figure 5.77). The heat shrink tubing seemed somewhat brittle and was easy to peel back from the plastic coupler. The splice's seals may not have remained intact during the specimen's exposure.

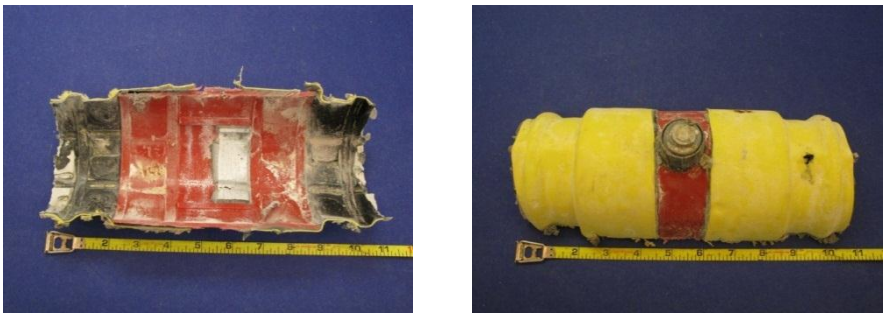

Figure 5.77: Specimen 3.2 North Duct Coupler Inner Surface (Left) and Outer Surface (Right)

5.2.7.4 Grout

The north tendon grout had transverse cracks every few inches along its length. No longitudinal cracks were found. Small voids, approximately 0.75 inches across, were found on the top surface of the grout. These voids were continuous over each half of the duct due to the duct's top longitudinal rib. The voids were slightly larger on the live end half of the grout than on the dead end half. The surface of all voids was uniformly dark gray in color. The end regions of the grout were much darker in color than the middle region, as shown in Figure 5.79. This indicates that segregation took place during or after grouting. The grout as a whole was very difficult to crack open, and its entire surface was very smooth to the touch. These observations suggest that the grout was very well consolidated. Segments of strand were visible along the bottom of the grout over much of its length. Chloride content at midspan of the grout was 0.48%.

The south tendon grout showed transverse cracks, but these cracks were only visible every few inches near midspan of the grout. Voids were observed in the top portion of the grout.

These voids were approximately 1 inch in width along the entire length of grout and were connected by the duct's top longitudinal rib (see Figure 5.79). The voids near the ends of the grout were white with a dark perimeter. Those near midspan were uniformly dark gray in color. The grout as a whole did not show any color change which might suggest density variation. Two strands were visible on the grout's lower surface centered at midspan, corresponding to the locations in the south duct which were gouged. Like the north duct grout, this grout was difficult to break in order to extract the strands within. In addition, the grout was very smooth to the touch and shiny in appearance, especially on its bottom surface. These observations suggest that the south duct grout was extremely well consolidated. Chloride content at midspan was 0.188%. Chloride content for grout in both ducts is shown in Figure 5.80.

Concentrations were well above the corrosion threshold in both tendons, indicating that breaches allowed chlorides to enter. The north tendon had a higher chloride content than the south, suggesting that the breach in the north duct coupler was more extensive than the breach in the south duct grout vent. Chlorides may have entered the north tendon through the coupler's grout vent, although damage incurred during autopsy does not allow this to be determined. Nothing suggests that chlorides entered the tendons through the anchorages. The extent of chloride travel along the tendon is not known because only one measurement per tendon was taken. However, the presence of strand corrosion along the entire strand suggests that chlorides traveled the entire length of both tendons through the strand interstices.

5.2.7.5 Strand

The north tendon strands were only slightly damaged. Small, isolated flecks of light corrosion or discoloration were found on one or more outer wires on some intervals, although the outer wires showed no damage at all on many intervals. The inner wires were slightly more damaged. However, all corrosion flecks were able to be scrubbed away with a scouring pad. Corrosion was most severe for the north duct strands in the region near midspan. Corrosion ratings were generally uniform along the entire length of the tendon.

The south tendon strands showed similar damage to that of the north strands. Some isolated flecks of corrosion were found on the strands' outer wires in a few intervals. Otherwise, the outer wires showed either discoloration or no damage at all. Again, the inner wires were more damaged, showing light surface corrosion spots in more intervals than the outer wires. All

corrosion spots could be removed with a scouring pad. Overall, the south duct strands were somewhat more damaged than the north duct strands. Corrosion ratings for the south duct strand were higher near the live end of the autopsy region than the dead end. A typical strand and inner wire are shown in Figure 5.79. Strand corrosion ratings are shown in Figure 5.80 and summarized in Table 5.17.

Similar to Specimen 2.2, the galvanized strand in this specimen was observed to have a much stronger bond with the surrounding grout than other types of strand. In addition, small bubbles were observed in the interstices of several strands, most prominently within a few inches of the end of the strands, as shown in Figure 5.78. This may be a sign that a chemical reaction occurred between the strands' zinc coating and the surrounding grout.

Figure 5.78: Specimen 3.2, Bubbles in Interstices of Galvanized Strand

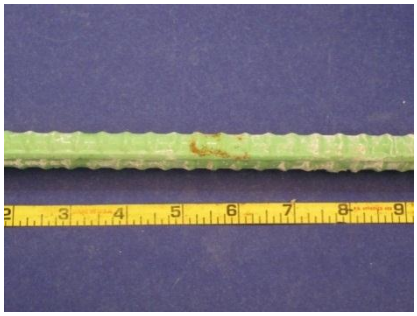

Longitudinal Bar

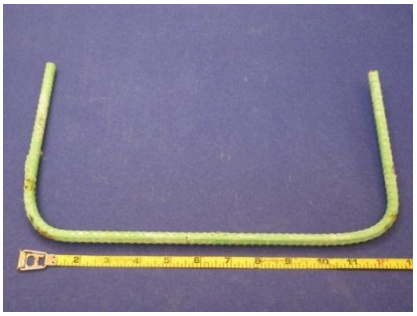

Stirrup

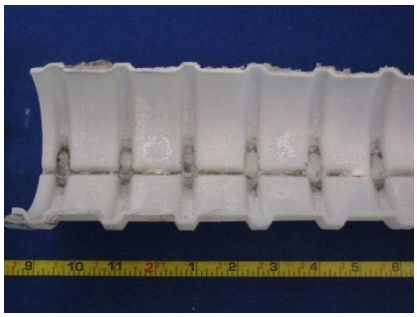

Top of North Duct

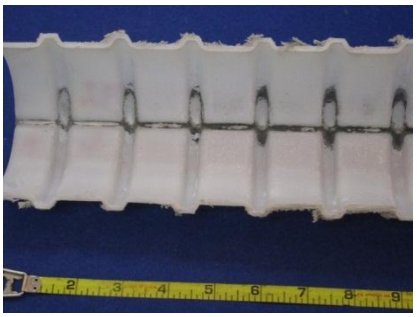

Top of South Duct

North Grout

South Grout

Strand

Inner Wire

Figure 5.79: Specimen 3.2 Main Autopsy Region Elements

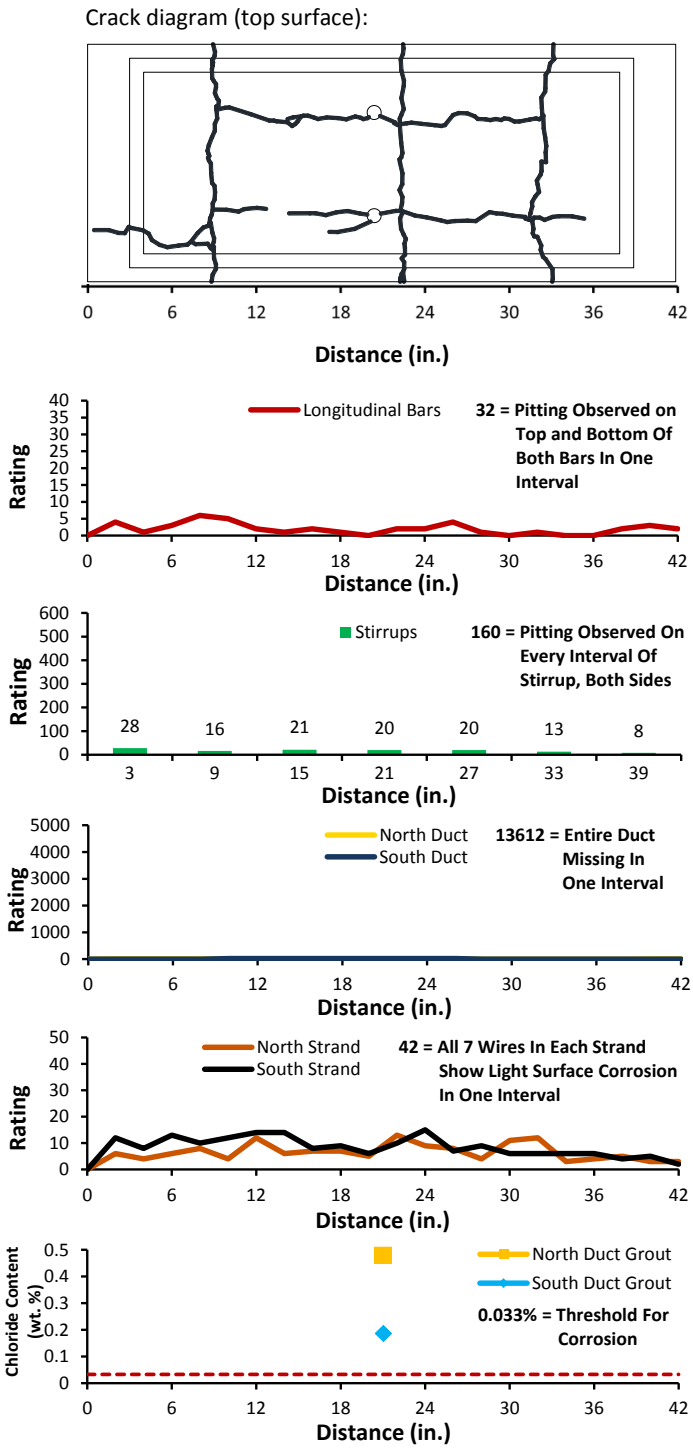

Figure 5.80: Specimen 3.2 Crack Map and Corrosion/Damage Rating Plots

5.2.7.6 Dead End Anchorages

The epoxy used to seal the exposed surfaces of both dead end anchorages was mostly intact on the bearing plates and mostly missing on the anchor heads. Both bearing plates showed only localized light to moderate corrosion over a small portion of their exposed area. Corrosion was much more widespread on the underside and along the lower interior edges of the bearing plates. Some localized discoloration was also found on the top and side surfaces. The duct tape used to splice the ducts to the anchorages was mostly intact at the time of autopsy. Some light corrosion was found on the north anchorage on the areas which had been covered by duct tape. The corrosion in this area was more severe on the south anchorage. Large patches of moderate corrosion were found on the inboard surface of the north anchor head, as well as light discoloration on its other surfaces. Only one small spot of corrosion was observed on the interior side of the south anchor head. The level of discoloration on the other surfaces was comparable to the north anchor head. The north and south anchorages and anchor heads are shown in Figure 5.81.

North Anchorage

South Anchorage

North Anchor Head

South Anchor Head

Figure 5.81: Specimen 3.2 Dead End Anchorages and Anchor Heads

The exterior of both anchorage zone ducts showed traces of chalky white residue. Isolated corrosion staining was also observed on both ducts where they were spliced to the anchorages. Scattered patches of shiny white crystals were found on the interior portions of both ducts. Evidence of small voids was also seen on the top interior portion of both ducts. The north duct had some light gouging due to strands rubbing near the anchorage splice. There was no such damage observed in the south duct. North and south ducts are shown in Figure 5.82. Anchorage zone duct corrosion ratings are shown in Figure 5.85 and summarized in Table 5.18.

Both north and south tendon anchorage zone grouts showed evidence of voids on their top surfaces. These voids did not appear to be connected by the top longitudinal rib of the duct. The bottom surfaces of both grouts were smooth and appeared extremely well consolidated. Like the main autopsy region grouts, the dead end anchorage grouts were very difficult to chip away. The south duct grout was much darker gray in color than the north duct grout, suggesting that segregation may have occurred during grouting. North and south tendon grouts are shown in Figure 5.82.

The dead end anchorage zone strands experienced localized discoloration and light surface corrosion along their entire lengths. The outer wires in all strands showed discoloration and flecks of corrosion which could be removed with a scouring pad over many intervals. Damage was the worst at the exposed strand ends and in the region where the wedges were located. The inner wire on each strand was typically more extensively corroded or discolored near the wedge region than the outer wires. Inner wire damage further into the specimen was comparable to that of the outer wires. All wedges were found to be intact with only light localized corrosion or discoloration on their outer surfaces. Typical strands, with and without wedges, are shown in Figure 5.82. Dead end anchorage zone strand corrosion ratings are shown in Figure 5.85 and summarized in Table 5.18.

Top of North Duct

Top of South Duct

North Grout

South Grout

Strands with Wedges

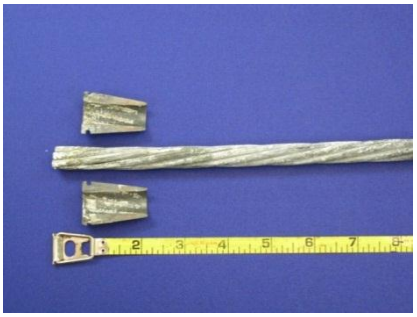

Strand

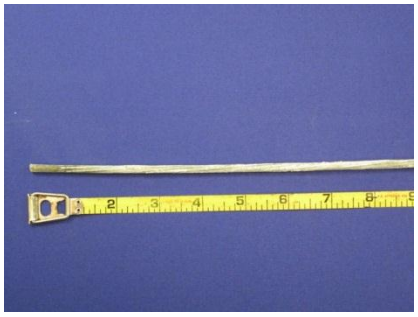

Inner Wire

Figure 5.82: Specimen 3.2 Dead End Anchorage Region Elements

5.2.7.7 Live End Anchorages

Most of the epoxy on the exposed surfaces of the live end anchorages was gone. The south bearing plate experienced light corrosion on some of its exposed surface, while the north bearing plate had moderate corrosion over the majority of its exposed area. The north and south bearing plates were moderately corroded on their bottom surfaces and on all inside edges of the bearing plates. This damage was more severe on the north anchorage than the south anchorage. Although the duct tape splices were mostly intact on both anchorages, there was extensive moderate corrosion and some pitting found underneath the duct tape. The north anchor head experienced widespread moderate corrosion on its inner surface and lighter localized corrosion on much of its other surfaces. The south anchor head was much less damaged, with light to moderate localized corrosion on its inside surface and extremely localized light corrosion or discoloration elsewhere. The north and south anchorages and anchor heads are shown in Figure 5.83.

North Anchorage

South Anchorage

North Anchor Head

South Anchor Head

Figure 5.83: Specimen 3.2 Live End Anchorages and Anchor Heads

The outer surfaces of both ducts showed a chalky white residue. Additionally, the outer surface of the north duct was significantly stained at the duct's interface with the bearing plate due to the corrosion which had occurred there. Inside the duct, evidence of small voids was found in the duct's upper ribs. The voids appeared to be connected by the duct's narrow longitudinal rib. Patches of shiny white crystals were found on the inside surfaces of the duct. In addition, several light scratches were found on the inside of the south duct. These most likely occurred while the strands were being threaded through the duct. Light scratches were seen in the north duct, but these were not nearly as extensive and occurred over only one interval. North and south ducts are shown in Figure 5.84. Live end anchorage zone corrosion ratings are shown in Figure 5.85 and summarized in Table 5.18.

Both north and south tendon grouts showed evidence of voids on their top surfaces. These voids appeared to be connected by the top longitudinal rib of the surrounding duct. Both grouts were extremely smooth to the touch. However, some variation in color on the grouts' surface suggests that segregation may have been an issue. The north grout was heavily stained near its interface with the bearing plate. Neither grout appeared to be cracked at the time of autopsy. North and south grouts are shown in Figure 5.84.

Damage to the live end anchorage zone strands was light to moderate. The outer wires of all strands showed some discoloration and localized light corrosion in most intervals. The inner wires showed similar damage, although corrosion was somewhat more widespread in the inner wires. Spots of corrosion which could not be scrubbed away were found on the inner wires of two of the north duct strands. Overall, corrosion ratings were highest where the strands had been exposed and where they had been inside the anchor heads. All wedges were intact, showing only localized light corrosion and discoloration. Most of this damage was observed on the outer surfaces of the wedges. Typical strands, with and without wedges, are shown in Figure 5.84. Live end anchorage zone strand corrosion ratings are shown in Figure 5.85 and summarized in Table 5.18.

Top of North Duct

Top of South Duct

North Grout

South Grout

Strands with Wedges

Strand

Inner Wire

Figure 5.84: Specimen 3.2 Live End Anchorage Region Elements

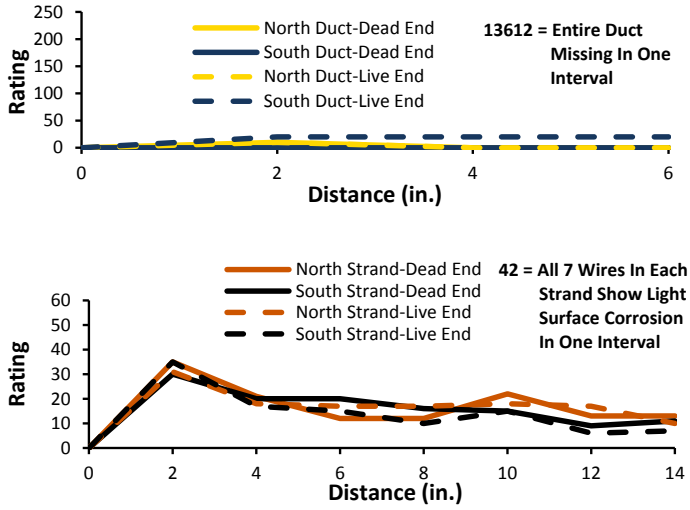

Figure 5.85: Specimen 3.2 Live and Dead End Anchorage Corrosion/Damage Ratings

Table 5.18: Specimen 3.2 Live and Dead End Anchorage Corrosion/Damage Rating Summary

	Dead End Anchorage			Live End Anchorage		
Component	**Maximum**	**Total**	**Generalized**	**Maximum**	**Total**	**Generalized**
North Duct	10	10	20	10	10	20
South Duct	0	0	0	20	60	120
North Strands	35	128	37	31	128	37
South Strands	30	121	35	35	105	30

5.2.7.8 Comparison of Anchorage Corrosion

The live end bearing plates and anchor heads appeared marginally more corroded than their dead end counterparts. Damage to the anchorage zone ducts was more severe at the live end than at the dead end. However, this is inconsequential because the damage was not caused by corrosion, nor was it severe enough to allow chloride ingress into the tendon. Damage to the strands was comparable in both anchorage regions. The strand corrosion rating plots are nearly identical for the live and dead end strands. No clear correlation between exposure and corrosion can be seen. These factors suggest that chlorides did not enter the specimen at its dead end, perhaps due to the absence of any large cracks on the specimen's dead end face. Again, it should be noted that the dripper system had not been operational for at least one year before autopsy.

5.2.8 Specimen 3.4: One-Way Plastic Duct, Hot-Dip Galvanized Strand

Figure 5.86: Specimen 3.4 Overall (Left) and Discoloration Around Surface Cracks (Right)

Table 5.19: Specimen 3.4 Corrosion/Damage Rating Summary

Component	Maximum	Total	Generalized
Longitudinal Bars	5	46	7
Stirrups	6	89	6
North Duct	10	180	51
South Duct	10	60	210
North Strands	12	150	14
South Strands	17	194	18

This specimen did not receive anchorage exposure during the testing period.

5.2.8.1 Appearance

Light scaling was observed in the saltwater tray as well as the north and south faces of the specimen. Some small surface air voids were present on the north and south faces of the specimen and in the saltwater tray. Many of the latter had been patched by grout spillage which occurred at the specimen's grout vents. There were many small flecks of a black residue in the saltwater tray which appeared to be a microbial or fungal growth. A faint dark discoloration was visible alongside several of the specimen's surface cracks. This discoloration extended about ½ inch on either side of the cracks, as shown in Figure 5.86. The protruding live end of the specimen's Dywidag bar appeared to have been run over by a vehicle during the test period. It is unknown what effect, if any, this may have had on stresses or cracking within the live end of the specimen.

The specimen had 5 transverse cracks. Three of these were continuous across the top surface, while the other 2 only extended a few inches into the saltwater tray. All transverse cracks extended down the north and south faces of the specimen. After construction, they had been sealed with epoxy which was still intact at the time of autopsy. Average width of the transverse cracks was 0.02 inches. Two longitudinal cracks were observed on the specimen's top face. Both passed through one grout vent, and the crack closer to the north face of the specimen was the longer of the two. Average width of the longitudinal cracks was 0.008 inches. In addition, some very small, random cracks were observed on the specimen's top face near the live end. Cracking extending from the live end anchorage pourback towards the re-entrant corner of the corbel had occurred during live load application. Most of these cracks had been sealed with mortar, but the cracks appeared to have propagated further towards the re-entrant corner during exposure. Some efflorescence was observed around the length of these cracks which had not been patched, as seen in Figure 5.87. This indicates the presence of moisture inside the specimen. Crack width data is shown in Figure 5.88, and the crack diagram is shown in Figure 5.92.

Figure 5.87: Specimen 3.4, Efflorescence at Live End Corbel and Pourback Cracks

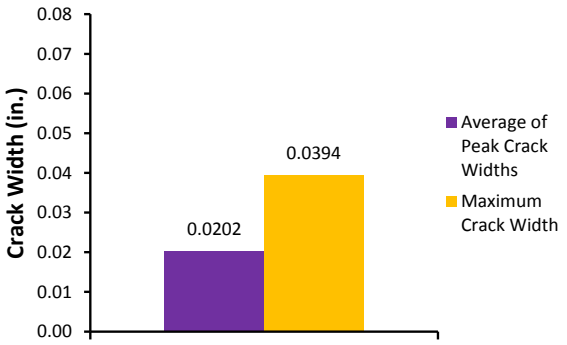

Figure 5.88: Specimen 3.4 Crack Data

5.2.8.2 Longitudinal Bars and Stirrups

Damage to both the north and south longitudinal bars was light, with most of the bars' surface area showing no signs of corrosion whatsoever (see Figure 5.91). Light localized surface corrosion and discoloration occurred at many of the points on the bars where stirrups had been tied. All visible corrosion was mild and could be removed with a scouring pad. The north bar was slightly more damaged than the south bar. Only isolated discoloration was observed on the south bar. Overall, corrosion ratings were highest on the intervals below the specimen's two largest transverse surface cracks. Longitudinal bar corrosion ratings are shown in Figure 5.92 and summarized in Table 5.19.

Corrosion observed in the stirrups was similarly mild. Light corrosion and discoloration was observed at the stirrups' bend points and along their horizontal portions, as shown in Figure 5.91. Moderate corrosion was seen on only two stirrups. Otherwise, all observed corrosion could be scoured away. Corrosion ratings showed little variation along the length of the autopsy region, although the five middle stirrups' ratings were slightly higher. Stirrup corrosion ratings are shown in Figure 5.92 and summarized in Table 5.19.

5.2.8.3 Duct

The exterior of the north duct was covered with a chalky white residue. No corrosion staining was observed. The pattern of the residue on the top of the duct in particular suggests that water was present there, as shown in Figure 5.91. Inside, the duct showed a shinier white residue along most of its length. Evidence of voids was found in the top inner portion of the duct. Most

of these voids appeared to be confined in the top transverse ribs of the duct. However, evidence of one continuous void was visible within approximately 6 inches of the live end of the autopsy region. This void was visible from the cut live end of the duct before the grout was extracted. The bottom interior portion of the duct was marked with intermittent light gouges which were found along nearly its entire length. The pattern of the gouges suggests that two or more strands were bearing directly on the duct before grouting occurred (see Figure 5.89).

Figure 5.89: Specimen 3.4, Strand Gouging on Bottom of North Duct

Damage to the south duct was similar to that of the north duct. Chalky white residue with apparent water marks was observed on the outside of the duct, and shiny white residue was found on the inside, as shown in Figure 5.91. Some extremely isolated corrosion staining was observed at a few points along the duct's length. The duct's midspan grout vent had been sealed with a zip tie, which was intact at the time of autopsy. No epoxy was found at the grout vent-duct interface. Inside the duct, evidence of voids was observed. The voids were isolated to the transverse ribs of the duct on the dead end half, while one continuous void was found on the live end half of the duct. This suggests that the grout vent at midspan may have slipped and blocked the flow of grout to the live end of the duct. Light gouges were seen along most of the duct's length on its bottom interior portion. It appeared that all three strands were bearing on the duct during the life of the specimen. Duct corrosion ratings are shown in Figure 5.92 and summarized in Table 5.19.

The north duct coupler was physically intact, and its two mechanical fasteners were functional at the time of autopsy. Similar discoloration to that of the north duct was observed on both the inner and outer surfaces of the coupler. Evidence of one small void was observed near the grout vent on the top inner surface of the coupler. The gasket on the bottom half of the

coupler was mostly intact, and a clear boundary between cement paste and grout residue was observed over most of its length. One breach in the gasket was found on the live end of the coupler, indicated by cement paste leaking through the gasket. The top gasket was in worse condition. The live end half of the gasket was breached and had allowed cement paste to fill almost 1/3 of the coupler's sealed area (see Figure 5.90). These breaches suggest that the gasket was not firmly applied to the full perimeter of the duct before concrete was cast around it.

Figure 5.90: Specimen 3.4 North Duct Coupler Outer Surface (Left) and Breach in Upper Gasket (Right)

5.2.8.4 Grout

The north tendon grout was cracked transversely every few inches along its length. Grout color was uniformly gray, although a few darker spots were found between duct ribs on the bottom of the grout. One large void, approximately 2 inches across, was found on nearly the entire live end half of the duct. Smaller voids, ranging in size from 1 to 1.5 inches, were found confined to the areas where the duct's ribs had been on the dead end half of the grout. The surface of the small voids was white with a gray perimeter. The surface of the large void was uniformly light gray, and some craze cracks were found at isolated points along the length of the void. Strands were visible on the surface of the grout over most of its length. All three strands were visible near the live end of the autopsy region (see Figure 5.91). Chloride content was 0.45% at midspan and 0.039% 6 inches from the live end of the grout.

The south tendon grout was similar in appearance to the north tendon grout. The south tendon grout was cracked every few inches along its length. No longitudinal cracks were found.

Some color variation was observed on the underside of the grout. The ends of the grout were darker in color than the interior region, suggesting that segregation had taken place (see Figure 5.91). One continuous void, about 1.5 inches wide, was observed along most of the live end half of the grout. On the dead end half of the grout, all voids were approximately 1 inch wide and isolated to the ribs of the duct. All voids were somewhat smaller than in the north grout, although their color was comparable. All three strands were visible on the underside of the grout along most of its length, and at least one strand was visible along the entire length of the grout. Chloride content was 0.36% at midspan. Chloride content for both ducts is shown in Figure 5.92.

The midspan grout chloride content of both tendons was above the corrosion threshold, showing that both the north duct coupler and the south duct grout vent were breached by chlorides during exposure. The grout vent located on the north duct coupler may have leaked as well, but this cannot be determined due to autopsy damage. It is not believed that any chlorides entered the tendon through the anchorages. The chloride content in the north tendon at 6 inches from the live end was much lower than midspan, although still above the corrosion threshold. Because no other means of chloride ingress into the duct were found, this means that chlorides entered at midspan and traveled along the live end of the tendon. The chlorides may have passed through the strand interstices or along the continuous void. Strand corrosion suggests that chlorides found their way to the strands in both tendons.

5.2.8.5 Strand

Damage to the north tendon strands was minor and relatively uniform along the length of the tendon. Small flecks of discoloration or light surface corrosion were observed on one or more outer wires on almost all intervals of every strand. The inner wires were similarly damaged, although corrosion spots appeared more frequently. All visible corrosion could be removed with a scouring pad.

The south tendon strands were slightly more damaged than the north duct strands. On the outer wires, discoloration and spots of corrosion were found on almost every interval of every strand. On one interval of one strand, this corrosion could not be removed with a scouring pad. The inner wires were uniformly discolored, and light corrosion spots were found along much of their length. Corrosion ratings were higher in the south strands than the north. Ratings reached their peak roughly 15 inches from the dead end of the autopsy region. A typical strand and inner

wire are shown in Figure 5.91. Strand corrosion ratings are shown in Figure 5.92 and summarized in Table 5.19.

As with previous specimens containing hot-dip galvanized strand, the strands in this specimen were observed to have a very strong bond with the surrounding grout. Also, some small bubbles were found in the strands' interstitial grout, suggesting that a chemical reaction may have occurred.

Longitudinal Bar

Stirrup

Top of North Duct

Top of South Duct

North Grout

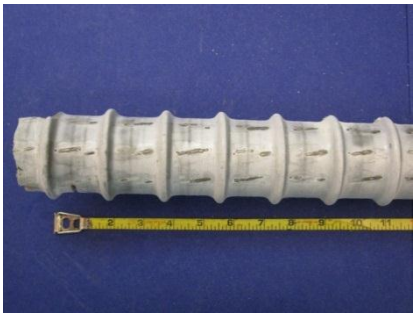

South Grout

Strand

Inner Wire

Figure 5.91: Specimen 3.4 Main Autopsy Region Elements

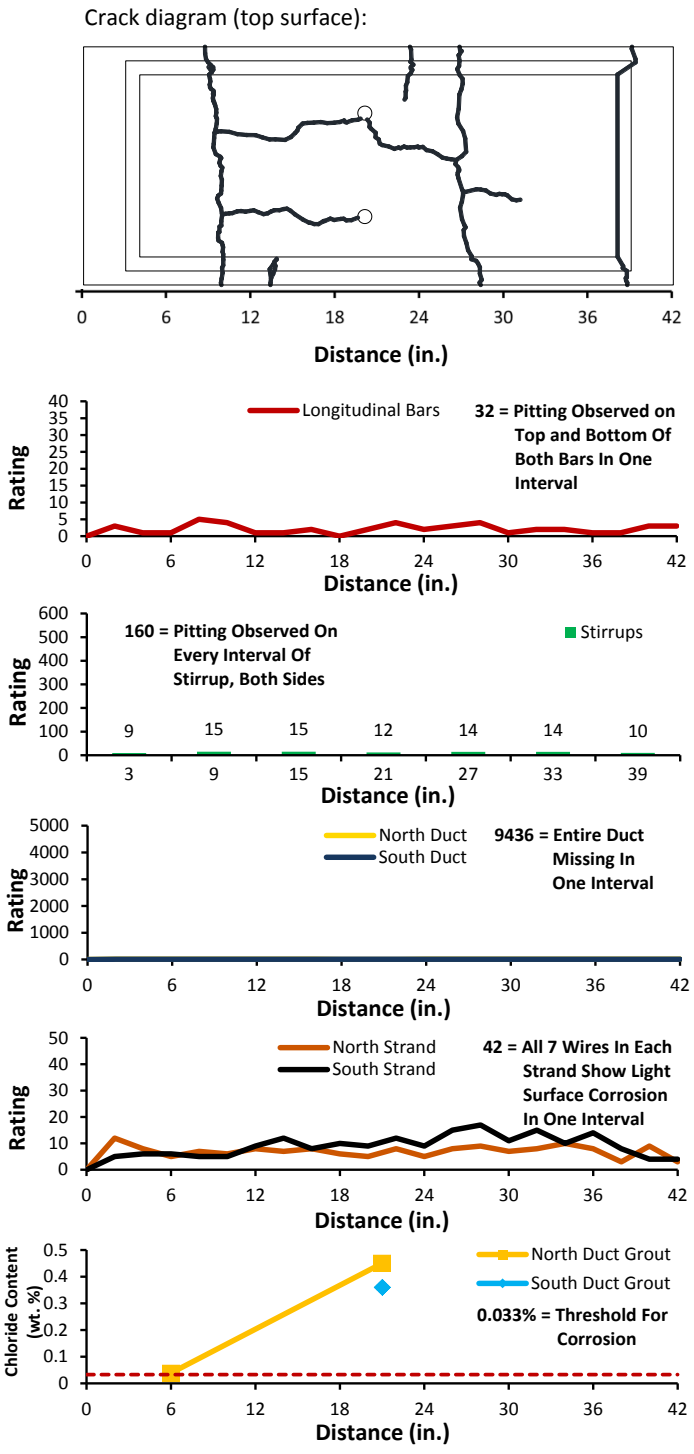

Figure 5.92: Specimen 3.4 Crack Map and Corrosion/Damage Rating Plots

5.2.8.6 Dead End Anchorage

The epoxy used to seal the exposed surfaces of the anchorages prior to applying the pourback were partially intact on the bearing plate and completely gone on the anchor head. The north bearing plate showed some very localized light surface corrosion, mostly on its lower half. Isolated light to moderate surface corrosion was found on the underside of the north bearing plate, mostly occurring near the grout vent located there. Some pitting was observed on the lower, inside edge of the bearing plate. The south bearing plate was more extensively corroded, with moderate surface corrosion occurring on most of its lower half. Moderate surface corrosion and some pitting were observed around the inside edges of the bearing plate, as well. The duct tape used to seal both bearing plates to their ducts was intact, with some light to moderate corrosion occurring on the anchorage surfaces beneath. The north anchor head showed only light surface corrosion on its side surface near the bearing plate, with faint discoloration occurring on other surfaces. The south anchor head was similar in appearance. However, the corrosion was less prominent and the discoloration more widespread. North and south anchorages and anchor heads are shown in Figure 5.93.

Table 5.20: Specimen 3.4 Anchorage Corrosion/Damage Rating Summary

Component	Maximum	Total	Generalized
North Duct	200	240	480
South Duct	0	0	0
North Strands	21	26	77
South Strands	33	28	84

North Anchorage

South Anchorage

North Anchor Head

South Anchor Head

Figure 5.93: Specimen 3.4 Anchorages and Anchor Heads

The outside surface of both ducts showed the same chalky white residue which was found on the ducts in the main autopsy region. Large deposits of cement paste were found in the splice region of both ducts. This occurred because the ducts are slightly smaller than the anchorage opening, which allowed paste to enter and adhere to the ducts. On their inner surface, both ducts also contained traces of a shiny white residue. Evidence of voids was found on the top inner portion of both ducts. These voids appeared to be contained within the ribs of the ducts. The north duct experienced light gouging, mostly near the duct's joint with the anchorage. No gouging was observed in the south duct. North and south ducts are shown in Figure 5.95. Anchorage zone corrosion ratings are shown in Figure 5.94 and summarized in Table 5.20.

The south tendon grout was severely damaged during extraction, so no meaningful observations could be made. The north tendon grout showed signs of small voids on its top surface and a long void within the anchorage itself. Over the region which had been covered by the north duct, the grout appeared to be well consolidated. The grout in this region was very dark and very hard to break. Two strands were visible on the grout's bottom surface over the entire

duct region. The grout was not observed to be cracked. North and south tendon grouts are shown in Figure 5.95.

The anchorage zone strands in both tendons showed similar levels of corrosion. Small flecks of light surface corrosion and discoloration were observed over the entire length of strand, generally on more than one wire per interval. Outer wire damage was greatest in the region which had been inside the wedges. Inner wire damage was uniform, with discoloration and light surface corrosion spots found along the entire length of wire on every strand. All wedges were physically intact, showing only mild surface corrosion on their outer surfaces and isolated spots of discoloration inside. Typical strands, with and without wedges, are shown in Figure 5.95. Anchorage zone strand corrosion ratings are shown in Figure 5.94 and summarized in Table 5.20.

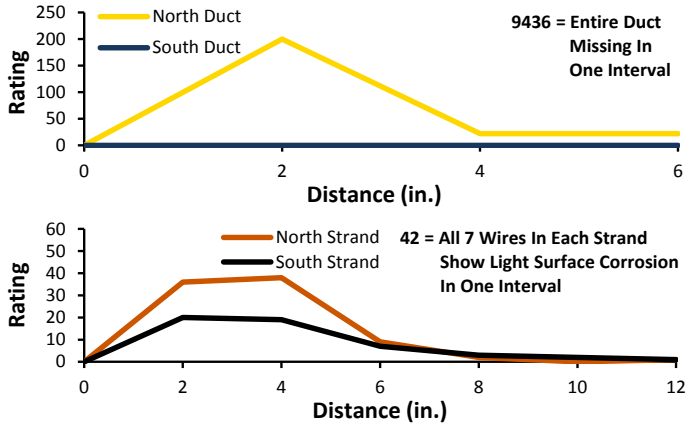

Figure 5.94: Specimen 3.4 Anchorage Zone Corrosion/Damage Ratings

Top of North Duct

Top of South Duct

North Grout

South Grout

Strands with Wedges

Strand

Inner Wire

Figure 5.95: Specimen 3.4 Anchorage Region Elements

5.2.9 Specimen 4.2: One-Way Plastic Duct, Stainless Steel Strand

Figure 5.96: Specimen 4.2 Overall (Left) and Discoloration Around North Grout Vent (Right)

Table 5.21: Specimen 4.2 Corrosion/Damage Rating Summary

Component	Maximum	Total	Generalized
Longitudinal Bars	4	26	4
Stirrups	10	78	6
North Duct	400	4740	1354
South Duct	250	2640	754
North Strands	6	6	1
South Strands	6	8	1

This specimen did not receive anchorage exposure during the test period.

5.2.9.1 Appearance

The specimen showed light scaling on its top, north, and south faces. Large aggregate was visible over a large portion of the edges surrounding the saltwater tray. Some shallow surface air voids were observed on the top, north, and south faces of the specimen. Those near the grout vents in the saltwater tray had been patched by the grout which spilled during the grouting process. Some faint corrosion and discoloration was observed around the base of the north grout vent, indicating the presence of corrosion within the specimen (see Figure 5.96).

Two transverse cracks were found on the specimen's top face. These cracks extended down the north and south faces of the specimen, although only one of the cracks was continuous over the entire width of the specimen. The epoxy used to seal the vertical side face portions of the transverse cracks was intact at the time of autopsy. Average width of the transverse cracks

was 0.02 inches. One short longitudinal crack was observed emanating from the south grout vent. The average width of this crack was 0.04 inches. Cracks extending from the anchorage pourbacks on both ends of the specimen toward the corbel re-entrant corner had formed during exposure. A small length of the cracks on the live end had been patched with mortar, indicating that they occurred during live load application. The remaining portion of the live end cracks and all of the dead end cracks formed after live load application. Some water was observed leaking from the unpatched portions of the cracks, indicating the presence of moisture inside the specimen (see Figure 5.97). Crack width data is shown in Figure 5.98, and the crack diagram is shown in Figure 5.102.

Figure 5.97: Specimen 4.2, Efflorescence and Moisture around Dead End Corbel Crack

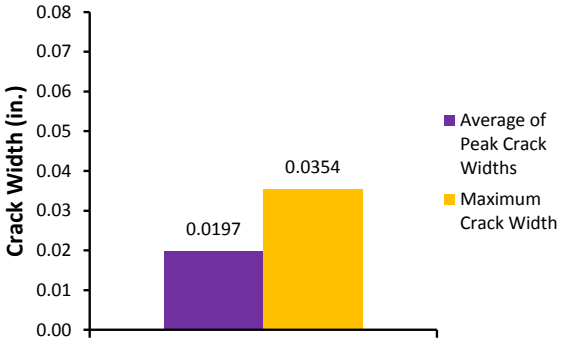

Figure 5.98: Specimen 4.2 Crack Data

5.2.9.2 Longitudinal Bars and Stirrups

Both the north and south longitudinal bars experienced no corrosion and very little discoloration. Isolated stain spots were found in the vicinity of the stirrup tie locations, as shown in Figure 5.101. Overall, damage was comparable on both bars, and the extent of staining did not coincide with the locations of the specimen's surface cracks. Longitudinal bar corrosion ratings are shown in Figure 5.102 and summarized in Table 5.21.

Corrosion damage to the stirrups was mild. Discoloration and light surface corrosion were generally found in the vicinity of the stirrups' bend points and midspan of their horizontal regions. Almost all visible corrosion could be removed with a scouring pad. However, stirrup #5, shown in Figure 5.101, showed pitting over one interval at its center. The highest corrosion ratings were observed in the stirrups underneath the specimen's transverse surface cracks. Stirrup corrosion ratings are shown in Figure 5.102 and summarized in Table 5.21.

5.2.9.3 Duct

The north plastic duct showed a large amount of chalky white residue on its outer surface. This residue formed small swirls near the live end of the duct, suggesting that small pockets of moisture may have been present there. Patches of shiny white crystals were found inside the duct. Evidence of a large, continuous void was found on the inner top portion of the duct, extending from the live end of the duct to the splice at midspan. Smaller voids were observed on the dead end half of the duct. These appeared to be confined to the top ribs of the duct. Gouges were observed on the duct's bottom interior surface, suggesting that at least one strand had been bearing on the duct over its entire length. Deep scratches, amounting to approximately 10% of the duct's thickness, were seen on the top interior surface of the duct along almost its entire length. This damage was likely caused by the highly curved strands as they were threaded through the duct prior to stressing (see Figure 5.101).

Damage to the south duct was comparable to that of the north duct. Chalky white residue was found on the outside of the duct, and isolated spots of shiny white crystals were found inside. Evidence of a large void was observed on the live end half of the duct's top interior surface. This void extended from 2 inches from the live end of the duct to just past midspan (see Figure 5.101). Smaller voids were found on the dead end half of the duct. These voids appeared to be completely contained within the top ribs of the duct. Extensive scratching was present on the

entire interior of the duct, amounting to about 10% of the duct's thickness in places. No gouges were observed. The epoxy used to seal the grout vent at its intersection with the duct was somewhat separated from the duct surface. It is unknown whether this occurred during autopsy or during exposure. Duct corrosion ratings are shown in Figure 5.102 and summarized in Table 5.21.

The north duct coupler was physically intact at the time of autopsy, and both of its mechanical fasteners were operational. The coupler showed similar discoloration to that of the north duct, both inside and out, as seen in Figure 5.99. Evidence of a large void was found on the top inside surface of the coupler. The gasket appeared mostly intact. However, one small breach was found on the lower, live end portion of the gasket. A small amount of cement paste had intruded into the inner portion of the coupler at that location, as shown in Figure 5.99. On the upper half of the coupler, a clear boundary between grout and gasket was observed, indicating that a positive seal was made there.

Figure 5.99: Specimen 4.2 Coupler Outer Surface (Left) and Lower Gasket Breach (Right)

5.2.9.4 Grout

The large curvature of the strands caused both the north and south grout to fracture along their lengths as the ducts were removed. Overall color appeared to be uniform for both grouts. Large, continuous voids, approximately 2 inches across, were present on the live end half of each grout, and smaller voids were seen on the dead end half (see Figure 5.101). These voids were approximately 0.75 inches in width. The smaller voids were mostly isolated by the ducts'

transverse ribs, although some bubbling and discoloration was observed between voids, as shown in Figure 5.101. This suggests that pressure was not uniform on the top of the grout. Chloride content was 0.39% at midspan of the north grout and 0.32% at midspan of the south grout. Chloride content for north and south grouts is shown in Figure 5.102.

The uniformly high chloride contents at midspan of both tendons indicate that the north duct coupler and the south duct grout vent were breached to a similar extent. The grout vent on the north duct coupler may have leaked as well, but it was too damaged from the autopsy to determine its soundness. The two anchorage pourbacks were intact, and there was no evidence that chlorides may have entered there. Large, continuous voids may have allowed chlorides to spread easily along both tendons. However, only one reading per tendon was taken and no signs of corrosion were found on the strands, so the extent of chloride penetration is unknown.

5.2.9.5 Strand

All strands in both the north and south tendons were nearly immaculate upon inspection. No corrosion or corrosion staining was found on the outer wires of any strand. The only discoloration observed was a light coating of white-gray grout residue (see Figure 5.101). This could easily be rubbed off over all intervals. When compared to a length of stainless steel strand which had been stored indoors for the duration of the exposure period, the strands extracted from the specimen showed no discernible difference in appearance, as shown in Figure 5.101. Small flecks of light surface corrosion were found at the dead end of every strand's inner wire, but this may have been due to water intrusion during the autopsy process. Strand corrosion ratings are shown in Figure 5.102 and summarized in Table 5.21.

The stainless steel strands were observed to have a much weaker bond with the surrounding grout than other strand types. Grout easily fell away from the strands after the ducts were removed due to the weak bond and the strands' large curvature. Additionally, the strands in both ducts showed evidence of debonding after the concrete had been chipped away from the autopsy region, as shown in Figure 5.100.

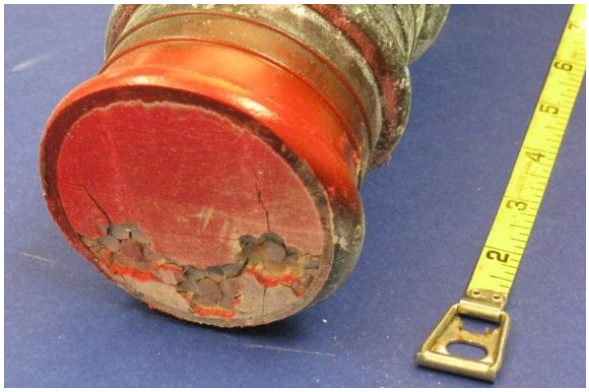

Figure 5.100: Specimen 4.2, Debonded Strands at Live End of South Duct

Longitudinal Bar

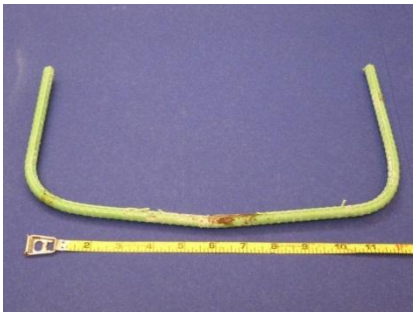

Stirrup

Top of North Duct

Top of South Duct

North Grout

South Grout

Strand

Comparison with Unused Strand

Figure 5.101: Specimen 4.2 Main Autopsy Region Elements

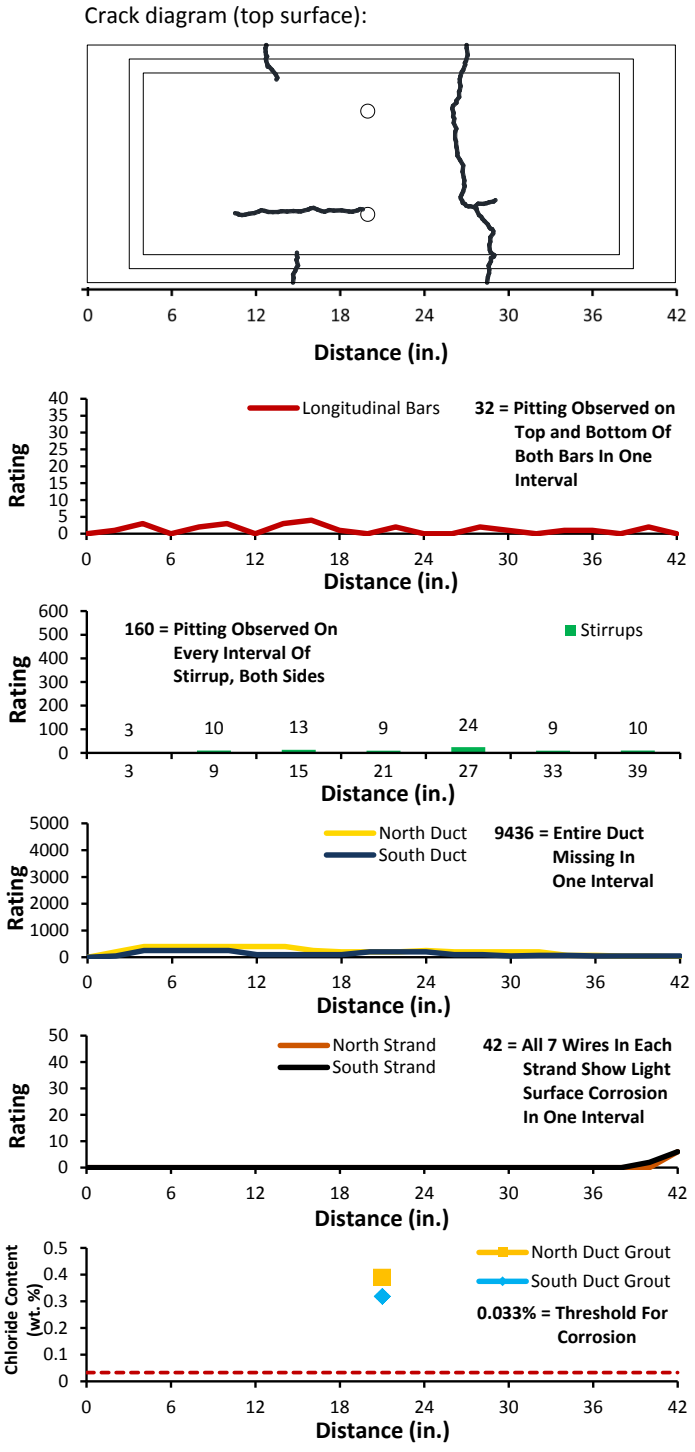

Figure 5.102: Specimen 4.2 Crack Map and Corrosion/Damage Rating Plots

5.2.9.6 Dead End Anchorages

The epoxy used to coat the exposed surfaces of both anchorages was partially intact on anchorages. Light to moderate surface corrosion was observed on the exposed surface of both bearing plates, tending to concentrate on the lower half of the bearing plates. Some pitting was observed on the bottom edge of the north bearing plate. The bottom edge of the south bearing plate had been cut off during autopsy, so no observations could be made there. Spots of light to moderate corrosion were found on the portions of the anchorages which were cast against concrete, tending to occur mostly on the underside of both bearing plates. The duct tape used to splice the ducts into the bearing plates was mostly intact. Only light discoloration was found on the anchorages beneath the duct tape. Moderate surface corrosion was found on the inner surface of both anchor heads, and light surface corrosion was present on much of their side and outer surfaces. North and south anchorages and anchor heads are shown in Figure 5.103.

North Anchorage

South Anchorage

North Anchor Head

South Anchor Head

Figure 5.103: Specimen 4.2 Anchorages and Anchor Heads

Table 5.22: Specimen 4.2 Anchorage Corrosion/Damage Rating Summary

Component	Maximum	Total	Generalized
North Duct	220	240	721
South Duct	0	0	0
North Strands	19	55	18
South Strands	14	51	17

Only a short length of anchorage zone duct was recovered for both the north and south anchorages. These duct segments were also heavily damaged, limiting the conclusions which could be drawn. Chalky white residue was present on the outer surface of both ducts, and a shinier white residue was found inside the ducts. No evidence of voids was observed. The north duct showed substantial scratches on its bottom interior surface and some faint scratches on its top interior surface. The strands appeared to have damaged the duct as they were being threaded through prior to stressing. No scratches or gouges were observed within the south duct. North and south tendon ducts are shown in Figure 5.104. Anchorage zone duct corrosion ratings are shown in Figure 5.105 and summarized in Table 5.22.

The north and south anchorage zone grouts shattered as the ducts were being removed, so observations were limited. Some small voids and bubbles were visible on the top surface of the south grout near the anchorage. Grout color was slightly darker near the interior of the specimen than near the anchor head, indicating that segregation may have occurred.

The north and south anchorage zone strands were not in the same condition as those in the main autopsy region of the specimen. Discoloration was found on all strands in the region where wedges had been applied, both on the inner and outer wires of every strand. The only corrosion present on the anchorage zone strands was one small spot found on the end away from the anchor head on the inner wire of one south duct strand. All discoloration could be wiped away to reveal clean strand underneath. Typical strands, with and without wedges, are shown in Figure 5.104. Anchorage zone strand corrosion ratings are shown in Figure 5.105 and summarized in Table 5.22.

Top of North Duct

Top of South Duct

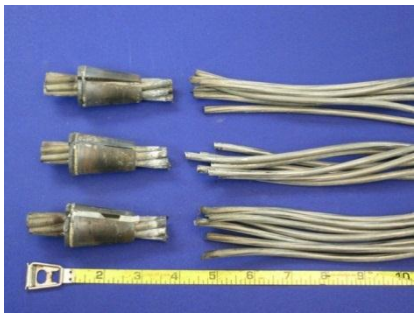

Strands with Wedges

Strand

Inner Wire

Figure 5.104: Specimen 4.2 Anchorage Region Elements

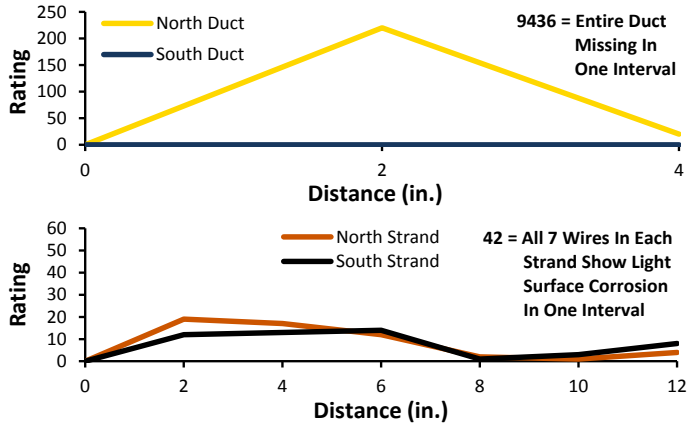

Figure 5.105: Specimen 4.2 Anchorage Corrosion/Damage Ratings

5.2.10 Specimen 7.1: Fully Encapsulated Tendon, Conventional Strand

Figure 5.106: Specimen 7.1 Overall (Left) and Corrosion Staining in Saltwater Tray Wells (Right)

Table 5.23: Specimen 7.1 Corrosion/Damage Rating Summary

Component	Maximum	Total	Generalized
Epoxy-Coated Longitudinal Bars	6	63	9
Uncoated Longitudinal Bars	32	360	51
Stirrups	6	128	9
Duct	10	80	23
Strands	19	296	28

This specimen was constructed such that the post-tensioning strands and hardware were electrically isolated. This required the use of longer, specially equipped anchorages. Accordingly, the specimen's pourback regions were made longer to accommodate this. Due to the additional width of the anchorage components, the specimen only had one tendon which ran down the centerline of the specimen. To ensure that the specimen could be properly monitored using AC impedance measurements, two additional, uncoated longitudinal bars were provided in the tension zone of the specimen. This allowed electrical current to flow efficiently from concrete to the reinforcement cage. This specimen received dead end anchorage exposure during the test period.

5.2.10.1 Appearance

Moderate scaling was observed on the specimen's saltwater tray. Some light scaling was also observed near the top of the specimen's north and south faces. Several small surface air

voids were visible on the north face of the specimen. Small puddles of grout were present around the live end and dead end grout vents. The live end grout vent was broken off near its base. Spots of severe corrosion staining were found in 3 of the 4 indentations within the saltwater tray, indicating the presence of corrosion inside the specimen (see Figure 5.106).

Several transverse cracks were present on the top face of the specimen. Although only one crossed the full width of the specimen, five of the cracks extended down both the north and south faces. The epoxy used to seal the vertical portions of the transverse cracks was intact at the time of autopsy. Two of the transverse cracks were connected to longitudinal cracks which ran approximately 6 inches from the south face of the specimen. Average crack width for all surface cracks was 0.015 inches. Some separation was found at the joint between the live and dead end pourbacks and the surrounding concrete. Also, one vertical crack was found near the midpoint of the pourback on both ends of the specimen. Efflorescence was observed around both cracks, indicating the presence of moisture inside the anchorage zones of the specimen (see Figure 5.107). Crack width data is shown in Figure 5.108, and the crack diagram is shown in Figure 5.111.

Figure 5.107: Specimen 7.1, Efflorescence Around Crack on Live End

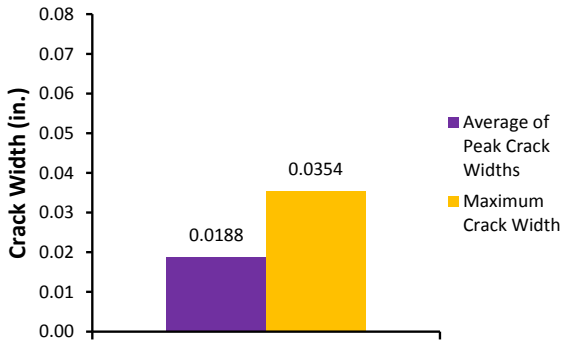

Figure 5.108: Specimen 7.1 Crack Data

5.2.10.2 Longitudinal Bars and Stirrups

Damage to the epoxy-coated longitudinal bars was minor. Spots of discoloration and light surface corrosion were observed at the points where stirrups had been tied, as shown in Figure 5.110. All corrosion could be removed with a scouring pad. The south epoxy-coated bar was slightly more damaged than the north bar. The uncoated longitudinal bars showed moderate to severe corrosion damage. Spots of corrosion were observed along most of the bars' length. Near midspan, both bars were also pitted over several intervals (see Figure 5.110). The south uncoated bar was substantially more damaged than the north bar. It showed pitting on almost half of its total length. Longitudinal bar corrosion ratings are shown in Figure 5.111 and summarized in Table 5.23.

The stirrups were mildly damaged. Spots of discoloration and light corrosion were generally observed at the stirrups' bend points as well as locations where the uncoated bars were tied, as shown in Figure 5.110. It is possible that much of the discoloration at these locations was transported there from the uncoated bars. Most of the corrosion present could be removed with a scouring pad. However, localized moderate surface corrosion was found on 4 of the 7 stirrups on at least one interval. Stirrup #3 was the most damaged, with nonremovable corrosion visible on top of its horizontal region over several intervals. This stirrup was located directly beneath the specimen's largest transverse surface crack. Stirrup corrosion ratings are shown in Figure 5.111 and summarized in Table 5.23.

5.2.10.3 Duct

The outside of the duct was extensively coated with chalky white residue. Some traces of corrosion products were found near the live end of the duct underneath the heat shrink sleeve. Inside, a shinier white residue was found, along with evidence of voids in the top inner ribs of the duct. These voids were uniform in size and did not appear to be continuous along the length of the duct (see Figure 5.110). Isolated light gouges were found on the duct's inner surface at various points along its length. It appeared that at least one strand had been bearing on the duct at those locations. Duct corrosion ratings are shown in Figure 5.111 and summarized in Table 5.23.

The dead end and live end couplers were completely intact. Both sets of fasteners were fully functional at the time of autopsy, and no cement paste appeared to have breached the gaskets at any point of either coupler (see Figure 5.109). The outer and inner surfaces of both couplers showed similar discoloration to that which was seen on the duct. Both primary heat shrink sleeves were also intact. Extensive paste intrusion was observed near the outer end of each sleeve, along with some corrosion staining, as shown in Figure 5.109. The sleeves had a somewhat loose fit on the ducts. It is unknown how much of the cement paste was introduced during construction and how much was a byproduct of the autopsy process. At the dead end coupler, an additional heat shrink sleeve had been applied to the top of the duct because the primary sleeve had split during its application. This additional sleeve was observed to be loose at the time of autopsy, although it may have been jarred loose during the extraction process.

Figure 5.109: Specimen 7.1 Live End Coupler (Left) and Live End Sheath (Right)

5.2.10.4 Grout

The specimen's grout was cracked every few inches along its length. These cracks were very faint, and no longitudinal cracks were observed. Voids which were approximately 1 inch wide were found along the top surface of the grout. These voids were confined by the upper ribs of the duct, but some small bubbles were also observed between ribs (see Figure 5.110). The bottom half of the grout was much smoother to the touch and much darker in color than the top half, as shown in Figure 5.110. This may indicate density variations within the grout. One strand was visible on the bottom surface of the grout at points along its length. Chloride contents were below the corrosion threshold along the length of the grout: 0.029% at midspan, and 0.030% and 0.027% at the live end and dead end couplers, respectively. Grout chloride content is shown in Figure 5.111. Because no breaches were found in the duct couplers, chlorides must have entered the tendon by some other means. Corrosion found on the anchorage components suggests that chlorides may have entered there. This is discussed in sections 5.2.10.6 and 5.2.10.7.

5.2.10.5 Strand

Corrosion damage to the strands was uniform and minor. The outer wires of each strand showed spots of discoloration and light surface corrosion over most intervals. All corrosion could be removed with a scouring pad (see Figure 5.110). The inner wire on each strand was somewhat more damaged, as shown in Figure 5.110. Corrosion which could not be removed was found in several intervals along each strand. Strand corrosion ratings are shown in Figure 5.111 and summarized in Table 5.23.

Coated Bar

Uncoated Bar

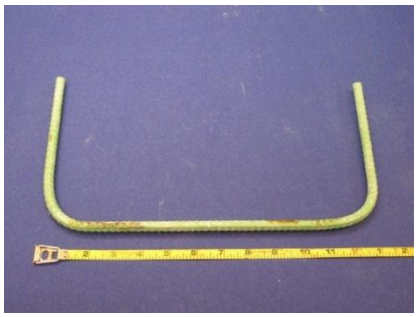

Stirrup

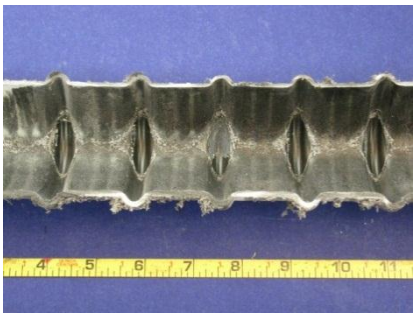

Top of Duct

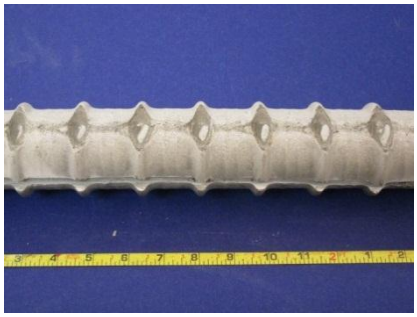

Top of Grout

Side of Grout

Strand

Inner Wire

Figure 5.110: Specimen 7.1 Main Autopsy Region Elements

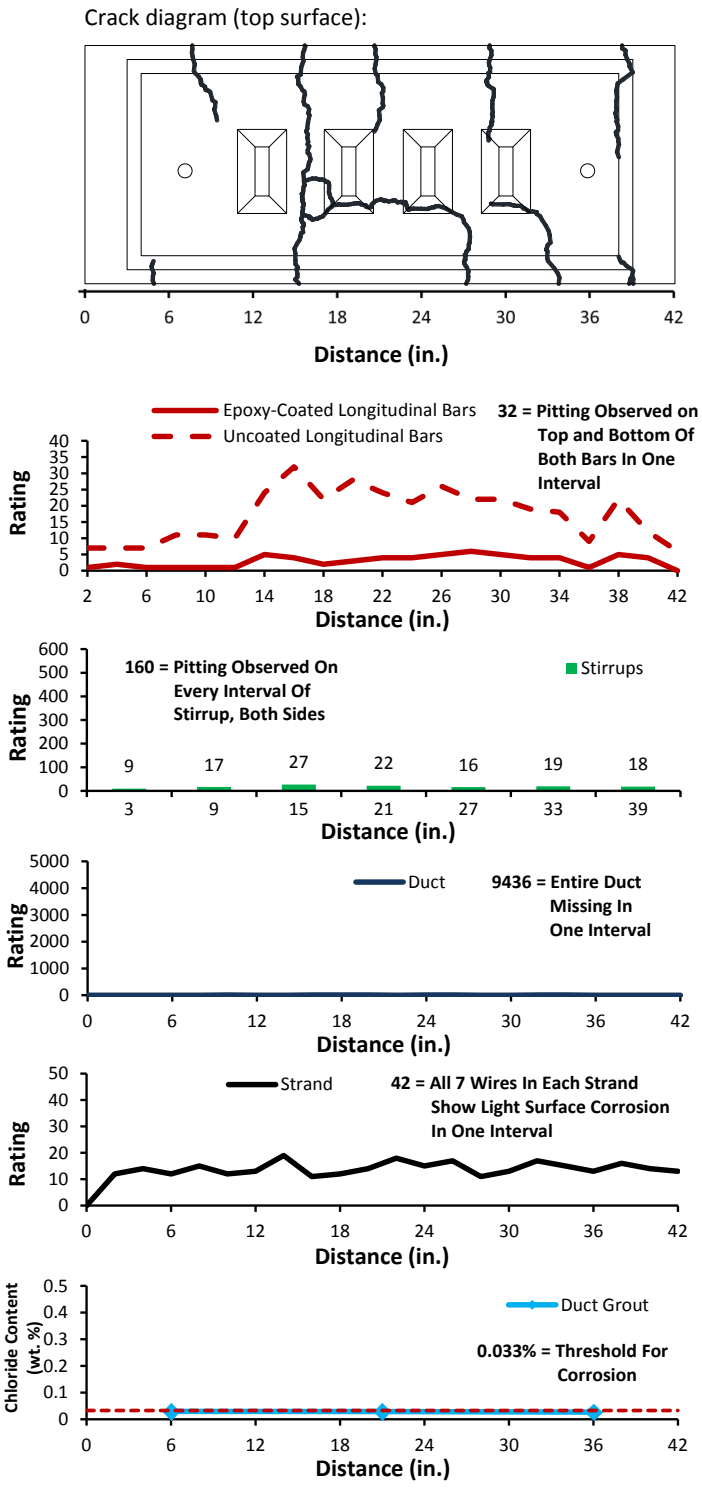

Figure 5.111: Specimen 7.1 Crack Map and Corrosion/Damage Rating Plots

5.2.10.6 Dead End Anchorage

The VSL CS-2000 anchorage system contained several cap components which will be described here in order from the end of the specimen toward the inside. See Figure 5.112 for the layout and names of these components. The outside of the grout cap was covered in chalky white residue. Some light corrosion staining was also observed on the top of its outer surface and along its outer lip. The retaining ring was severely pitted around the top of its outer face. Localized pitting and corrosion was found elsewhere on the retaining ring, mostly on or near its outer edges. The insulation plate showed widespread corrosion staining on both of its faces. The discoloration was most severe near the top of the plate. The bearing plate showed widespread moderate surface corrosion on the surface in contact with the insulation plate. Lighter corrosion was also observed around the bearing plate's forward edge. Some light to moderate surface corrosion was observed on the rear of the bearing plate. The anchor head was lightly discolored over much of its exposed surfaces. The surface which had been bearing on the bearing plate showed widespread moderate corrosion and some pitting. Also, a small "window" of corrosion was observed on the top, outer surface of the anchor head. A grout void which was similar in shape to the "window" appeared to have been located there. This may have been a chloride ingress point. Anchorage components are shown in Figure 5.113.

Figure 5.112: Specimen 7.1 Anchorage Components, from Top: Grout Cap, Retaining Ring, Insulation Plate, Bearing Plate

Anchorage

Grout Cap

Insulation Plate

Bearing Plate

Anchor Head

Figure 5.113: Specimen 7.1 Dead End Anchorage Cap Components

The trumpet was completely intact at the time of autopsy. Chalky white residue was observed on the outer surface of the trumpet. Some localized corrosion staining was observed near the bearing plate. Inside the trumpet, lines were visible in the shiny grout residue which suggested that the grout was cracked longitudinally there. The trumpet is pictured in Figure 5.115. Trumpet damage ratings are shown in Figure 5.118 and summarized in Table 5.24.

The grout inside the grout cap was not cracked. The top third of the grout cap was slightly darker than the rest, and a clear boundary was visible between these regions, as shown in

Figure 5.114. This may have occurred because grouting was completed in stages. It is possible that the time between stages was too great. A void was observed on the top of the grout within the grout cap adjacent to the insulation plate. The corroded "window" of the anchor head was visible beneath the void. Some corrosion products were found around the perimeter of the void, and the void appeared to terminate at the location of the grout cap vent. The grout within the trumpet was also uncracked, contradicting evidence found to the contrary inside the dead end trumpet. The grout was darker on its bottom surface along its whole length, as shown in Figure 5.115. This indicates that segregation may have occurred. A small void surrounded by dark bubbling was found on the top of the grout.

Figure 5.114: Specimen 7.1 Dead End Grout Cap Showing Grout Discontinuity

The dead end anchorage zone strands were somewhat damaged but overall in good condition. The outer wires of each strand showed spots of discoloration or light surface corrosion over most of their length. All corrosion could be scrubbed away with a scouring pad. The inner wires were more damaged, with light to moderate surface corrosion occurring over all intervals, as shown in Figure 5.115. On the inner wires of two strands, the heaviest corrosion occurred on the intervals which had been located inside the anchor head. Light to moderate surface corrosion was found on the exterior of all three wedges. The interior of each wedge was not damaged. A typical strand is shown with and without wedges in Figure 5.115. Dead end anchorage zone strand corrosion ratings are shown in Figure 5.118 and summarized in Table 5.24.

Top of Trumpet

Grout

Strands with Wedges

Strand

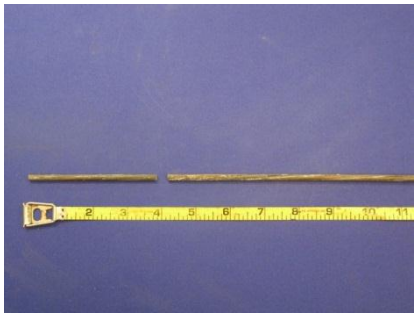

Inner Wire

Figure 5.115: Specimen 7.1 Dead End Anchorage Region Elements

5.2.10.7 Live End Anchorage Components

The orientation of the components within the live end anchorage cap is shown in Figure 5.112. The grout cap was covered in white, chalky residue and showed moderate corrosion staining along its outer lip. Localized moderate corrosion and pitting were found on all surfaces of the retaining ring. The most severe damage occurred near the top of the ring. The insulation plate was lightly stained on both sides. Staining was most severe in the vicinity of its inner edge. The bearing plate showed widespread moderate corrosion and some localized pitting on the

surface it shared with the insulation plate. The corrosion near the middle of this outer surface was burnt orange in color, while the corrosion around the bearing plate's outer edge was a much darker red. The inboard side of the bearing plate had localized light to moderate surface corrosion, mostly occurring on its upper portion. Many small spots of light surface corrosion were observed on the outer surfaces of the anchor head, while moderate surface corrosion covered much of the surface which had rested on the bearing plate. A small "window" of moderate corrosion was found on the upper surface of the anchor head. This appeared to coincide with the location of small grout void there and may have been another chloride ingress point for the tendon. Anchorage cap components are shown in Figure 5.116.

Anchorage

Grout Cap

Insulation Plate

Bearing Plate

Anchor Head

Figure 5.116: Specimen 7.1 Live End Anchorage Cap Components

The live end trumpet was similar in appearance to the dead end trumpet. Chalky white residue was found on its outer surface, along with small areas of corrosion staining on the portion of the trumpet which had been inside the bearing plate. Shiny white residue was present on the inner surfaces of the trumpet. Lines in this residue suggested that the grout may have been cracked there. The live end trumpet is pictured in Figure 5.117. Trumpet damage ratings are shown in Figure 5.118 and summarized in Table 5.24.

The grout within the live end grout cap was uncracked and showed similar evidence of a cold joint near its top surface to that observed within the dead end anchorage. A large void was visible on the top surface of the grout, and some light corrosion staining was present around its edges all the way to the location of the grout vent. The "window" of corrosion on the top of the anchor head was visible within the void. The grout within the trumpet was cracked transversely on its end nearest to the inside of the specimen. These cracks appeared to correspond to the pattern observed on the inside of the trumpet. Some efflorescence was observed in the vicinity of these cracks, as shown in Figure 5.117. It is unknown whether this was due to chlorides or bleed water from the grout. One longitudinal crack was also observed extending along the middle of the grout from the inside end to the bearing plate. The bottom half of the grout appeared much darker in color than the top half, indicating that segregation may have occurred during grouting. A very small void was present on top of the grout near the bearing plate.

The live end anchorage strands were somewhat less damaged than the dead end strands. Discoloration spots were visible along many of the outer wires' length in all three strands, as shown in Figure 5.117. Occasional spots of light surface corrosion were observed on the outer wires. These did not occur solely in the anchor head regions of each strand. The inner wires were more corroded. Localized light surface corrosion was present on all intervals (see Figure 5.117). With the exception of one interval on one of the outer wires, this corrosion could be removed with a scouring pad. All three wedges were substantially intact, although spots of moderate surface corrosion were found on their outer surfaces. Typical live end anchorage region strands, with and without wedges, are shown in Figure 5.117. Live end anchorage zone strand corrosion ratings are shown in Figure 5.118 and summarized in Table 5.24.

Top of Trumpet

Grout

Strands with Wedges

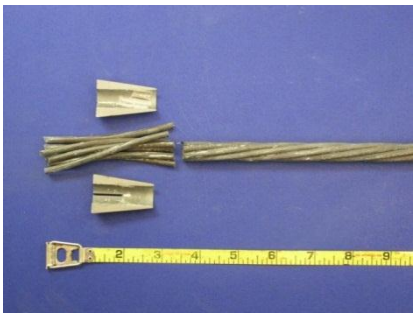

Strand

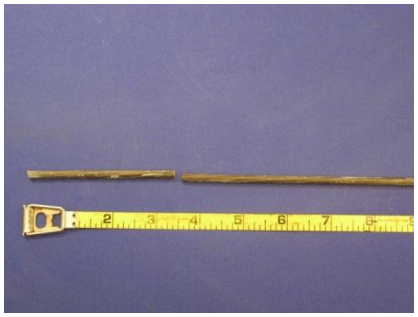

Inner Wire

Figure 5.117: Specimen 7.1 Live End Anchorage Region Elements

Table 5.24: Specimen 7.1 Anchorage Corrosion/Damage Rating Summary

	Dead End Anchorage			Live End Anchorage		
Component	**Maximum**	**Total**	**Generalized**	**Maximum**	**Total**	**Generalized**
Trumpet	0	0	0	0	0	0
Strands	28	163	36	20	140	31

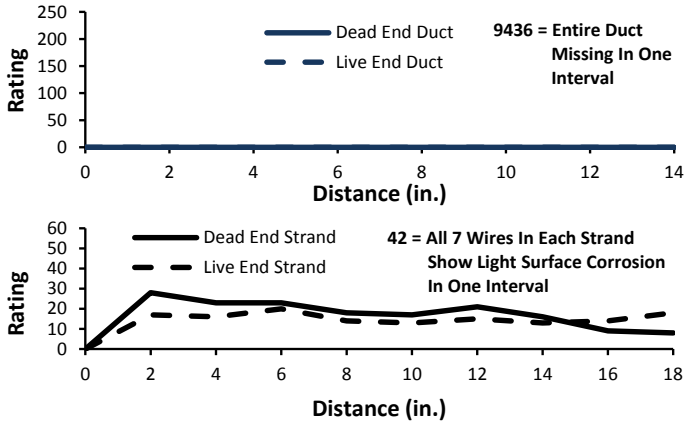

Figure 5.118: Specimen 7.1 Anchorage Corrosion/Damage Ratings

5.2.10.8 Comparison of Anchorage Corrosion

Damage to the dead end anchorage cap components was slightly more severe than the damage to the live end components. Trumpet damage was not severe enough to allow chloride ingress into the anchorage. Therefore, trumpet damage ratings will not be considered here. Strand corrosion ratings were slightly higher for the dead end strand on all but the two innermost intervals of the anchorage regions. Generalized corrosion for the live end strands was 5 units higher than that for the dead end strands. Given that damage was uniformly more severe for dead end anchorage components than for their live end counterparts, it is possible that the corrosion was affected by the saltwater spray applied to the dead end during the test period. The vertical cracks which displayed efflorescence also support this hypothesis, although the extent of efflorescence was similar on both ends of the specimen. Further, it appears that chlorides entered the tendon through the anchorage caps. Due to the similar appearance of the corroded "window" on both anchorage caps, the chlorides originated from the saltwater pond and not the dripper. From the anchorages, chlorides were able to traverse the entire tendon within the strand interstices, which resulted in the uniform corrosion ratings observed in the main autopsy region.

However, the difference in corrosion damage between the ends of the specimen was not drastic enough to conclude with certainty that exposure worsened the corrosion at the dead end. Note that the saltwater exposure system had not been operational for at least one year prior to autopsy.

5.2.11 Control Specimen: Galvanized Duct, No Strand

Figure 5.119: Control Specimen Overall Appearance

Table 5.25: Control Specimen Corrosion Rating Summary

Component	Maximum	Total	Generalized
Longitudinal Bars	0	0	0
Stirrups	0	0	0
North Duct	0	0	0
South Duct	0	0	0

This specimen was cast as part of the 6 series but was never fitted with strand nor loaded. It remained in indoor storage in the south bay of Building 24 for the duration of the exposure period. As the autopsy process was being planned, it was determined that this specimen should be autopsied to provide a baseline level of damage to which other specimens could be compared.

5.2.11.1 Appearance

The beam was in near-immaculate condition at the time of autopsy, as shown in Figure 5.119. Some light scaling had taken place along the edges of the saltwater tray. Small surface air voids were visible on the north and south faces of the specimen, as well as within the saltwater tray. No cracks were observed at any location on the specimen, as it had never been stressed.

5.2.11.2 Longitudinal Bars and Stirrups

None of the epoxy-coated bars or stirrups within the specimen showed any signs of corrosion whatsoever (see Figure 5.120). Longitudinal bar and stirrup corrosion ratings are shown in Figure 5.121 and summarized in Table 5.25.

5.2.11.3 Duct

The outside of both the north and south ducts was covered in a dull gray residue, as seen in Figure 5.120. No corrosion damage was found on the outer surfaces of either duct. Because the ducts had not been grouted, their inner surfaces were exposed to air for the entire exposure period. As this was not consistent with conditions inside the ducts of the exposure specimens, the inside surfaces of the control specimen were not evaluated for corrosion. Duct corrosion ratings are shown in Figure 5.121 and summarized in Table 5.25.

Figure 5.120: Control Specimen Rebar Cage and Ducts

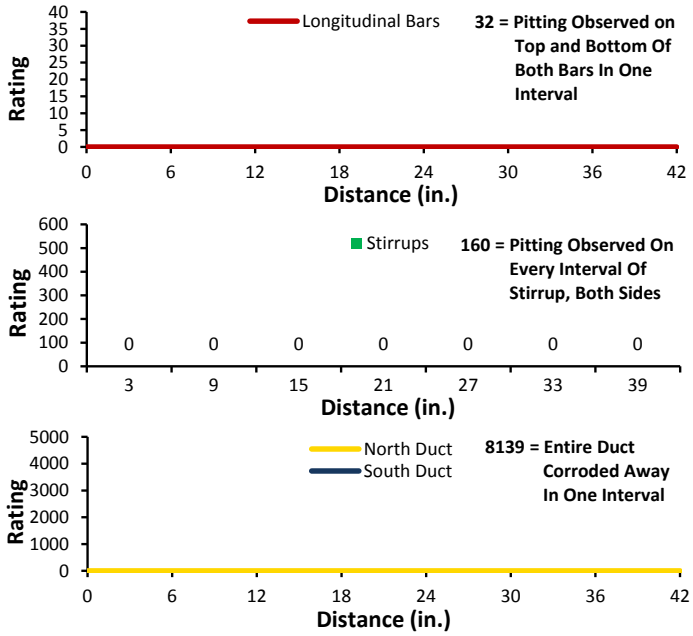

Figure 5.121: Control Specimen Corrosion Ratings

5.2.11.4 Dead End Anchorages

A uniform layer of light surface corrosion was present on the exposed surface of the bearing plates. Localized light to moderate surface corrosion was found along the outside edges of the bearing plates, as well as on the portions of the anchorages around which concrete had been cast. The duct tape used to make the connection between the ducts and bearing plates was intact. A small amount of light surface corrosion was found beneath the duct tape on both bearing plates. North and south anchorages are shown in Figure 5.122.

Some spots of discoloration were present on the outside of the north and south ducts in the area where the duct tape had been applied. This is shown in Figure 5.122. The inner surfaces of the ducts were not evaluated because they had spent several years exposed to air. Anchorage zone duct corrosion ratings are shown in Figure 5.123 and summarized in Table 5.26.

North Bearing Plate

South Bearing Plate

Top of North Duct

Top of South Duct

Figure 5.122: Control Specimen Anchorages and Ducts

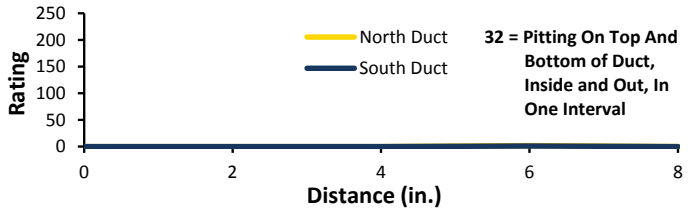

Figure 5.123: Control Specimen Anchorage Corrosion Ratings

Table 5.26: Control Specimen Anchorage Corrosion Rating Summary

Component	Maximum	Total	Generalized
North Duct	2	2	3
South Duct	1	1	1

CHAPTER 6

Analysis of Results

6.1 OVERALL OBSERVATIONS FROM FORENSIC ANALYSIS

6.1.1 Specimen Appearance and Cracking

The surface concrete of all specimens developed scaling in and around the saltwater tray. In many cases, the north and south faces of the specimens were also affected. Shallow surface air voids were visible in the saltwater trays of all specimens. Isolated spalling was found around the surface cracks and pourback joints of some specimens. Corrosion staining was visible on the top surface of several specimens, most often near the base of one or both grout vents.

Most specimens displayed wider and more numerous top surface cracks than had been observed immediately after live load application. Cracks were also found on one or both corbels of several specimens. When present, these corbel cracks were longer than had been noted immediately after live load application. Efflorescence or water stains were found around the corbel cracks in most cases, indicating that moisture was present inside the specimens at those locations. Crack ratings for all specimens are shown in Figure 6.1. The highest crack ratings occurred in Specimens 2.2 and 2.4, while the lowest crack ratings were computed for Specimens T.2 and 4.2. Crack ratings do not show a strong correlation with duct type. In fact, the two highest and two lowest crack ratings were found in one specimen with plastic ducts and one with galvanized steel, respectively. This suggests that galvanized duct corrosion, while quite extensive, was not extensive enough to cause surface cracking.

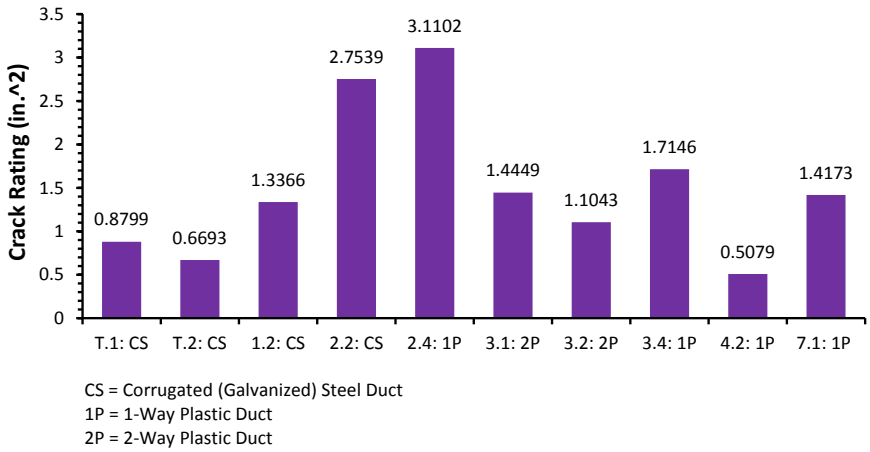

Figure 6.1: Crack Ratings

6.1.2 Longitudinal Bars and Stirrups

Overall, the specimens' epoxy-coated reinforcing elements were in good condition. Corrosion damage was mild and limited to small areas of each bar or stirrup. In between these regions, the epoxy coating was completely intact. Discoloration and corrosion tended to occur at locations where damage to the epoxy coating was likely to have occurred, such as points where the bars had been tied or lifted with a crane. Pitting and area loss were extremely rare. Discoloration was the most common form of corrosion damage.

Generalized longitudinal bar and stirrup corrosion ratings are shown in Figure 6.2 and plotted with crack ratings for each specimen. In general, it appears that specimens with higher crack ratings also tend to have higher longitudinal bar and stirrup corrosion ratings. For most specimens, it was observed during autopsy that corrosion ratings were highest for the regions of the bars and stirrups located directly underneath each specimen's surface cracks. Figure 6.2 builds on this finding by linking the extent of epoxy-coated bar corrosion to crack rating.

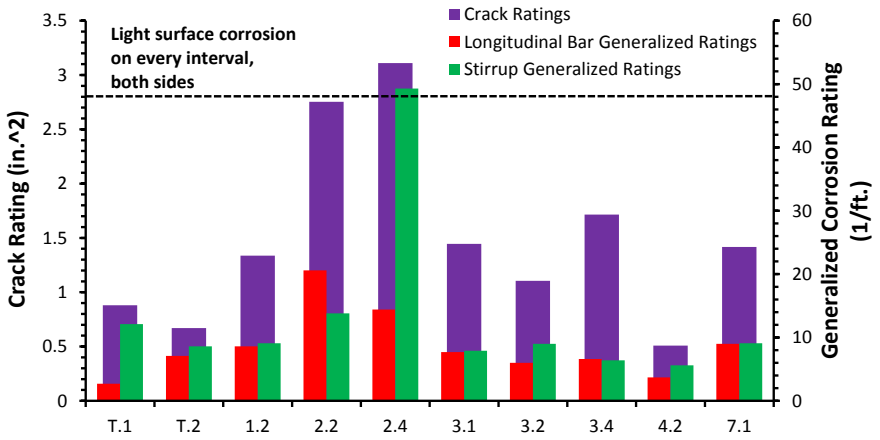

Figure 6.2: Generalized Longitudinal Bar and Stirrup Corrosion Ratings and Crack Ratings

6.1.3 Duct

Galvanized steel ducts performed very poorly, with every one showing area loss and pitting over a portion of its length. Substantial area loss and pitting were present at locations of grout voids. Corrosion and discoloration were less localized, appearing over larger portions of the ducts' length. Damage was most severe along the portions of duct which were located beneath each specimen's transverse cracks.

The plastic ducts were found to be only lightly damaged at the time of autopsy. This damage was caused either by strands scratching the inner surface of the duct while being threaded through the specimen, or by one or more strands gouging into the duct during stressing. Damage ratings were highest in Specimen 4.2, which contained stainless steel strand. The highly curved stainless steel strand scratched the ducts during strand placement, resulting in high damage ratings for this specimen.

No holes or leaks were found in any of the plastic ducts, indicating that the ducts themselves did not allow chlorides to enter the tendons. However, breaches were observed in the heat shrink or mechanical couplers used to connect the two halves of the north duct on all but one specimen. Also, the epoxy used to seal the grout vent to the south duct was observed to be loose on all specimens. This provided a route for chlorides to enter the tendon and may explain the high chloride levels in all tendons with plastic ducts except for Specimen 7.1.

6.1.4 Grout

Grout condition varied by specimen. Some grouts were smooth, consistent in color, and extremely difficult to break open during autopsy. Others were somewhat rough to the touch, showed color variations, and shattered after the duct was removed. This suggests that pressure was not well-controlled during the grouting process. Overall, grout quality improved in specimens which were cast later in the construction sequence. All grouts showed voids to some extent. Most voids were limited to the extreme top portions of each duct's transverse ribs, but some were substantially larger and extended along large portions of the tendon. Strands were visible on the bottom surface of many grouts. For some specimens, the grout did not consolidate well around the strands at these locations. The bond strength between grout and strand varied by strand type. Nearly all grout chloride levels were at or above the 0.033% threshold for corrosion, regardless of whether the grout voids were continuous. This, combined with the uniform strand corrosion which was observed, implies that chlorides entered the ducts and traveled along the strand interstices.

6.1.5 Strand

Conventional strands showed discoloration or light corrosion spots on their outer wires and somewhat more severe corrosion spots on their inner wires. The spots were most frequent in the regions which had been in direct contact with the surrounding duct. Galvanized strands showed similar damage. However, most corrosion on the outer wires of each galvanized strand occurred on the zinc coating, while damage to the inner wire occurred on the bare interstitial steel. Copper clad strands were uniformly coated with a black patina, which appeared glossier on the inner wires than the outer wires. Stainless strand was covered with a light coating of grout residue but was otherwise immaculate.

6.1.6 Anchorages

The exposed surfaces of the bearing plates and anchor heads showed patches of light to moderate corrosion. Inside the specimens, corrosion was most prominent on the underside of the bearing plates, suggesting that voids may have formed there during casting and that moisture was able to enter. Anchorage region ducts showed similar damage to their counterparts in the main autopsy region. Grouts were similar in appearance, but voids were smaller in size. Anchorage region strands were most corroded at their outer tips and at the regions which had been located

inside the anchor head. Wedges were almost always intact, although many displayed light to moderate surface corrosion.

There is little evidence to show that the presence of anchorage drippers had any effect on the corrosion of the anchorage post-tensioning components. In fact, corrosion was nearly uniform within both anchorages of the three dead end exposure specimens. This indicates that anchorage corrosion occurred due to other factors, such as exposure to air prior to pourback application or chloride ingress from the saltwater bath.

6.2 ANALYSIS OF VARIABLES

6.2.1 Strand Type

Because the different strand types corroded in different ways, direct comparison among them is difficult. Generalized strand corrosion ratings are plotted with maximum chloride content for both tendons in each autopsy specimen in Figure 6.3. Note that the plots are organized by strand type.

For tendons with conventional strand, only Specimen 7.1 (electrically isolated tendon) had a maximum chloride content below the corrosion threshold. The north duct of Specimen T.2 had the highest strand corrosion rating but one of the lowest grout chloride concentrations. The south tendon of Specimen T.1, the north tendon of T.2, and the tendon in Specimen 7.1 all had similar generalized strand corrosion ratings. However, the maximum chloride content of these tendons varied dramatically, showing that corrosion rating is not dependent on chloride concentrations once the corrosion threshold has been exceeded.

The copper clad strands all took on a uniform black patina during their life. As a result, their generalized strand ratings were identical. However, all maximum chloride concentrations were above the corrosion threshold, varying from 0.11% to 0.25%. Therefore, corrosion of copper-clad strand was independent of chloride content above the corrosion threshold for copper-clad strand.

For the specimens with hot-dip galvanized strand, generalized corrosion ratings were relatively uniform. However, chloride concentrations ranged from 0.08% to 0.48%. Again, this suggests that corrosion of galvanized strand was independent of chloride concentration past the corrosion threshold.

Only one specimen with stainless steel strands was autopsied. Generalized strand corrosion ratings were very low in both tendons of Specimen 4.2, while maximum chloride concentrations were about ten times higher than the corrosion threshold. This shows that the stainless steel strands were extremely corrosion resistant.

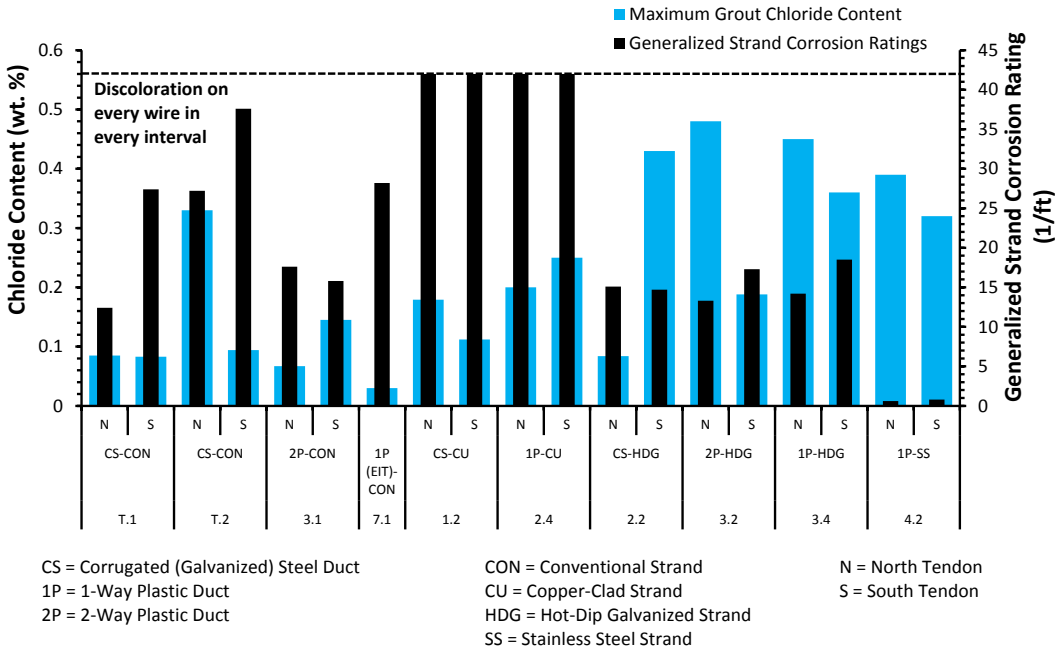

Figure 6.3: Generalized Strand Corrosion Ratings and Maximum Tendon Chloride Content, Organized by Strand Type

Figure 6.4 shows generalized strand corrosion ratings plotted with crack ratings for each specimen. The corrosion ratings shown represent the average of the tendons in each specimen. For each individual strand type, there is no clear correlation between strand corrosion rating and crack rating. High crack ratings do not necessarily correspond to high corrosion ratings. If cracking is assumed to indicate the extent of chloride ingress, this data confirms that strand corrosion does not depend on chloride content above the corrosion threshold.

Overall, the stainless steel strands performed the best. Copper-clad strands also showed no corrosion. Hot-dip galvanized and conventional strands had spots of discoloration and corrosion but were substantially intact. Based on observed corrosion damage alone, stainless steel strand would be best suited to prolonging the service life of a structure.

The role of grout in controlling strand corrosion cannot be neglected. Grout quality was not quantified in this study. Subjectively, the density and texture of tendon grout varied from specimen to specimen. The test specimens were grouted with a hand pump, not an electric pump as is the standard in the post-tensioning industry[7]. Had an electric pump been used, grout voids may have been much smaller or eliminated altogether. This may have slowed the spread of chlorides through the tendons. It is important to note that regardless of grout quality, grout is not prestressed like the rest of a post-tensioned structure. Therefore, it will crack under service loads. If chlorides are present in a tendon, they can travel down these cracks to strand level.

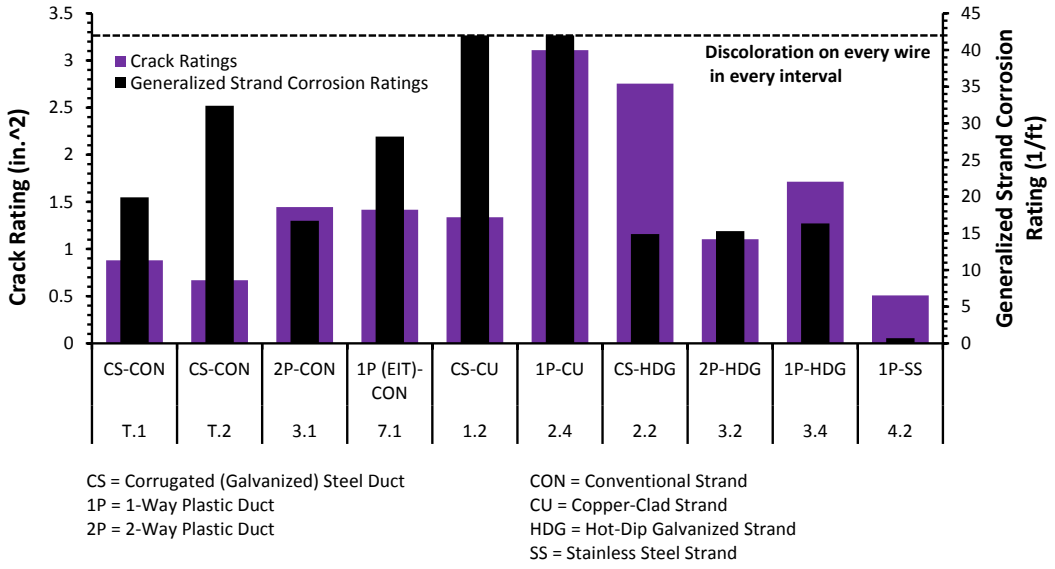

Figure 6.4: Average Generalized Strand Corrosion Ratings and Crack Ratings, Organized by Strand Type

6.2.2 Duct Type

The autopsy specimens contained galvanized steel duct or one of three types of plastic duct from two suppliers. Specimen 7.1, which was electrically isolated, contained the same type of one-way plastic duct as Specimens 3.4 and 4.2. In Figure 6.5, average generalized duct corrosion or damage ratings for each specimen are plotted with crack ratings.

Among the four specimens with galvanized steel ducts, corrosion ratings increased with crack ratings for Specimens T.1, 1.2, and 2.2. However, the highest duct corrosion ratings

occurred for Specimen T.2, which had the lowest crack rating. This suggests a correlation between crack rating and duct corrosion rating, but other factors must also influence the extent of corrosion. From the forensic analysis, it was clear that corrosion initiated in the galvanized steel ducts at locations corresponding to each specimen's transverse surface cracks. For Specimen T.2, cracking allowed duct corrosion to initiate at crack locations, then travel along the length of the large voids as chlorides continued to enter the tendons. Therefore, crack location and the presence of grout voids are just as important as crack rating in determining the extent of duct corrosion.

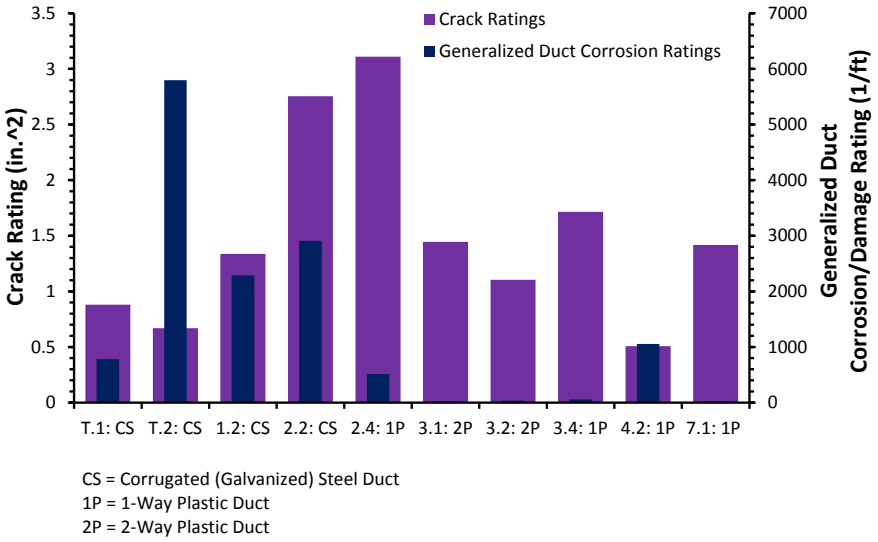

Figure 6.5: Average Generalized Duct Corrosion/Damage Ratings and Crack Ratings

Damage ratings were very low for the plastic ducts. Unlike the steel ducts, the plastic ducts were only damaged during strand placement and stressing. The ducts in Specimen 4.2 were most severely damaged during strand placement due to the stainless steel strands' high curvature. The presence of chlorides at duct level due to cracking did not affect the duct damage in the way that it would for steel ducts. No one type of plastic duct appeared to be less robust than any other, and all ducts were intact at the time of autopsy. Variation in plastic duct damage ratings depended more on strand curvature than on the structural integrity of the ducts. This was especially evident in Specimen 4.2, which had relatively high damage ratings due to the highly

curved stainless steel strands it contained. The plastic ducts in Specimen 2.4 were also damaged in this manner by the copper-clad strands.

Figure 6.6 shows generalized duct corrosion and damage ratings plotted with maximum chloride content in each tendon. For the steel ducts, chloride content seemed to increase in each tendon along with the generalized corrosion rating in the surrounding duct. However, the highest overall chloride contents occurred in tendons with plastic ducts. This is a puzzling result, given the extensive area loss in the steel ducts. However, it confirms the presence of leaks in the couplers of the north plastic ducts and the grout vents of the south plastic ducts, as observed during the autopsy process. Plastic duct damage ratings showed no correlation to the grout chloride content.

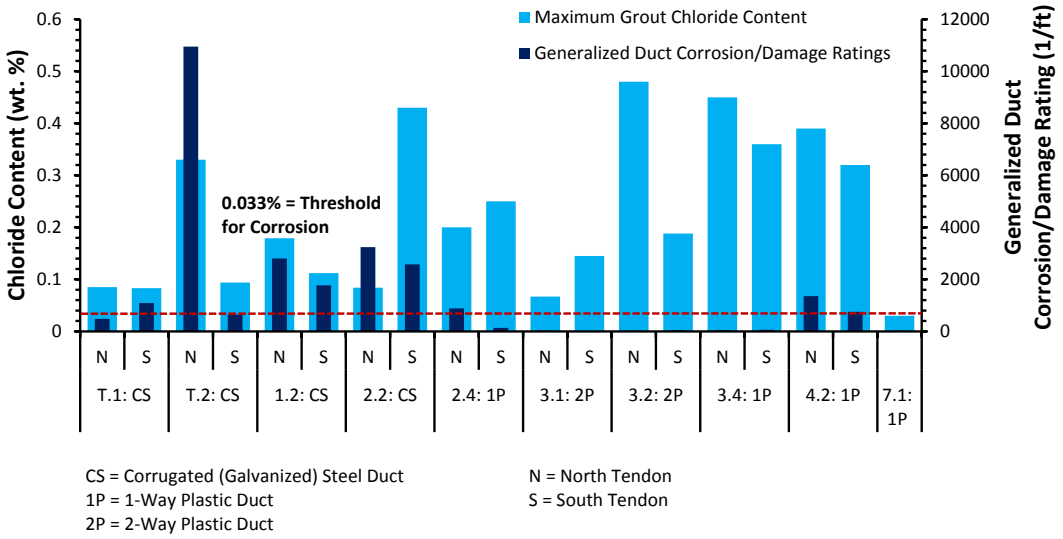

Figure 6.6: Generalized Duct Corrosion/Damage Ratings and Maximum Grout Chloride Content

In all, the plastic ducts were physically intact at autopsy, while the galvanized steel ducts were moderately to severely corroded. Although more chlorides were present inside the plastic ducts than the steel ducts, plastic ducts can provide a greater level of corrosion protection for a post-tensioned structure if all points of possible chloride ingress, such as grout vent connections, are properly sealed. Even in high chloride environments, the ducts themselves will never produce corrosion products in the presence of chlorides. This enables the plastic duct to act as a barrier, preventing or stopping the spread of corrosion throughout a post-tensioned structure.

6.2.3 Coupler Type

The specimens with galvanized steel ducts did not contain couplers. In each specimen with plastic ducts, the two halves of the north duct were connected with one of three couplers: GTI slip-on, GTI snap-on, or VSL snap-on. For each specimen, Figure 6.7 shows the chloride content within the tendon grout at the location of each coupler.

The highest grout chloride concentration was found inside the GTI heat shrink coupler within Specimen 3.2. The lowest concentrations were found in both VSL snap-on couplers inside Specimen 7.1, although these couplers had the benefit of being covered with an additional plastic sheath. Both chloride concentrations in Specimen 7.1 were below the corrosion threshold. The presence of chlorides within the couplers confirms that breaches had occurred, as observed during autopsies. For each coupler which was installed in more than one specimen, chloride concentrations vary significantly. This suggests that the integrity of the couplers depends more on workmanship during construction than on coupler type and manufacturer. The inexperience of the project team at construction time may have resulted in couplers which were not properly installed and which allowed chloride ingress during exposure.

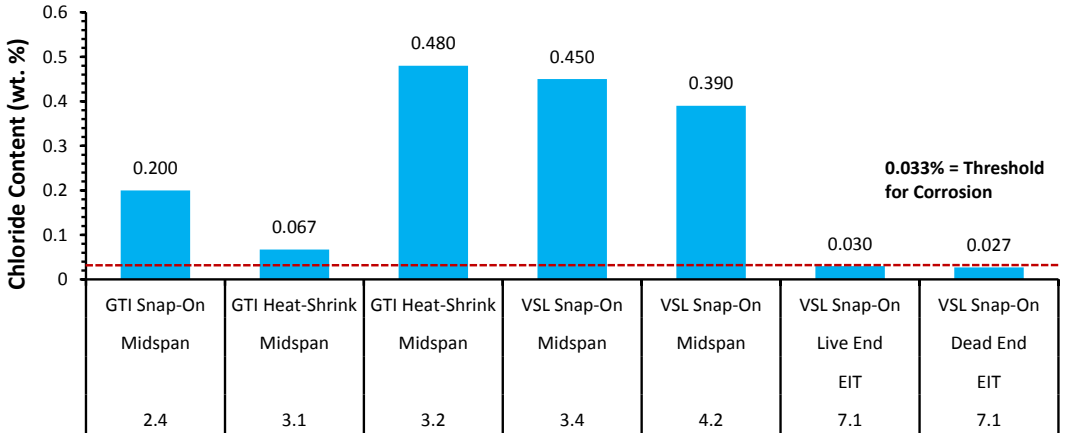

Figure 6.7: Grout Chloride Contents at Coupler Locations

For all specimens with one coupled and one uncoupled plastic duct, grout chloride concentrations at midspan are plotted in Figure 6.8. From this figure, it is clear that chloride levels at midspan were well above the corrosion threshold in both tendons of each specimen. While chloride levels were generally higher in the north tendons, concentrations were of similar

magnitude in the corresponding south tendons. This is most clear for Specimens 2.4, 3.4, and 4.2, for which both chloride concentrations were nearly equal. This trend confirms that the grout vents at midspan of the south ducts were indeed breached by chlorides during the exposure period.

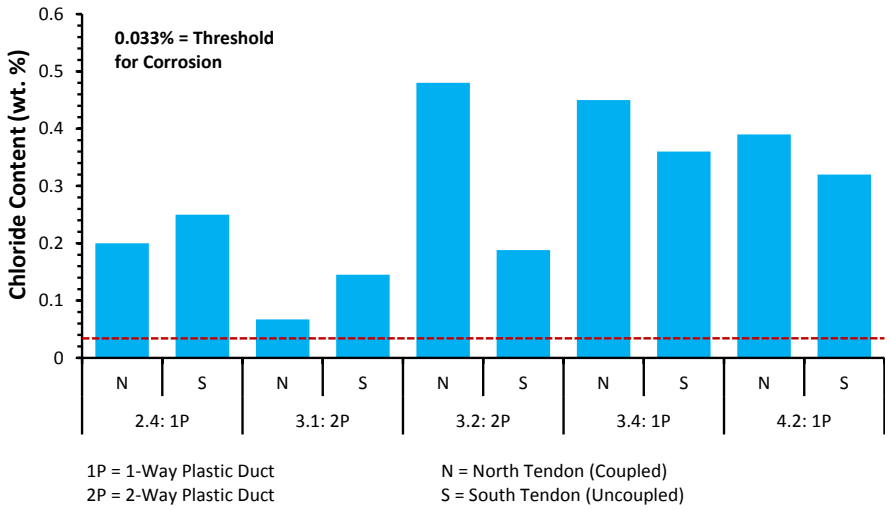

Figure 6.8: Midspan Grout Chloride Contents for Specimens with Two Plastic Ducts

6.2.4 Anchorage Type

Of the autopsy specimens, only T.2 had been constructed with galvanized bearing plates. Corrosion occurred at similar locations on the galvanized and non-galvanized bearing plates. Most corrosion was found on the underside of the bearing plates and on their end surfaces. The galvanized bearing plates were generally less corroded, and the corrosion which was found had occurred on the zinc, not on the steel beneath (see Figure 6.9).

Specimens T.1 and T.2 were both constructed with steel ducts and conventional steel strand, so these specimens can be used to compare the effects of bearing plate type on other elements within the specimens. Less corrosion was found on the bearing plate splice regions of the ducts in Specimen T.2 than Specimen T.1. This suggests that the galvanized bearing plates may have acted as a sacrificial anode and reduced corrosion in the galvanized ducts connected to them. Conversely, slightly more corrosion was found on the anchorage region strands in Specimen T.2 than in T.1. This may have been galvanic corrosion caused by the difference in potentials between the zinc bearing plates and the plain steel strands.

Figure 6.9: Underside View of Anchorage with Non-Galvanized Bearing Plate (Left) and Galvanized Bearing Plate (Right)

The galvanized bearing plates in Specimen T.2 performed better than the non-galvanized plates in Specimen T.1. However, the effect of the galvanizing zinc on the corrosion of other steel elements is not fully understood and should be carefully weighed before opting for galvanized bearing plates in a post-tensioned structure. In addition, the non-galvanized bearing plates on all other autopsy specimens showed corrosion but remained structurally intact after four years of exposure. This casts doubt on the need for galvanized components in the first place.

6.2.5 Fully Encapsulated System

Specimen 7.1 was constructed such that its tendon was electrically isolated from all other elements in the specimen. Figure 6.2 shows that the epoxy-coated mild steel components inside Specimen 7.1 were corroded to about the same extent as other specimens with non-isolated plastic ducts, as would be expected. The crack rating for Specimen 7.1 was comparable to that of the other specimens. As shown in Figure 6.3, the generalized strand corrosion rating for Specimen 7.1 was the second highest among all specimens with conventional strand. Only the south tendon of Specimen T.2 experienced a higher rating. The generalized duct damage rating was very low, even compared to other specimens with VSL one-way plastic ducts (see Figure 6.5). This can be attributed to the low curvature of the conventional strand and to the robust construction of the VSL electrically isolated anchorage components. Grout chloride content was below the corrosion threshold at all points along the tendon. This confirms that the couplers and

heat shrink sleeves applied at the trumpet-duct joints remained watertight for the entire life of the specimen. The grout chlorides must have entered the duct at some other location.

In general, corrosion damage in Specimen 7.1 was minor and comparable to other specimens. It is significant that this was the only specimen which did not have any grout chloride concentrations above the corrosion threshold. Had the exposure period lasted longer, this may have become an important factor in the corrosion protection of the strands. If a very long service life is desired for a post-tensioned structure, electrically isolated systems might be a viable option.

6.3 COMPARISON OF MONITORING AND FORENSIC DATA

6.3.1 Half-Cell Potential Data

6.3.1.1 Half-Cell Potential Data vs. Observed Corrosion Damage

Average final half-cell potentials for each specimen are shown in Figure 6.10 with generalized longitudinal bar and stirrup corrosion ratings. All specimens except for 7.1 ended the test period with an average half-cell potential within the 90% chance of corrosion region, indicating that corrosion is very likely to be present[14]. Specimen 7.1 ended the test period in the uncertain corrosion category. Corrosion was present to some extent on the bars and stirrups in all specimens. In the sense of predicting the presence of corrosion, the final half-cell potential method was accurate. However, the half-cell potentials did not correlate well to the magnitude of the stirrup and longitudinal bar generalized corrosion ratings. Thus, the half-cell method did not accurately predict the relative severity of corrosion for the mild steel components in the autopsy specimens.

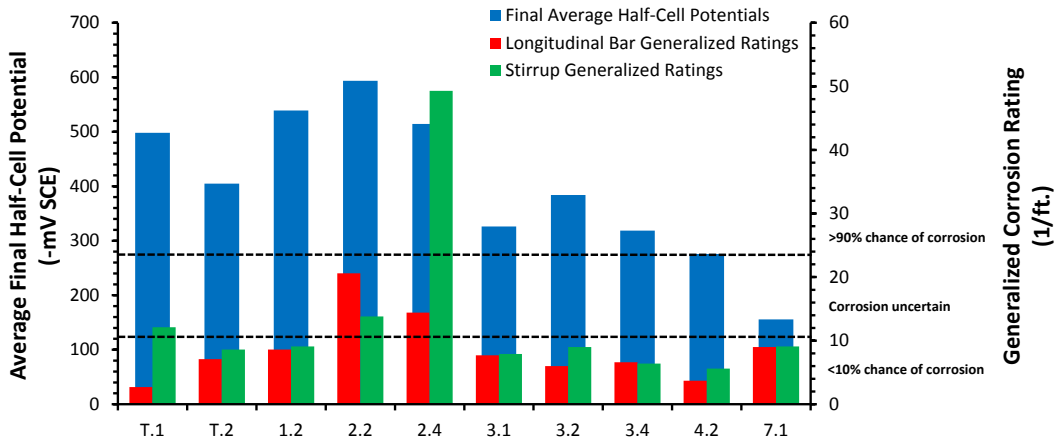

Figure 6.10: Average Final Half-Cell Potentials and Generalized Longitudinal Bar and Stirrup Corrosion Ratings

Average final half-cell potentials for the north and south tendon in every specimen are shown in Figure 6.11 plotted with generalized duct corrosion ratings. Only the specimens with galvanized steel ducts were considered because the half-cell method would be unable to predict damage to the plastic ducts. For these four specimens, final average half-cell readings were all in the greater than 90% chance of corrosion range. This might indicate that half-cell readings predicted corrosion in those specimens. However, almost all of the specimens with plastic ducts also had readings within the 90% probability range, as shown in Figure 6.10. It is likely that the presence of duct corrosion made the half-cell readings more negative, but they were already very negative due to rebar corrosion.

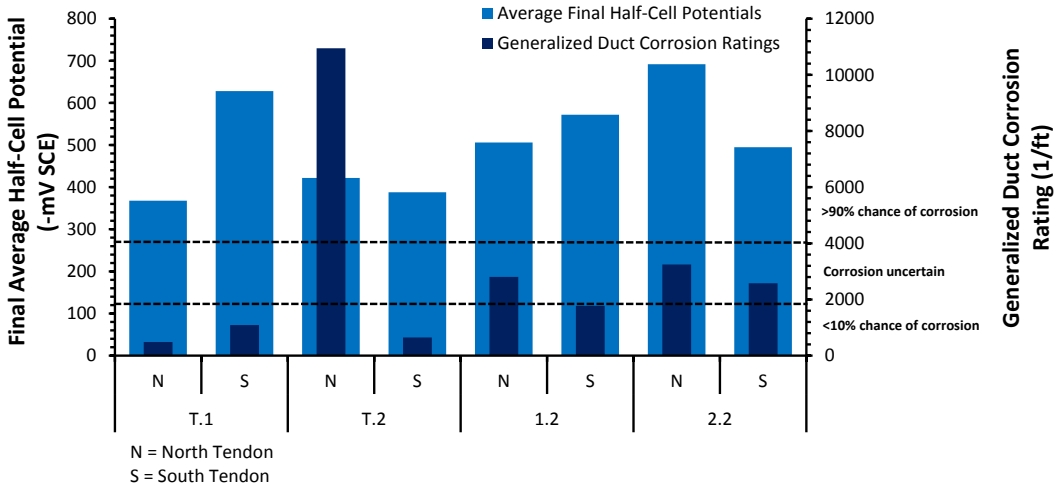

Figure 6.11: Average Final Half-Cell Potentials and Generalized Duct Corrosion Ratings for Specimens with Galvanized Steel Duct

Figure 6.12 shows average final half-cell potentials plotted with generalized strand corrosion ratings for north and south tendons of each Specimen, grouped by strand type. Final half-cell potentials for all seven tendons with conventional strand indicated that corrosion was uncertain or more than 90% likely. Because all conventional strands had some corrosion, the half-cell method was accurate in this regard. However, no relationship can be seen between the final half-cell potential and generalized corrosion rating.

The copper-clad strands all had identical strand corrosion ratings. Half-cell potential readings for the tendons in Specimens 1.2 and 2.4 were similar, and all four were within the 90% chance of corrosion range. Because the black patina on the strands in every specimen was so uniform, it is unknown how half-cell potentials correlate to copper-clad strand corrosion.

The three specimens with hot-dip galvanized strands all showed similar generalized corrosion ratings. Final average half-cell potentials were all above the 90% threshold and generally decreased from Specimen 2.2 to 3.2 to 3.4. In this case, a slight correlation can be seen between half-cell potential and strand corrosion rating.

Almost no corrosion was found on the stainless steel strands in Specimen 4.2. However, the final average half-cell potentials for the two tendons in that specimen indicated that corrosion was uncertain or more than 90% likely. The half-cell method was not accurate for stainless steel strands.

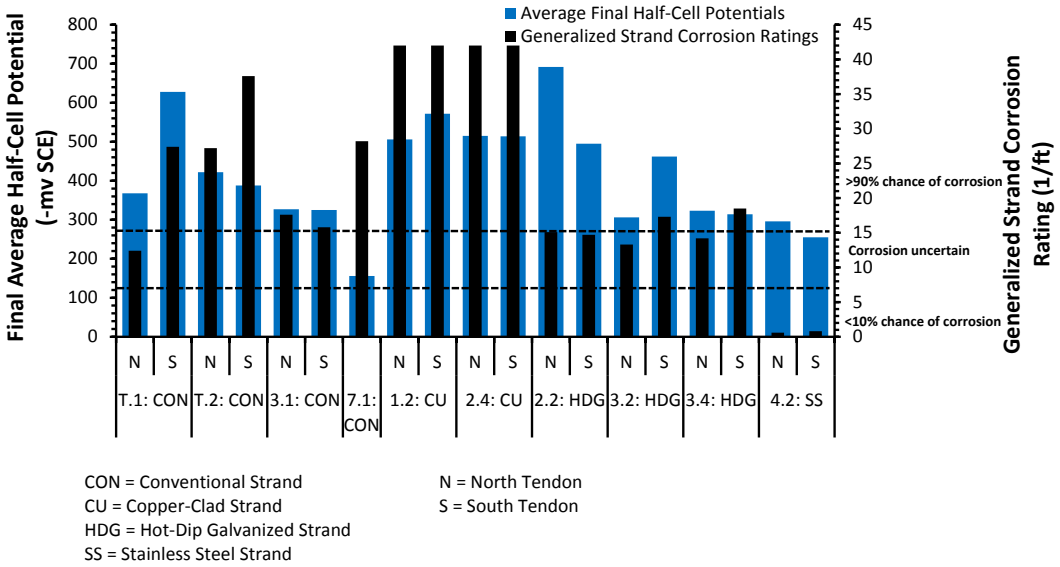

Figure 6.12: Average Final Half-Cell Potentials and Generalized Strand Corrosion Ratings

Overall, strand corrosion was found in all specimens which had a final half-cell reading in the uncertain or 90% probability range. However, all specimens had corrosion in their epoxy-coated mild steel elements. The galvanized ducts were also corroded in every specimen which was built with them. Therefore, the half-cell method successfully predicted the presence of corrosion only because all specimens had some corroded elements. The method did not predict which elements were corroded or their extent of corrosion. Therefore, the half-cell method is not suitable for predicting post-tensioning corrosion.

For all specimens except for Specimen 7.1, the steel elements of the specimens were all in contact at various points throughout the reinforcement cage. It was not possible to isolate the potential of each steel element within the specimen, even though measurements were taken separately at both tendons of each specimen. Like any other non-destructive monitoring technique, the half-cell method was not designed to stand alone[14]. Further research on non-destructive testing methods is required in order to develop a method which will accurately predict corrosion in post-tensioned structures.

6.3.1.2 Time to Corrosion vs. Observed Corrosion Damage

In Chapter 4, corrosion was assumed to initiate when the most negative half-cell reading within a specimen exceeded the 90% chance of corrosion threshold. The number of days to onset

of corrosion for each specimen is shown in Figure 6.13 along with generalized longitudinal bar and stirrup corrosion ratings.

There was not much variation in the time to onset of corrosion among most autopsy specimens, which makes comparison difficult. Times to corrosion onset tended to be lower for specimens with higher bar and stirrup corrosion ratings, although this trend is not universal. The longest time to corrosion onset was observed in Specimen 4.2, which also had the least amount of corrosion on its bars and stirrups.

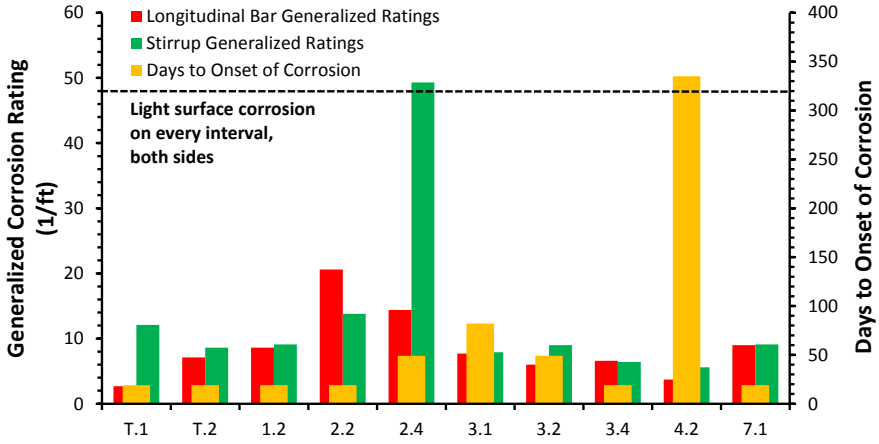

Figure 6.13: Longitudinal Bar and Stirrup Generalized Corrosion Ratings and Days to Onset of Corrosion

The number of days to corrosion is shown in Figure 6.14 along with the generalized duct corrosion/damage ratings for each specimen. All four specimens with galvanized steel duct were heavily damaged, and all four had the lowest time to corrosion onset at 19 days each. The six specimens with plastic duct showed much more variation in their time to onset of corrosion. Specimens 3.4 and 7.1 took only 19 days, while Specimen 4.2 took 335 days to initiate corrosion. This shows that elements inside specimens with plastic ducts generally take longer to begin corroding. This is logical because a post-tensioning duct has a substantial amount of surface area and is one of the first elements to be reached by chlorides from a surface crack. If the duct is plastic, it will not corrode like a steel duct would. The plastic duct will therefore block chloride penetration into the tendon for much longer, resulting in less corrosion and a longer amount of time with less negative half-cell potentials.

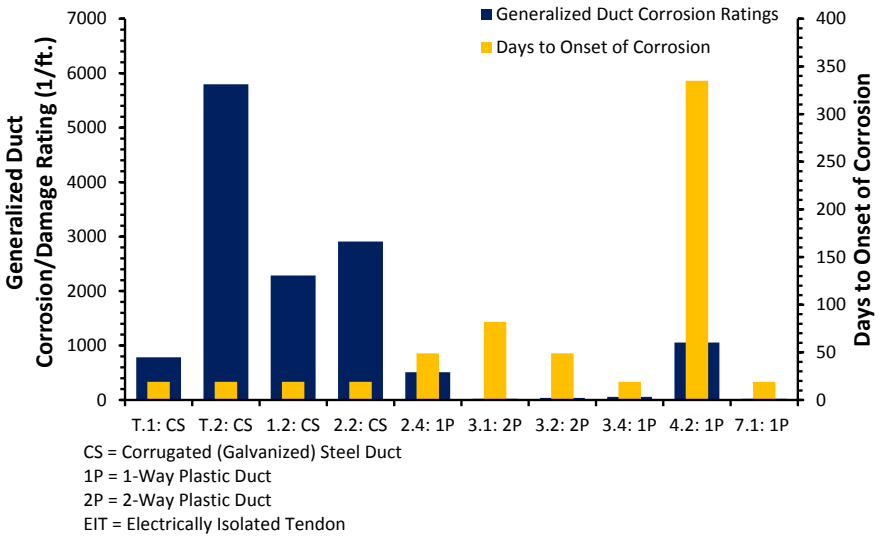

Figure 6.14: Generalized Duct Corrosion/Damage Ratings and Days to Onset of Corrosion

The number of days to onset of corrosion is shown in Figure 6.15 along with generalized strand corrosion ratings for each specimen, arranged by strand type. Among the four specimens with conventional strands, Specimen 3.1 had the lowest corrosion rating and the longest time to initiation of corrosion. The other three specimens started corroding at 19 days and had much higher generalized corrosion ratings. The two specimens with copper-clad strands showed little difference in time to onset of corrosion. The difference could be attributed to Specimen 1.2 having steel ducts and Specimen 2.4 having plastic ducts. Strand corrosion ratings were relatively uniform for the specimens with hot-dip galvanized strands, and corrosion began by the first or second half-cell reading for all three specimens. Specimen 4.2, built with stainless steel strands, showed the longest time to onset of corrosion.

From this data, it seems that corrosion was most likely to occur early in specimens with steel duct and any type of strand other than stainless steel. The fact that all four specimens with galvanized ducts began corroding immediately suggests that corrosion tended to initiate at the ducts, then spread to the bars and stirrups and inside the tendons. However, all specimens had corrosion on their bars and stirrups, even the specimens with plastic ducts. This means that corrosion may have initiated on the bars and stirrups. The low number of days to corrosion onset in most of the specimens indicates that corrosion was not limited by oxygen or chlorides, as can be the case if cracks are narrow or if moisture remains in cracks continuously.

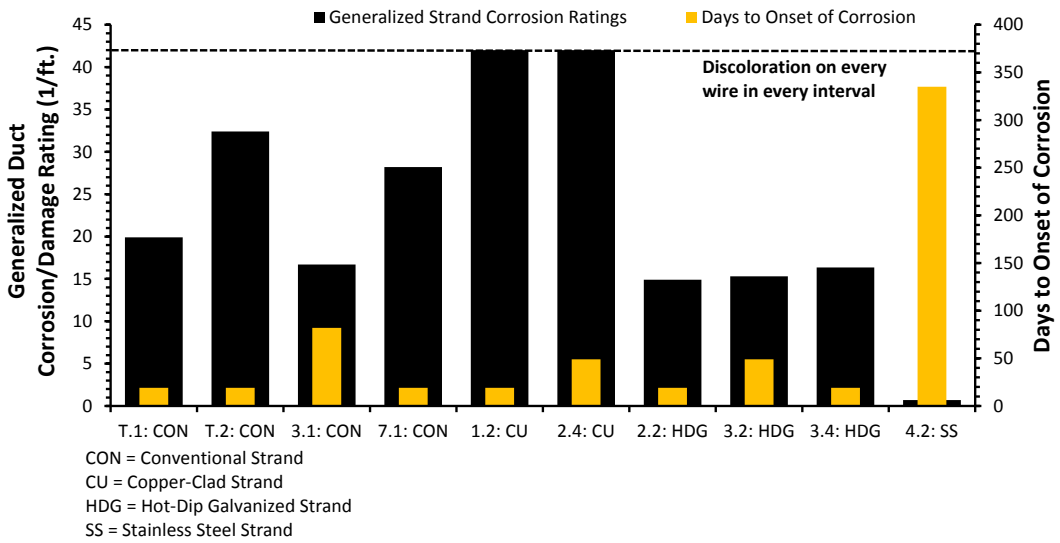

Figure 6.15: Generalized Strand Corrosion Ratings and Days to Onset of Corrosion

6.3.2 AC Impedance Data

AC impedance data serves as an indicator of the watertightness and electrical isolation of a tendon. As such, there is not yet a consensus in literature on how measured AC impedance values might directly indicate the presence or probability of corrosion. As mentioned in Chapter 4, a 30% or greater drop in measured resistance indicates the ingress of moisture into a tendon[4]. Resistance versus exposure time for Specimen 7.1 is shown in Figure 6.16 with the locations of 30% decreases marked with green squares. The first of these decreases occurred 25 days into exposure. According to the half-cell potential data, corrosion was initiated at 19 days when the most negative half-cell potential was first measured within the 90% probability of corrosion region. If the first 30% decrease is assumed to indicate the onset of corrosion, both methods predicted approximately the same time to corrosion initiation.

Specific resistance can be used to ascertain the level of damage to a post-tensioning duct. In general, higher values of specific resistance indicate a lesser probability of damage or holes in the duct[4]. Given the questions surrounding the monitorability of Specimen 7.1 which were presented in Chapter 4, this will not be discussed here.

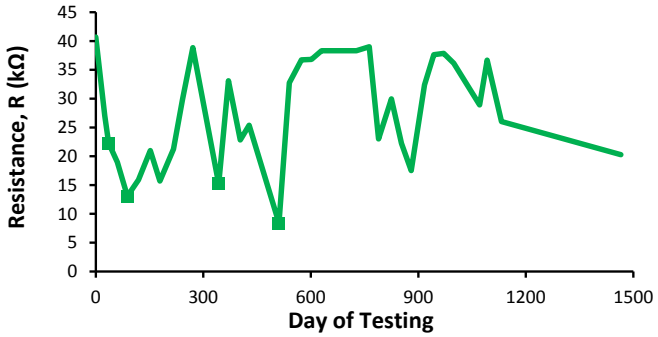

Figure 6.16: Resistance versus Time for Specimen 7.1

6.3.3 Chloride Penetration Data

The longitudinal bars and stirrups in all specimens were present at a depth of approximately 1 inch from the surface of the saltwater tray. Therefore, the concrete chloride sample extracted from that depth on the top surfaces of the specimens represents the chloride concentrations at bar and stirrup level. Chloride contents from the top surface of each specimen at 1-inch depth are shown in Figure 6.17 alongside generalized longitudinal bar and stirrup corrosion ratings.

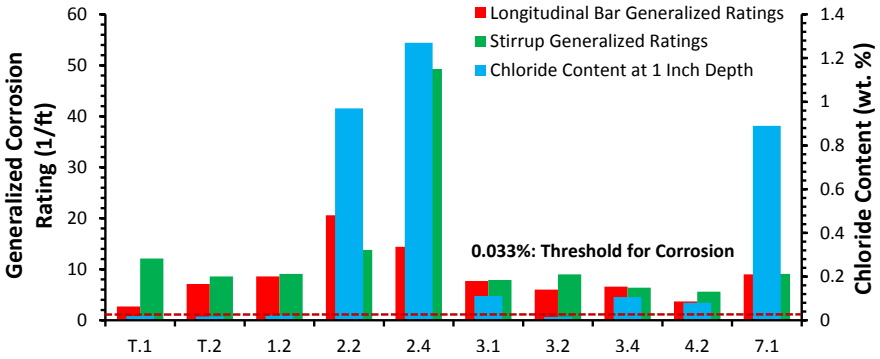

Figure 6.17: Generalized Longitudinal Bar and Stirrup Corrosion Ratings and Top Surface Chloride Content at 1-Inch Depth

Chloride samples were not extracted from the top surface at depths any greater than 1 inch. Therefore, the effect of chloride content on galvanized duct corrosion will not be examined here.

Six of the ten autopsy specimens had chloride concentrations greater than the corrosion threshold at 1-inch depth. The two specimens with the highest chloride concentrations also had the highest longitudinal bar and stirrup corrosion ratings. In general, higher corrosion ratings occurred in the specimens which had higher chloride contents, although this trend was not as clear for lower chloride contents. Specimen 7.1 had low bar and stirrup corrosion ratings in spite of a chloride concentration of almost 1% at bar level. This may be due to the additional indentations in that specimen's saltwater tray which may have caused an irregular chloride distribution.

6.4 COMPARISON WITH PROJECT 0-1405 RESULTS

A portion of TxDOT Project 0-1405 involved the construction, exposure testing, and autopsy of twenty-seven large scale beam specimens. Exposure initiated on the first set of beams in 1998, and the last set of beams was autopsied in 2006. This project can be considered the forerunner of Project 0-4562, as many of the lessons learned from the autopsies were used to fine-tune the corrosion resistance of the 0-4562 specimens and to better isolate variables for study. Salas performed autopsies on twelve of the Project 0-1405 specimens after 3.5 to 4.5 years of exposure[8]. His results are compared to the author's results after four years of exposure in this section.

6.4.1 Appearance

The 0-1405 autopsy specimens were poor in appearance. Most specimens had moderate to severe staining on their top surface. Expansive stresses due to internal corrosion resulted in extensive surface cracking in addition to the pre-existing flexural cracks on some specimens. The large cracks provided easy ingress for chlorides from the top surface saltwater pond, and corrosion easily spread to regions of the specimens where no flexural cracks had been present.

The Project 0-4562 specimens were much better in appearance. Limited staining was observed on a few specimens, although some efflorescence was present on the top and end face surface cracks of several others. Additional cracks formed on some specimens after live load application, but there is no evidence to suggest that these cracks were the result of expansive stresses due to corrosion products within the specimens. The external appearance of typical specimens from both projects is shown in Figure 6.18.

Figure 6.18: Typical Specimen from Project 0-1405[8] (Left) and Project 0-4562 (Right)

6.4.2 Longitudinal Bars and Stirrups

Uncoated rebar was used to form the longitudinal bars and stirrups of each 0-1405 specimen. These bars were found to have serious corrosion over most of the autopsy region. This corrosion resulted in substantial area loss, especially in the partially prestressed specimens. Crack width was observed to have a direct effect on the corrosion of reinforcement.

Project 0-4562 specimens made use of epoxy-coated rebar. Some discoloration and corrosion were present at locations where the coating was most likely to have been disturbed, such as bar curves and lifting points. Pitting was even found on occasion. However, most of the bars' and stirrups' epoxy coating remained intact, preventing widespread corrosion to those components. This indicates substantial value in the use of epoxy-coated reinforcement in aggressive exposures. A typical longitudinal bar from both projects is shown in Figure 6.19.

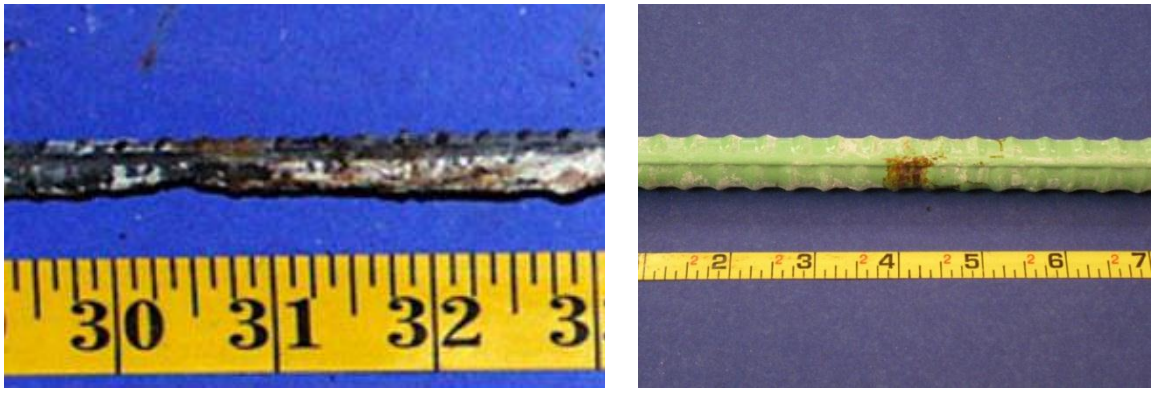

Figure 6.19: Typical Longitudinal Bar from Project 0-1405[8] (Left) and Project 0-4562 (Right)

6.4.3 Ducts

The galvanized steel ducts experienced pitting and area loss in several 0-1405 specimens, with the worst corrosion occurring at locations of grout voids. "Industry standard" (duct tape) and heat shrink splices performed very poorly, allowing chloride ingress at splice locations. Salas did not include any specimens with plastic ducts in his autopsies.

Galvanized duct corrosion was comparable in the 0-4562 specimens. Despite very little visible corrosion on the outer surface of the specimens, the galvanized duct within experienced substantial area loss and some pitting. This damage occurred mostly around transverse surface cracks and the locations of grout voids. Typical steel ducts from both projects are shown in Figure 6.20. The comparable damage in the ducts indicates that the testing conditions were generally compatible in both projects.

Figure 6.20: Typical Galvanized Steel Duct from Project 0-1405[8] (Left) and Project 0-4562 (Right)

6.4.4 Grout

Grout type and grouting procedure were test variables for Project 0-1405. Specimens were constructed with different grout types using both industry standard and "poor" grouting techniques. Voids or evidence of porosity were found in all tendons. Grouting techniques were found to improve grout quality, although the improvement was offset by obsolete and underdesigned grout mixes.

Project 0-4562 specimens were constructed using prebagged grout, and a hand pump was used to inject the grout. Grout quality varied from specimen to specimen. Much smaller voids were present in all specimens, mostly limited to the upper flutes of the surrounding duct. Some evidence of segregation was observed on several grouts, suggesting that pressure was not uniform during grouting. However, overall grout quality was much improved over that of Project 0-1405.

6.4.5 Strands

Conventional strand was found to be severely corroded in the Project 0-1405 specimens. Area loss and pitting were common, and some strands fractured during the autopsy process. Non-flow-filled epoxy-coated strand fared no better, as damage to the coating allowed moisture to enter and travel down the length of the strand. Galvanized strand began corroding later than the other strand types, but it was still heavily corroded and pitted.

Conventional strand in the Project 0-4562 specimens showed spots of discoloration and light corrosion, mostly occurring at points which were in direct contact with the duct. Galvanized

strand was similarly damaged, with corrosion occurring mostly on the protective zinc covering and not on the steel itself. Copper-clad and stainless steel strands were observed to have debonded slightly during the autopsy process, calling their bond strength into question. No fractures or other types of failure were observed. The improved plastic duct and better grout quality in Project 0-4562 helped control strand damage.

6.4.6 Corrosion Ratings

Average generalized corrosion ratings from both projects for each component type are shown in Figure 6.21. Because none of the Project 0-1405 specimens autopsied by Salas had plastic ducts, only the four Project 0-4562 specimens with galvanized ducts were considered for this comparison. Due to the epoxy-coated reinforcement which was used in Project 0-4562, corrosion in those longitudinal bars and stirrups was much less severe than what was observed by Salas. Accordingly, generalized ratings for those components are so low they do not show up in the plots. Strand corrosion was also much less severe in Project 0-4562 specimens. This may have been due to the better overall grout quality which was achieved in those specimens.

Duct corrosion ratings were substantially higher in Project 0-4562 specimens, as shown in Figure 6.21. This occurred because level of prestress and live load were variables in Project 0-1405. The varying prestress and live load levels caused the flexural crack widths in those specimens to vary drastically. Conversely, the crack ratings of Project 0-4562 specimens were held constant as a control variable, resulting in similar corrosion ratings among the four specimens with galvanized duct. The ducts from 0-1405 specimens which had narrower cracks were much less corroded than those with wider cracks, thereby reducing the average generalized rating.

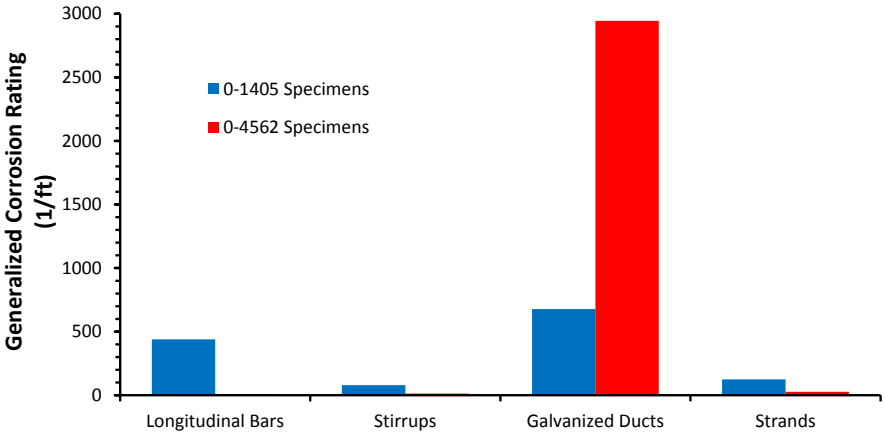

Figure 6.21: Generalized Corrosion Ratings for All Components of Project 0-1405 and Project 0-4562 Among Specimens with Galvanized Steel Ducts

CHAPTER 7
Cost Analysis

7.1 RATIONALE

If properly implemented, the new corrosion-resistant post-tensioning materials studied in this thesis could be capable of extending the service life of a bridge by delaying or eliminating the onset of corrosion. However, it is important for designers to understand the additional construction costs that each upgrade entails. In this chapter, cost estimates for each of the main project variables are presented and analyzed. Quantities are based on what would be found in a typical segmental bridge.

7.2 METHODOLOGY

Unit costs of post-tensioning materials can vary widely based on the scale of the structure for which they are acquired. To achieve a uniform comparison, the author chose to analyze costs for the FM 2031 Gulf Intracoastal Waterway (GIWW) bridge in Matagorda, Texas (see Figure 7.1). This structure consists of a three-span, 680-foot-long cast-in-place post-tensioned segmental box girder bridge and 19 additional precast prestressed concrete approach spans. The bridge was opened to traffic in 2009[23]. Post-tensioning material quantities were obtained from TxDOT[24]. To simplify the cost comparison, only quantities of longitudinal post-tensioning materials for the three post-tensioned spans were considered. Those quantities are shown in Table 7.1. Only "neat" quantities were included. Auxiliary items such as grout vents and plugs were not considered.

Figure 7.1: FM 2031 Bridge over Gulf Intracoastal Waterway in Matagorda, Texas[25]

Table 7.1: Matagorda GIWW Bridge Longitudinal Post-Tensioning Quantities

Item	Quantity	Unit
2″ Duct	2720	Ft.
3″ Duct	9891	Ft.
4″ Duct	18180	Ft.
2″ Coupler	176	Each
3″ Coupler	783	Each
4″ Coupler	1452	Each
7-Strand Anchorage	8	Each
12-Strand Anchorage	88	Each
19-Strand Anchorage	160	Each
0.6″ 7-Wire Strand	267403	Ft.

Costs for each type of duct and anchorage examined in this thesis were obtained from a post-tensioning supplier. Strand costs were obtained from the Federal Highway Administration[1] and from estimates of the post-tensioning supplier. Strand and duct estimates were provided in a unit price per foot. Coupler cost estimates were given as a price per coupler. Anchorage estimates were given as a package price per bearing plate, anchor head, and corresponding number of wedges. Because electrically isolated tendons are not currently used in the United States, prices were obtained from a source in Switzerland. These costs were converted to U.S. dollars using the market exchange rate at 5:00 PM EST on Friday, November 12, 2010[26]. All cost

estimates exclude shipping, handling, and markup by the post-tensioning supplier. On-site labor costs were assumed to be identical for all materials.

7.3 COST DATA AND ANALYSIS

The baseline cost was defined as the official published construction cost of $16 million[23]. Figure 7.2 shows the percent increase in the total construction cost for each combination of strand, duct, and anchorage based on the cost estimates which were obtained by the author.

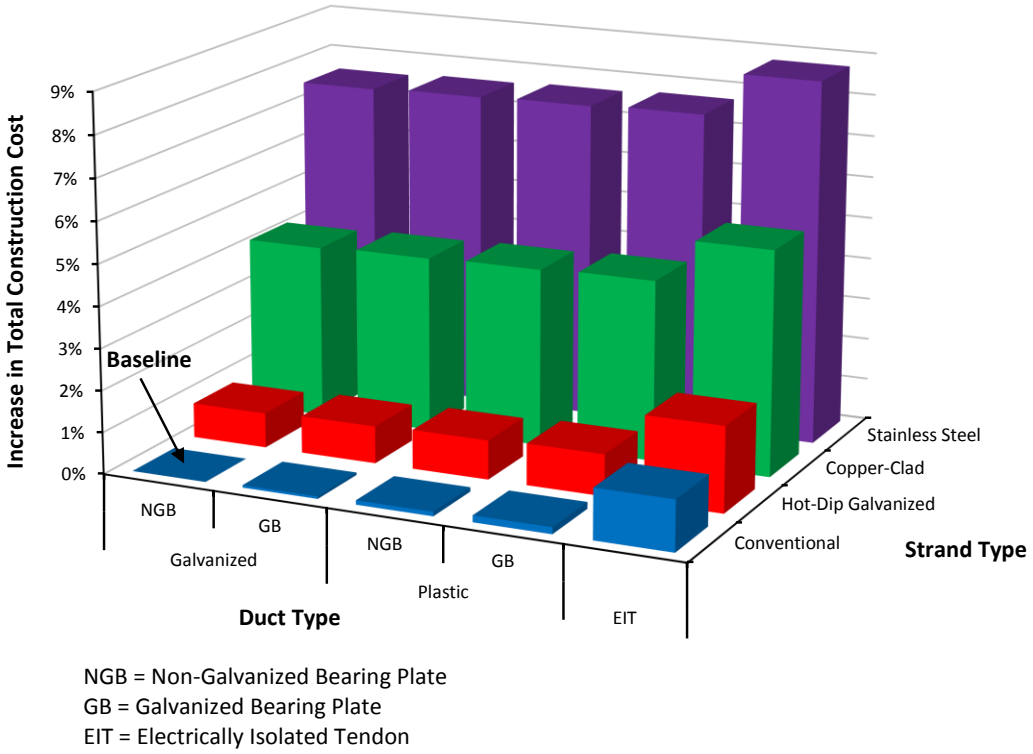

NGB = Non-Galvanized Bearing Plate
GB = Galvanized Bearing Plate
EIT = Electrically Isolated Tendon

Figure 7.2: Percent Increase of Total Construction Cost for Each Project Variable

From Figure 7.2, it is clear that costs increase as more protection is provided. Galvanized bearing plates cost more than non-galvanized bearing plates. Systems with plastic ducts cost more than those with galvanized ducts. Electrically isolated systems are the most expensive. Strand costs increase with how "exotic" they are. The highest overall cost increase would occur if the Matagorda bridge were constructed with electrically isolated tendons and stainless steel strand. Regardless of materials, the total construction cost increases are all less than 10%. Strand

type makes the biggest difference in construction cost, while duct and anchorage type have less of an effect.

Percent increase in construction costs are plotted in Figure 7.3 for each type of duct and bearing plate for conventional strand only. This better illustrates the cost increases associated with duct and bearing plate type. The incremental cost increases for plastic ducts and galvanized bearing plates are approximately 0.10% and 0.05%, respectively. The electrically isolated tendon costs are much greater, resulting in about 1.2% higher construction costs.

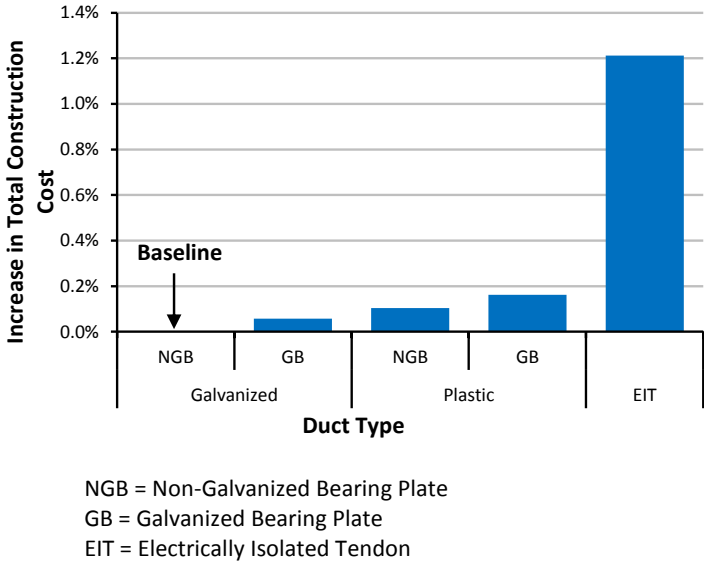

Figure 7.3: Percent Increase in Construction Costs for Conventional Strand

It is important to consider that total costs of a bridge include maintenance and repair over the life of the structure. Even if a durability upgrade results in slightly higher construction costs, it may reduce lifetime costs due to lower ongoing expenditures and a longer service life. Consider a simple numerical example. Assume that a bridge costs 10% more to construct with stainless steel strand than with conventional steel strand. Assume also that the service life of the structure would increase from 50 years to 100 years. According to Grau, 1% of construction cost is a reasonable estimate for the annual maintenance expenditures of a bridge[27]. Assume that this cost would remain the same for both conventional and stainless steel strand. Treating 100 as an arbitrary unitless construction cost, total costs for the bridge with conventional strand are: 100 + 50 years * 1 per year = 150. Amortized over the service life of the structure, this is a cost of 3 per

year. For the structure with stainless steel strand: 110 + 100 * 1 per year = 210. Cost per year of service in this case is 2.1. With stainless steel strand, lifetime cost decreases by 30%.

This is a simplified example. A true life cycle cost analysis must consider real costs and the effect of inflation. More importantly, it must be established to what extent different post-tensioning materials prolong the service life of a bridge. As part of Project 0-1405, Grau[27] performed life cycle cost analyses based on macrocell corrosion tests performed by West[10] and Salas[8]. By assuming that a decrease in corrosion rating corresponded to the same proportional decrease in maintenance costs, she was able to compute lifetime costs on an arbitrary structure for each project variable. This was not possible here because too few specimens were autopsied to obtain meaningful service life estimates for each project variable. Additionally, the corrosion rating system does not account for material type. For example, it would be meaningless to compare corrosion ratings among specimens with copper-clad strand because all copper-clad strand had the same corrosion rating regardless of duct type.

CHAPTER 8
Design Recommendations

8.1 CRACK CONTROL

Corrosion damage to the longitudinal bars, stirrups, and galvanized steel ducts was most severe at flexural crack locations. If a post-tensioned structure is uncracked, chlorides must travel through the concrete pore space in order to reach reinforcing elements. This would delay the onset and propagation of corrosion greatly. Therefore, it is recommended that post-tensioned structures in aggressive environments be designed as fully prestressed.

8.2 EPOXY-COATING OF MILD REINFORCEMENT

The epoxy-coated mild steel reinforcement showed minimal corrosion which mostly occurred at the points where it had been handled or disturbed in some way. It is recommended that epoxy-coated rebar fulfill the applicable ASTM standard. The rebar must also be handled with care to avoid damaging the coating. Any defects which arise during handling or construction should be patched with the appropriate repair compound prior to casting. In many instances, coating damage was caused by the coated rebar ties which were used to construct the reinforcement cages of the autopsy specimens. It is therefore recommended that epoxy-coated rebar be tied with plastic ties to minimize coating damage.

8.3 DUCT TYPE

Galvanized steel duct performed very poorly and should not be used in aggressive environments. The plastic ducts studied here were robust enough to prevent significant damage during casting and post-tensioning. Their use is recommended in aggressive environments. However, chlorides were able to enter continuous plastic ducts through grout vent openings which had been drilled on-site and inadequately sealed. Therefore, it is recommended that all grout vents be installed at couplers equipped with integral grout vents and positively attached grout hoses for maximum watertightness.

8.4 COUPLER TYPE

In many cases, chlorides entered the plastic ducts through breaches in the seal between coupler and duct. It is recommended that any duct couplers be installed under the supervision of

Post-Tensioning Institute certified inspectors or equivalent. Additionally, duct pressure testing should be conducted in accordance with the TxDOT Standard Specification. For the internal longitudinal ducts of segmental bridges, duct couplers should be installed at segment joints to protect the tendon from chloride intrusion. Alternatively, the segmental duct joints should be swabbed with epoxy to protect them from within.

8.5 GROUT TYPE

Because grout was injected with a hand pump, the grout in the autopsy specimens was not always well-consolidated and showed some large voids. It is recommended that anti-bleed and/or thixotropic grout be used for internal bonded post-tensioning tendons. Additionally, grout should be injected using the equipment, personnel, and procedures specified in the TxDOT Standard Specification.

8.6 STRAND TYPE

Damage to all strands was minimal. It is recommended that strand be chosen on the basis of cost, mechanical properties, availability, and contractor familiarity. All strands should be installed and tensioned according to TxDOT specifications.

8.7 ANCHORAGE REGIONS

Galvanized bearing plates showed no substantial benefit over non-galvanized bearing plates. Anchorage pourbacks performed well on autopsy specimens, with most showing little shrinkage cracking and very good consolidation. On dripper specimens, this appears to have prevented chlorides from entering the tendons at the anchorages. Therefore, anchorage region pourbacks should be carefully placed with the proper epoxy and mortar materials. This will ensure low permeability and prevent chloride ingress.

8.8 ELECTRICALLY ISOLATED SYSTEMS

The strands and duct in the fully encapsulated specimen autopsied here performed similarly to those found in the non-encapsulated specimens. However, despite AC impedance data suggesting that the duct was not watertight, chloride concentrations were below the corrosion threshold throughout the entire tendon. This is a marked improvement over all other specimens, most of which showed chloride concentrations well above the corrosion threshold. When

properly installed under the supervision of a certified inspector, this system may enable bridges to achieve a long service life.

8.9 HALF-CELL POTENTIAL MEASUREMENTS

Half-cell measurements were able to predict the presence of corrosion in the autopsy specimens. However, the method could not determine the particular components which were corroding. Further development in the area of non-destructive corrosion testing is necessary to accurately assess corrosion in post-tensioned structures.

8.10 AC IMPEDANCE MEASUREMENTS

This method is only applicable to fully encapsulated tendons. If the tendons are properly installed, this method may offer a simple means of establishing their soundness. However, further testing is necessary to establish its accuracy.

8.11 CHLORIDE CONTENT

Concrete or grout chloride content above the corrosion threshold indicates that the probability of corrosion for an unprotected element is high at that location. For a structure with epoxy-coated reinforcement or plastic duct, chloride content is not an accurate predictor of corrosion if the protective layers are undamaged. In addition, chloride concentrations do not adequately predict the extent or severity of corrosion.

CHAPTER 9

Summary, Conclusions, and Recommendations for Future Testing

9.1 SUMMARY

Ten full-scale post-tensioned beam specimens were subjected to 4 years of aggressive cyclic ponded saltwater exposure. Three of those specimens were additionally exposed to saltwater spray once per month on one anchorage face. Non-destructive monitoring was conducted during the exposure period. This consisted of half-cell potential measurements, AC impedance measurements (for specimens with fully encapsulated tendons), and regular visual inspections. Chloride samples were extracted from the specimens at the end of exposure. After 4 years, the specimens were autopsied, and all reinforcing elements from the middle of each specimen were examined for corrosion and damage. Anchorage regions were also autopsied and examined for corrosion.

9.2 CONCLUSIONS

9.2.1 Strand Type

All strand types showed a low level of corrosion. Elevated grout chloride levels in many specimens suggest that chlorides were able to travel within strand interstices along the entire length of the tendons. Corrosion was more severe within the anchor heads than in the main autopsy regions of the specimens.

9.2.1.1 Conventional Strand

Conventional strands showed discoloration or light surface corrosion spots on their outer wires and somewhat more severe corrosion on their inner wires. The spots were most frequent in the regions which had been in direct contact with the surrounding duct.

9.2.1.2 Hot-Dip Galvanized Strand

Damage to the hot-dip galvanized strand was similar to that of the conventional strand. On the outer wires of each strand, corrosion occurred in the zinc coating. However, corrosion on the inner wire occurred on the bare steel which was not covered with zinc during the galvanizing process. Galvanized strand had a very strong bond with the surrounding grout and was very

difficult to remove. Small bubbles found in the interstices of some galvanized strand suggest that the zinc may have reacted with the grout chemically.

9.2.1.3 Copper-Clad Strand

Copper-clad strand in the main autopsy region assumed a glossy black patina on all wires. The patina was darker and glossier on the inner wires than the outer wires. Dezincification may have occurred near the ends of some copper-clad strands. In the anchorage region, the wedges penetrated the copper coating and caused the underlying steel to corrode there.

9.2.1.4 Stainless Steel Strand

The stainless steel strand in the main autopsy region showed very little corrosion. For the most part, the strand appeared to be brand new. Some light corrosion occurred in the anchorage region strands. These strands had a very weak bond with the surrounding grout, which resulted in debonding during autopsy.

9.2.2 Duct Type

9.2.2.1 Galvanized Steel Duct

The galvanized steel duct performed very poorly. Every duct autopsied showed area loss and pitting. These were most prevalent at the locations of grout voids within the tendon. Corrosion initiated at the locations where surface cracks intersected with the ducts and spread from there.

9.2.2.2 Plastic Duct

Plastic ducts sustained some scratching and gouging during tensioning but were structurally intact. No substantial difference was observed among the three types of plastic duct examined in the autopsies. While no leaks were found in the ducts, chlorides entered the non-coupled plastic ducts through inadequately sealed grout vents at midspan. A major finding from this study is that all grout vents should be installed at couplers equipped with integral grout vents and positively attached grout hoses for maximum watertightness.

9.2.3 Coupler Type

The two heat-shrink couplers examined here were very brittle at the time of autopsy and showed signs of breaches. Several of the mechanical snap-on couplers also showed signs of breaches. High chloride content in the coupled plastic ducts indicates that chlorides entered either through these breaches or through the grout vent which was attached to the top of each coupler.

9.2.4 Anchorage Type

There was no appreciable difference between the galvanized and non-galvanized bearing plates, although only one specimen with the former was autopsied for this thesis. Anchorage pourback quality appeared to play a greater role in anchorage protection than galvanization.

9.2.5 Fully Encapsulated System

Strand corrosion in the fully-encapsulated tendon was comparable to the non-encapsulated tendons in other specimens. However, chloride concentrations were below the corrosion threshold along the entire tendon. It seemed that chlorides did not enter the tendon through the couplers, as was observed on other specimens. However, there was evidence suggesting that chlorides may have entered through the anchorages.

9.2.6 Accuracy of Non-Destructive and Destructive Measurements

9.2.6.1 Half-Cell Potential Measurements

The half-cell method was able to predict corrosion in the specimens. However, it could not be determined in which reinforcing element the corrosion was taking place.

9.2.6.2 AC Impedance Measurements

AC impedance measurements indicated that the electrically isolated tendon was barely monitorable and that chlorides may have entered the tendon during the exposure period. AC impedance readings can be used to detect duct defects, but this was not possible for the autopsy specimen due to its lack of monitorability.

9.2.6.3 Concrete Chloride Samples

Chloride levels were above the corrosion threshold at rebar level in the specimens, and all rebar showed some corrosion at that level. However, chloride content cannot adequately predict the presence of corrosion in epoxy-coated reinforcement. Additionally, chloride content cannot predict the extent of corrosion.

9.3 RECOMMENDATIONS FOR FUTURE TESTING

It has already been determined that the remaining 14 beam specimens will be autopsied in 2012. The following recommendations concern the exposure and autopsy of those specimens.

- Take grout chloride samples at regular intervals along all tendons. This will better illustrate the transport of chlorides along the tendons.
- Take grout chloride samples at both anchorage regions of the dripper specimens.
- During the last one or two wet cycles prior to autopsy, tint the saltwater in the top depression of one specimen with a dye tracer. If the hypotheses of this thesis are true, the saltwater will infiltrate the tendon and travel along its length inside the strand interstices. Upon autopsy, the dye will be visible inside the specimen to illustrate the path of chloride intrusion.
- Conduct a full life cycle cost analysis for each material using all autopsy data.
- Test the accuracy of the AC impedance method using DC impedance. Dr. Markus Büchler of SGK in Switzerland has suggested a method to accomplish this.
- Determine the exact chloride content threshold for corrosion based on the cement content of the concrete and grout used in the test specimens.

For future corrosion studies:

- Focus on workmanship and ease of installation of post-tensioning systems. Small breaches in improperly installed couplers and grout vents caused severe chloride ingress in the specimens studied here. Future work should focus on how to minimize or eliminate installation problems such as these.
- Continue developing better grout mixes. Grout voids provide an easy avenue for chloride travel in a tendon, so minimizing grout voids should remain a priority.

Ensure that grout chloride content specifications are followed so that chlorides are not introduced to the tendon through the grout itself.

- Concrete and plastic have different coefficients of thermal expansion. As such, temperature variation may result in gaps between embedded grout vents and the surrounding concrete, providing easy access for chlorides. Study the effect of applying a flexible, waterproof membrane around grout vents at the concrete surface to prevent chloride ingress there.
- As improved post-tensioning systems continue to be installed in new bridges, conduct field inspections to determine their effectiveness in-situ. With time, this will also provide estimates for service life increases associated with various materials.
- Develop and refine new and existing non-destructive monitoring methods for post-tensioned structures.

APPENDIX

Material and Specimen Information

A.1 MATERIAL SUPPLIERS

Suppliers for all materials used in the Project 0-4562 beam specimens are listed below. Shaded entries indicate that contact information has been updated since specimen construction.

Material	Supplier	Contact
Bearing Plates	VSL USA	Jordan Stephenson jstephenson@vsl.net 817-545-4807
Galvanized Steel Duct		
PT Plus Plastic Duct and Couplers		
Hot Dip Galvanized Strand*		
0.6" Strand Anchor Heads		
Wedges		
EIT Systems*	VSL Switzerland	Hans-Rudolf Ganz hansrudolf.ganz@vsl.com
76mm One-Way Ribbed Plastic Duct*	GTI	Joe Harrison joe.harrison@gti-usa.com 281.240.0550
76mm Couplers*		
85mm Two-Way Ribbed Plastic Duct*		
85mm Coupler*		
Stainless Strand*	Techalloy	Jim Beitz jbeitz@techalloy.com 815.923.2131
Stainless Clad Strand*	DSI	Ron Bonomo ron.bonomo@dsiamerica.com
Copper Clad Strand*	Copperweld	Milton Lamb mlamb@copperweld.com info@copperweld.com
Epoxy Coated Strand*	Sumiden Wire	Steve Yoshida stevey@sumiden.com
Type V Epoxy*	Unitex	Susan Wintz 816.231.7700
Epoxy Coated Rebar	ABC Coating	Mary Boyette 972.937.9841 orders@abccoatingtx.com
Concrete	Capitol Aggregates	Ron Taff

* - Material Donated to Research Project

A.2 LIST OF SPECIMENS

All Project 0-4562 beam specimens are listed below. Specimen identification is made according to the naming system in Chapter 2.

Casting Group	Specimen Name	Specimen ID
T	T.1	TEST-GA-CON-CS-CG-T
	T.2	TEST-NGA-CON-CS-CG-T
1	1.1	NGA-CON-CS-CG-1
	1.2	NGA-CU-CS-CG-1
	1.3	NGA-SC-CS-CG-1
	1.4	GA-CON-CS-CG-1
2	2.1	NGA-FF-CS-CG-2
	2.2	NGA-HDG-CS-CG-2
	2.3	NGA-CON-1P-CG-2
	2.4	NGA-CU-1P-CG-2
3	3.1	NGA-CON-2P-CG-3
	3.2	NGA-HDG-2P-CG-2
	3.3	NGA-CU-2P-CG-3
	3.4	NGA-HDG-1P-CG-3
4	4.1	NGA-SS-CS-CG-4
	4.2	NGA-SS-1P-CG-4
	4.3	Comparison-Epoxy-4
	4.4	Comparison-Uncoated-4
5	5.1	GA-CON-2P-CG-5
	5.2	NGA-SC-2P-CG-5
	5.3	NGA-SS-2P-CG-5
6	6.1	NGA-EG-CS-CG-6
	6.2	NGA-EG-1P-CG-6
	6.3	NGA-EG-2P-CG-6
7	7.1	EIT-CON-CG-7
	7.2	EIT-CON-CG-7
	7.3	EIT-HDG-CG-7
	7.4	EIT-FF-CG-7

= Autopsy Specimens

A.3 CORROSION RATINGS

Corrosion ratings for all autopsy specimens are listed below.

Specimen	Main Autopsy Region Corrosion/Damage Ratings											
	Longitudinal Bars		Stirrups		North Duct		South Duct		North Tendon Strands		South Tendon Strands	
	Total	Generalized	Total	Generalized	Total	Generalized	Total	Generalized	Total	Generalized	Total	Generalized
T.1	19	3	169	12	1680	480	3800	1086	130	12	288	27
T.2	50	7	120	9	38318	10948	2256	645	286	27	395	38
1.2	60	9	128	9	9813	2804	6190	1769	441	42	441	42
2.2	144	21	193	14	11350	3243	9017	2576	159	15	154	15
2.4	101	14	690	49	3100	886	475	136	441	42	441	42
3.1	54	8	110	8	120	34	40	11	185	18	166	16
3.2	42	6	126	9	80	23	180	51	140	13	182	17
3.4	46	7	89	6	180	51	210	60	150	14	194	18
4.2	26	4	78	6	4740	1354	2640	754	6	1	8	1
7.1	63/360	9/51	128	9	80	23			296	28		

Specimen	Dead End Anchorage Corrosion/Damage Ratings							
	North Duct		South Duct		North Tendon Strands		South Tendon Strands	
	Total	Generalized	Total	Generalized	Total	Generalized	Total	Generalized
T.1	35	52	17	25	107	36	94	31
T.2	27	40	19	28	127	42	107	36
1.2	15	30	16	32	135	45	127	42
2.2	16	32	13	26	86	29	52	17
2.4	0	0	0	0	156	52	153	51
3.1	0	0	30	60	130	37	139	46
3.2	10	20	0	0	128	37	121	35
3.4	240	480	0	0	77	26	84	28
4.2	240	721	0	0	55	18	51	17
7.1	0	0			163	36		

Specimen	Live End Anchorage Corrosion/Damage Ratings							
	North Duct		South Duct		North Tendon Strands		South Tendon Strands	
	Total	Generalized	Total	Generalized	Total	Generalized	Total	Generalized
3.1	30	60	0	0	126	36	117	33
3.2	10	20	60	120	128	37	105	30
7.1	0	0			140	31		

REFERENCES

1. Corven, J. and Moreton, A, "Post-Tensioning Tendon Installation and Grouting Manual," Federal Highway Administration, Tallahassee, FL, May 26, 2004.

2. Schokker, A.J., "Improving Corrosion Resistance of Post-Tensioned Substructures Emphasizing High-Performance Grouts," Ph.D. Dissertation, The University of Texas at Austin, May 1999.

3. ACI Committee 222, "Corrosion of Metals in Concrete" (ACI 222R-01), American Concrete Institute, Farmington Hills, MI, 2001.

4. *fib* Bulletin 33, "Durability of Post-Tensioning Tendons," Fèdèration Internationale du Bèton, Lausanne, Switzerland, 2006.

5. Raiss, M.E., "Re-Design of Post-Tensioned Bridges to Improve Buildability and Durability," Second Workshop on Durability of Post-Tensioning Tendons, Zürich, Switzerland, October 2004.

6. Florida Department of Transportation, "New Directions for Florida Post-Tensioned Bridges," Corven Engineering, Inc., Volume 1 of 10, Tallahassee, FL, February 15, 2002.

7. Ahern, M.E., "Design and Fabrication of a Compact Specimen for Evaluation of Corrosion Resistance of New Post-Tensioning Systems," M.S. Thesis, The University of Texas at Austin, May 2005.

8. Salas, R.M., "Accelerated Corrosion Testing, Evaluation, and Durability Design of Bonded Post-Tensioned Concrete Tendons," Ph.D. Dissertation, The University of Texas at Austin, August 2003.

9. Turco, G.P., "Durability Evaluation of Post-Tensioned Concrete Beam Specimens After Long-Term Aggressive Exposure Testing," M.S. Thesis, The University of Texas at Austin, August 2007.

10. West, J.S., "Durability Design of Post-Tensioned Bridge Substructures," Ph.D. Dissertation, The University of Texas at Austin, May 1999.

11. Texas Department of Transportation, "Standard Specifications for Construction and Maintenance of Highways, Streets, and Bridges," 2004.

12. VSL, "Grouting of Post-Tensioning Tendons," VSL Report Series 5, VSL International Ltd., Lyssach, Switzerland, 2002.

13. ASTM, "Standard Test Method for Determining Effects of Chemical Admixtures on the Corrosion of Embedded Steel Reinforcement in Concrete Exposed to Chloride Environments," ASTM G109-07, American Society for Testing and Materials, Philadelphia, PA, 2007.

14. ASTM, "Standard Test Method for Corrosion Potentials of Uncoated Reinforcing Steel in Concrete," ASTM C876-09, American Society for Testing and Materials, Philadelphia, PA, 2009.

15. Elsener, B., "Monitoring of Electrically Isolated Post-Tensioning Tendons," Structural Concrete: Journal of the *fib*, Vol. 6, No. 3, September 2005.

16. ASTM, "Standard Test Method for Acid-Soluble Chloride in Mortar and Concrete," ASTM C1152/C1152M-04, American Society for Testing and Materials, Philadelphia, PA, 2004.

17. ASTM, "Standard Practice for Conventions Applicable to Electrochemical Measurements in Corrosion Testing," ASTM G3-89, American Society for Testing and Materials, Philadelphia, PA, 1989.

18. Bundesamt für Strassen, "Massnahmen zur Gewährleistung der Dauerhaftigkeit von Spanngliedern in Kunstbauten," ASTRA Richtlinie 12 010, 2007.

19. Ganz, H.R., Email Correspondence, October 19, 2010.

20. Ganz, H.R., Email Correspondence, November 5, 2010.

21. ACI Committee 201, "Guide for Conducting a Visual Inspection of Concrete in Service" (ACI 201.1R-08), American Concrete Institute, Farmington Hills, MI, 2001.

22. Wheat, H.G., Email Correspondence, May 27, 2010.

23. Van Lunduyt, D., "The Gulf Intracoastal Waterway Bridge at Matagorda, Texas," Aspire: The Concrete Bridge Magazine, Winter 2010, pp. 20-23.

24. Turco, G.P., Email Correspondence, October 15, 2010.

25. Frank, D., "FM 2031 Bridge, GIWW," U.S. Coast Guard Office of Waterways Management: Bridge Program Division, Presentation to U.S. Department of Homeland Security, August 14, 2009.

26. USD/CHF Market Exchange Rate, Yahoo Finance, Obtained November 12, 2010, 5 PM EST.

27. Grau, K.A., "Survey of Costs, Economic Analysis, and Design Guidelines for Corrosion Protection Methods for Post-Tensioned Concrete Bridges," M.S. Thesis, The University of Texas at Austin, May 2005.

VITA

Gregory Edward McCool was born in 1986 in Minneapolis, Minnesota. He graduated high school from Maple Grove Senior High in 2004 and immediately spent a year in Germany attending college preparatory school as an exchange student. After arriving stateside, he enrolled at the University of Notre Dame and received his Bachelor of Science in Civil Engineering in 2009. That fall, he enrolled at the University of Texas at Austin to pursue a Master of Science degree in Structural Engineering. He graduated from the University of Texas in December 2010.

Permanent Address: 9374 Rosewood Ln N
Maple Grove, MN 55369

This thesis was typed by the author.